OPTICAL AND OPTOGENETIC CONTROL OF CELL PROLIFERATION AND SURVIVAL

by

Eva Gschaider-Reichhart

8th January, 2018

A thesis presented to the
Graduate School
of the
Institute of Science and Technology Austria, Klosterneuburg, Austria
in partial fulfillment of the requirements
for the degree of
Doctor of Philosophy

I hereby declare that this dissertation is my own work and that it does not contain other people's work without this being so stated; this thesis does not contain my previous work without this being stated, and the bibliography contains all the literature that I used in writing the dissertation.

I declare that this is a true copy of my thesis, including any final revisions, as approved by my thesis committee, and that this thesis has not been submitted for a higher degree to any other university or institution.

I certify that any republication of materials presented in this thesis has been approved by the relevant publishers and co-authors.

Signature: _____

Gschaider-Reichhart Eva

8th January, 2018

ABSTRACT

The aim of this thesis was the development of new strategies for optical and optogenetic control of proliferative and pro-survival signaling, and characterizing them from the molecular mechanism up to cellular effects. These new light-based methods have unique features, such as red light as an activator, or the avoidance of gene delivery, which enable to overcome current limitations, such as light delivery to target tissues and feasibility as therapeutic approach. A special focus was placed on implementing these new light-based approaches in pancreatic β-cells, as β-cells are the key players in diabetes and especially their loss in number negatively affects disease progression. Currently no treatment options are available to compensate the lack of functional β-cells in diabetic patients.

In a first approach, red-light-activated growth factor receptors, in particular receptor tyrosine kinases were engineered and characterized. Receptor activation with light allows spatio-temporal control compared to ligand-based activation, and especially red light exhibits deeper tissue penetration than other wavelengths of the visible spectrum. Red-light-activated receptor tyrosine kinases robustly activated major growth factor related signaling pathways with a high temporal resolution. Moreover, the remote activation of the proliferative MAPK/Erk pathway by red-light-activated receptor tyrosine kinases in a pancreatic β-cell line was also achieved, through one centimeter thick mouse tissue. Although red-light-activated receptor tyrosine kinases are particularly attractive for applications in animal models due to the deep tissue penetration of red light, a drawback, especially with regard to translation into humans, is the requirement of gene therapy.

In a second approach an endogenous light-sensitive mechanism was identified and its potential to promote proliferative and pro-survival signals was explored, towards light-based tissue regeneration without the need for gene transfer. Blue-green light illumination was found to be sufficient for the activation of proliferation and survival promoting signaling pathways in primary pancreatic murine and human islets. Blue-green light also led to an increase in proliferation of primary islet cells, an effect which was shown to be mostly β-cell specific in human islets. Moreover, it was demonstrated that this approach of pancreatic β-cell expansion did not have any negative effect on the β-cell function, in particular on their insulin secretion capacity. In contrast, a trend for enhanced insulin secretion under high glucose conditions after illumination was detected. In order to unravel the detailed characteristics of this endogenous light-sensitive mechanism, the precise light requirements were determined. In addition, the expression of light sensing proteins, OPN3 and rhodopsin, was detected. The observed effects were found to be independent of handling effects such as temperature differences and cytochrome c oxidase dependent ATP increase, but they were found to be enhanced through the knockout of OPN3. The exact mechanism of how islets cells sense light and the identity of the photoreceptor remains unknown.

Summarized two new light-based systems with unique features were established that enable the activation of proliferative and pro-survival signaling pathways. While red-light-activated receptor tyrosine kinases open a new avenue for optogenetics research, by allowing non-invasive control of signaling *in vivo*, the identified endogenous light-sensitive mechanism has the potential to be the basis of a gene therapy-free therapeutical approach for light-based β-cell expansion.

ABOUT THE AUTHOR

Eva Gschaider-Reichhart completed her Bachelor of Science in Medical and Pharmaceutical Biotechnology at the University of Applied Sciences IMC Krems and her Master of Science in Molecular Biotechnology at the University of Applied Sciences Campus Vienna, before joining the PhD program of IST Austria in September 2013. In 2015 she received a full fellowship of the doctoral program "Molecular Drug Targets", financed by the Austrian Science Fund (FWF).

Her main research interest is the field of synthetic physiology with a special focus on cell signaling and optogenetics. During her Bachelor's degree, she worked on the research project "The regulation of the insulin-like growth factor family by transforming growth factor β in benign and malignant human prostate cells" with the Klocker group at the Medical University Innsbruck at the "Department for Experimental Urology" from July to December 2010, and her results were part of a publication in the journal The American Journal of Pathology. During her PhD, Eva was involved in different projects focusing on engineering and applying different light-based cell signaling systems. The results of these projects were published in different high-impact journals, such as *EMBO Journal, Nature Chemical Biology* and *Angewandte Chemie International Edition*. One part of her main PhD project was published in 2016 in *Angewandte Chemie International Edition*. She also presented her research results in different conferences such as the *ASCB Annual Meeting* (New Orleans, USA), the *Gordon Research Seminar on FGFs in Development & Disease* (Hong Kong, S.A.R. China), the *12th International Congress of Cell Biology* (Prague, Czech Republic) and the *53rd Annual Meeting of the EASD* (Lisbon, Portugal).

ACKNOWLEDGMENTS

First and foremost, I would like to thank my supervisor Harald Janovjak for providing me with the opportunity to work on my very interesting projects. He consistently allowed me to work on my projects very independently, but steered me in the right direction whenever necessary. The door to Harald's office was always open whenever I had questions or needed support for problem solving. I also would like to thank him for the many hours of reviewing all my abstracts, presentations, applications and my thesis draft during my whole PhD.

Special thanks also to Martina Düfer (University of Münster, Institute of Pharmaceutical and Medicinal) and her lab members, for their very warm welcome in their lab in summer 2015 and their generosity to teach me the fundamentals of my second project, the isolation of primary islets. Moreover, I would like to thank them for answering all my uncertainties regarding experimental setups and islets handling during the last two years.

I also want to acknowledge the very successful and straightforward collaboration with Stefan Kubicek (CeMM Research Center for Molecular Medicine, Austrian Academy of Sciences) who provided me with human islet samples, as well as King-Wai Yau (Johns Hopkins University School of Medicine Preclinical Teaching) for supporting the project by providing us a OPN3 knockout mouse strain as well as for all the fruitful discussions.

Moreover I want to thank all the past and present members of the lab for their advice, and discussions; their support in times of frustration and troubles and also for celebrating our successes together. In particular I would like to thank Alvaro Ingles-Prieto, Alexandra-Madeleine Tichy and Stephanie Kainrath for all the constructive discussions, their experimental support and for revising all my thesis drafts.

Finally, I must express my very profound gratitude to my husband for providing me with unfailing support and continuous encouragement throughout the whole process of researching and writing this thesis.

This accomplishment would not have been possible without the support of all the people mentioned and many others left unmentioned. Thank you.

LIST OF PUBLICATIONS APPEARING IN THESIS

1. Kainrath S.**,** Stadler M.**, Reichhart E.**, Distel M. & Janovjak H. (2017). Green light-induced inactivation of receptor signaling using cobalamin-binding domains. **Angewandte Chemie International Edition in English,** 56(16): 4608-4611

2. **Reichhart E.**, Ingles-Prieto A., Tichy A.M., McKenzie C. & Janovjak H. (2016). A phytochrome sensory domain permits receptor activation by red light. **Angewandte Chemie International Edition in English,** 55(21): 6339-6342

3. Ingles-Prieto A., **Reichhart E.**, Muellner M.K., Nowak M., Nijman S.M., Grusch M. & Janovjak H. (2015). Light-assisted small molecule screening against protein kinases. **Nature Chemical Biology,** 11(12) 952-954

4. Grusch, M.*, Schelch K.*, Riedler R.*, **Reichhart E.**, Differ C., Berger W., Ingles-Prieto A. & Janovjak H. (2014). Spatio-temporally precise activation of engineered receptor tyrosine kinases by light. **EMBO Journal,** 33(15): 1713-1726

* Shared first authorship

TABLE OF CONTENTS

LIST OF FIGURES

LIST OF TABLES

LIST OF EQUATIONS

LIST OF ABBREVIATIONS

APC	Antigen presenting cells
AdoCbl	Adenosylcobalamine
ADP	Adenosin diphosphat
AppA	Activation of photopigment and puc expression A
ATP	Adenosine triphosphate
BG	Blue-green
BLUF	Blue light sensors using flavin adenine dinucleotide
BSA	Bovine Serum Albumin
°C	Degree Celsius
$[Ca^{2+}]i$	Intercellular Ca^{2+}
CcO	Cytochrome c oxidase
CCT	C-terminal domain
cGMP	Cyclic guanosine monophosphate
CIB1	Calcium and integrin-binding protein 1
CIP	Alkaline Phosphatase, Calf Intestinal
cm	Centimeter
CMV	Cytomegalovirus (promoter)
CMRL	Connaught medical research laboratories medium
CNG channels	Cyclic nucleotide gated channels
CO_2	Carbon dioxide
COP1	Constitutive photomorphogenic 1
CPH1S	CPH1 sensory domain
CPH1So	CPH1 codon optimized sensory domain
CRYs	Cryptochromes
DAG	Diacyl glycerol
DAPI	4',6-Diamidino-2-phenylindole dihydrochloride
DMEM	Dulbecco's modified eagle medium
DMSO	Dimethylsulfoxid
DNA	Deoxyribonucleic acid

dNTP	Deoxyribonucleotide triphosphate
DPP-4	Dipeptidyl peptidase-4
E.Coli	*Escherichia coli*
EDTA	Ethylenediaminetetraacetic
EdU	5-ethynyl-2'-deoxyuridine
ELISA	Enzyme-linked immunosorbent assay
Em	Emission
En2SA	Mouse Engrailed2 intron splice acceptor
Erk	Extracellular signal-regulated kinase
Ex	Excitation
FAD	Flavin adenine dinucleotide
FBS	Fetal Bovine Serum
FGF2	Fibroblast growth factor 2
FKBP	FK506 binding protein
FMN	Flavin mononucleotide
FRT	Flippase recognition target
g	Gramm
GAF	cGMP-specific phosphodiesterase adenylate cyclase FhlA
GD	Gestational diabetes
gDNA	Genomic DNA
GFR	Growth factor receptor
GIP	Glucose-dependent insulinotropic polypeptide
GK	Glucokinase
GLP-1	Glucagon-like peptide 1
GLUT-2	Glucose transporter-2
G6P	Glucose-6-phosphate
G_t	G-protein transducin
hActbP	Human β-actin promoter
H_2O	Water
HCl	Hydrochloride

HGF	Hepatocyte growth factor
HEK293	Human Embryonic Kidney 293
HEPES	4-(2-hydroxyethyl)-1-piperazineethanesulfonic acid
IEQ	Human islet equivalent
IIDP	Integrated Islet Distribution Program
IP_3	Inositol trisphosphate
IR	Insulin receptor
IRES	Internal ribosome entry site
L	Liter
LOV	Light-oxygen-voltage
M	Molar
MAPK	Mitogen-activated protein kinase
mCer3	mCerulean3
mFGFR1	Murine fibroblast growth factor receptor
mg	Milligram
MHC	Major histocompatibility complex
min	Minutes
ml	Milliliter
mm	Millimeter
mM	Millimolar
MODY	Maturity onset diabetes of the young
MTHF	Methenyltetrahydrofolate
MxCarH	*Myxococcus xanthus*
mV	mVenus
neo	Neomycin-resistance gene
OFSC	Orbital fat stem cells
OPN3	Opsin 3
OPN4	Opsin 4
OPN5	Opsin 5
OPN1LW	Long-wave-sensitive opsin

OPN1MW	Medium-wave-sensitive opsin
OPN1SW	Short-wave-sensitive opsin
Opto-RTK	Optogenetic-receptor tyrosine kinases
pA	SV40 polyadenylation site
pAkt	Phosphorylated Akt
PAS	PER-ARNT-SIM
PBS	Phosphate-buffered saline
PCB	Phycocyanobilin
PCR	Polymerase chain reaction
PDE6	Phosphodiesterase 6
PEI	Polyethylenimine
pErk	Phosphorylated Erk
PFA	Paraformaldehyde
PHY	Phytochrome-specific GAF-related domain
PIP_2	Phosphatidylinositol 4,5-bisphosphate
PHR	Photolyase homology region
PI3K	Phosphoinositid-3-kinase
PIF	Phytochrome interacting factors
PL	Photolyase
PLC	Phospholipase C
PLO	Poly-L-ornithine
PPARγ	Proliferator-activated receptors gamma
Rac1	Ras-related C3 botulinum toxin substrate 1
RCF	Relative centrifugal force
RER	Rough endoplasmic reticulum
RFU	Relative fluorescence units
RLU	Raw light units
RPMI 1640	Roswell park memorial institute 1640 medium
RNA	Ribonucleic acid
rpm	Revolutions per minute

RRP	Readily releasable pool
RT	Reverse transcriptase
-RT	Minus RT control
RT-PCR	Reverse transcriptase-polymerase chain reaction
RTK	Receptor tyrosine kinases
rtrkB	Rat tropomyosin receptor kinase B
SD	Standard deviation
SDS	Sodium dodecyl sulphate
sec	Seconds
SEM	Standard error of the mean
TAE	Tris-acetate-EDTA
TD1	Type 1 diabetes
TD2	Type 2 diabetes
T_m	Melting temperature
Tris-HCl	Trizma hydrochloride
Trypsin-EDTA	Trypsin-ethylenediaminetetraacetic acid
TtCarH	*Thermus thermophilus*
U	Units
µg	Microgram
µl	Microliter
µM	Micromolar
UV-B	Ultraviolet-B
V	Volt
VDCC	Voltage-dependent Ca^{2+} channels

CHAPTER 1: LITERATURE REVIEW

1.1 Photoreceptors

1.1.1 Photoreceptor introduction

The ability to sense light is widespread among prokaryotes and eukaryotes. Light is a major stimulus that initiates a signal upon absorption of a photon, transmits this signal through complex molecular and metabolic pathways, and ultimately results in modified behavior.[1] In microbes and plants, light modifies biological activities such as light-induced movements and phototropism, whereas in mammalians, light mediates vision and the regulation of the circadian rhythm.[2,3] Light is directly absorbed by protein molecules known as photoreceptors.[3] Photoreceptors have evolved in diverse biological systems to sense light, and their absorption spectrum ranges over specific regions of the electromagnetic spectrum, covering the ultraviolet, visible and near-infrared region (Figure 1.1).[3] Because the polypeptide backbone and amino acid side chains of photoreceptors do not absorb light in this range, almost all photoreceptors need a prosthetic light-absorbing cofactor, known as a chromophore, to be functional. Chromophores act as the primary photon acceptor and can be covalently or non-covalently bound to the photoreceptor. The corresponding chromophore of each photoreceptor is responsible for its specific absorption spectrum (Figure 1.1).[3] In response to photon absorption, photoreceptors undergo different structural rearrangements, including the opening of transmembrane ion channels, the unfolding of terminal secondary structure motifs as well as the formation or disruption of protein-protein interactions, such as hetero- and homodimerization or oligomerization.[4,5] Photoreceptors are commonly classified into six different classes by their chemical nature and the photochemistry of their chromophore: ultraviolet-B (UV-B) light photoreceptors, flavin-binding photoreceptors, xanthopsins, adenosylcobalamine-binding photoreceptors, phytochromes and opsins.[3,5,6]

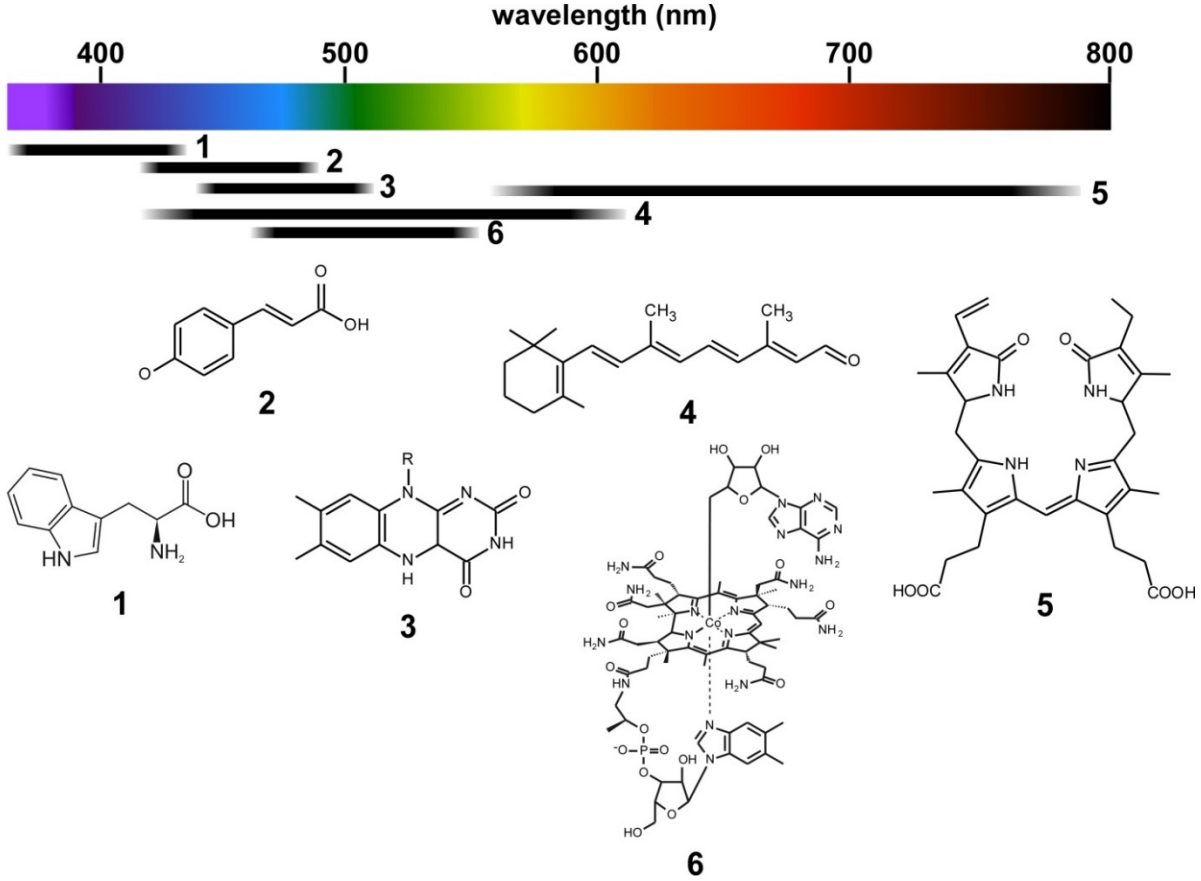

Figure 1.1 Absorption spectra of different chromophores. The specific chromophore of each photoreceptor is responsible for its specific absorption spectrum. Chromophores of main photoreceptor classes: (1) tryptophan, (2) p-coumaric acid, (3) flavin, (4) retinal, (5) tetrapyrroles, (6) adenosylcobalamine.

1.1.2 UV-B light photoreceptors

UV-B light is a key environmental signal that is specifically recognized by plants to promote UV adaption and survival in sunlight. Although UV-B (280–315 nm) represents less than 0.5% of total sunlight energy reaching the earth's surface, it causes photomorphogenic responses in plants that modify their biochemical composition, photosynthetic competence and morphogenesis.[5,7] UV-B is absorbed by the UVR8 photoreceptor, which is a β-propeller protein originally identified in *Arabidopsis thaliana*.[5] The UVR8 protein is localized in the cytoplasm and the nucleus, but upon UV-B irradiation it accumulates in the nucleus, where it interacts with the E3 ubiquitin ligase, constitutive photomorphogenic 1 (COP1), which is a central regulator of UV-B and visible light responses.[5,8] This UV-B-dependent nuclear localization of the receptor is necessary for its activation.[5] In its inactive state, UVR8 is present as a homodimer, whereas absorption of UV-B light leads to the dissociation of UVR8 dimers into monomers within seconds.[5] UV-B-dependent monomerisation of the *Arabidopsis thaliana* UVR8 homodimers is independent of the host cell and can be reproduced in yeast or human cells, by expressing the UVR8 receptors in these cells.[9] The structural change from a dimer to monomer requires a chromophore, which perceives UV-B irradiation and initiates the photoreceptor mediated signal transduction.[5] UVR8 is a noteworthy photoreceptor, because in

contrast to other known photoreceptors that use a prosthetic cofactor, UVR8 uses specific tryptophan amino acids as a chromophore for UV-B light absorption.[5,7] The investigations of the physiological role of UVR8 are still at an early stage. Initial studies focused on gene regulation by UVR8 and demonstrated its importance in UV protection.[7] There is solid evidence that UVR8 and COP1 act together to mediate photomorphogenic UV-B responses by promoting the expression of the basic leucine-zipper transcription factor elongated hypocotyl 5, which is one of the most important promoters of photomorphogenesis.[5,7] Nevertheless all discoveries are derived from studies with *Arabidopsis thaliana.* Therefore, much remains to be studied about the physiological role of UVR8 in other, diverse species.[7]

1.1.3 Flavin-binding photoreceptors

Blue light (300–500 nm) in particular acts to promote a wide variety of photomorphogenic responses in plants, including seedling establishment, phototropism and circadian clock regulation.[10] Flavin-binding photoreceptors sense blue light through a riboflavin derivative cofactor, and are further subdivided into cryptochromes (CRYs), proteins containing light-oxygen-voltage (LOV) domains, and blue light sensors using flavin adenine dinucleotide (BLUF).[10,11] Genetic analyses in the model plant *Arabidopsis thaliana* have been used to identify the molecular basis of blue light receptors and their mechanism of action.[10] In general, the photoexcitation of the flavin cofactor leads to changes in redox and protonation states that ultimately modify the protein conformation and its molecular interactions.[11]

1.1.3.1 CRYs

CRYs were the first plant blue light receptors to be characterized at the molecular level. Although they were first identified in *Arabidopsis thaliana,* they are present throughout the biological kingdom, from archaebacteria to mammals.[10,12] CRYs are key components of various light-dependent responses such as photoperiodic control of flowering in plants and entrainment of the circadian clock in plants and animals.[3,11,12] CRYs exhibit significant homology to the photolyase (PL) family of proteins, which are blue-light-activated enzymes found in both prokaryotes and eukaryotes that catalyze light-dependent repair of damaged DNA following exposure to UV-B irradiation.[10,11,13] CRYs bind two different chromophores at their N-terminal chromophore binding domain, flavin adenine dinucleotide (FAD) and methenyltetrahydrofolate (MTHF). FAD is bound non-covalently within the PL homology region (PHR) and functions as the primary light sensor, whereas MTHF serves as an antenna cofactor to harvest and transfer additional light energy to the FAD chromophore from the near UV region (370–390 nm).[10] The N-terminal chromophore binding domain is highly conserved among all classes of CRYs and PLs, whereas the C-terminal domains (CCTs), which are the effector domains and important for CRY signaling, are of variable length and poorly conserved, even among CRYs of the same species. In animals, CRYs are divided into two subtypes based on their responsiveness to light: Type I CRYs act as circadian photoreceptors (as in Drosophila), whereas Type II CRYs exert their function without responding to light (as in mouse, human, and other vertebrates). Some vertebrates, such as zebrafish have both types of CRYs.[12] In *Arabidopsis thaliana,* three CRYs have been identified, which are also the best characterized ones to date: CRY1, CRY2 and CRY3. CRY1 and CRY2 exhibit no DNA repair activity but instead, upon blue light

absorption, directly or indirectly regulate transcription by interacting with other proteins, such as the basic helix-loop-helix transcription factor calcium and integrin-binding protein 1 (CIB1) and COP1 to control various processes, such as plant growth or flowering. CRY2 undergoes blue-light-dependent ubiquitination and degradation in the nucleus and functions preferentially under low light conditions.[10] In contrast, CRY3 localizes to mitochondria and chloroplasts to repair UV-induced lesions in single-stranded DNA and in loop structures of double-stranded DNA.[10,14,15] In all CRYs, the PHR domain and the CCT are proposed to form a closed or inactive conformation in the dark, while blue light absorption by the PHR domain triggers a conformational change in the CCT to produce an open or active conformation that initiates signaling.[10] Upon photoexcitation, it is generally agreed that a series of biophysical and biochemical changes mediated by FAD lead to structural rearrangement, protein modification (phosphorylation) and interaction with signaling proteins including (e.g. CIB1 and COP1) (Figure 1.3 C).[16] However, the mechanism by which the FAD to $FADH^{\bullet}$ transition within the PHR domain is propagated to induce the proposed conformational change within the CCT is still not fully understood.[10] Based on the different absorption spectra it is argued that the oxidized from of FAD, which strongly absorbs blue light ($\lambda_{max} \approx 450$ nm), is most likely present in the dark and inactive state of the photoreceptor. Irradiation of the PHR domain results in a sequential electron transfer from three tryptophan residues to reduce FAD to $FADH^{\bullet}$.[17] However, while extensive structural, spectroscopic, biochemical, and computational studies have been brought to bear on the associated light-sensing mechanisms, many of the resolved features and their implications remain controversial.

1.1.3.2 LOV

LOV domains were first identified in the plant photoreceptor phototropin, but LOV domains have since been discovered in several plant, fungi, archaea and bacterial proteins, such as the fungal light-adaptation protein Vivid, and YtvA, a LOV protein from *B. subtilis* involved in stress responses.[3,11] LOV domains are a subset of the PER-ARNT-SIM (PAS) domain superfamily that uses a non-covalently bound flavin cofactor, flavin mononucleotide (FMN) or FAD that absorbs UVA and blue light.[11,18] Upon light absorption, a covalent bond between the cofactor and a conserved cysteine residue is formed.[11] This leads to conformational changes which, in plant phototropins, induce the C-terminal α-helix (Jα) to undock from the LOV core and unfold, consequently inducing downstream effector functions (Figure 1.3 B). In other LOV proteins, activation can induce dimerization or rotation of LOV domain subunits (Figure 1.3 A).[19] The induced signaling mechanisms depend on various factors such as the oligomeric state, the flanking helical content, and the character of the effector domain.[11] Usually, the photoreaction is fully reversible and the signaling state thermally reverts to the ground, dark state. However, despite similar sequence and structure, individual LOV domains differ distinctly in the kinetics and quantum yield of their photocycle. The basis for these differences may be linked to protein flexibility or to solvent accessibility, or the specific environment of the flavin chromophore in the protein core, where mutations can strongly affect photocycle kinetics.[3] Although the photochemistry of the LOV flavin is relatively well defined, some key issues remain unresolved. These include the identity of intermediates preceding adduct formation, proton transfer during the reaction, and in particular, factors influencing the highly

variable dark-state recovery rates, where timescales vary between seconds to hours.[11,18]

1.1.3.3 BLUF

BLUF domains are a family of photosensor domains that use FAD to detect blue light. They predominantly occur in prokaryotes and they were first identified and are most extensively studied in activation of photopigment and *puc* expression A (AppA) from *Rhodobacter sphaeroides,* where they regulate photosynthetic gene expression. BLUF domains are also found in eukaryotes, such as euglenozoa and fungi.[3] They exist either as isolated domains or covalently linked to effector domains, which are mostly involved in cyclic nucleotide metabolism.[3,20] BLUF domains are oligomeric and have a ferredoxin-like module with two helices aligned in parallel to a five-stranded mixed parallel/antiparallel β-sheet.[11] The FAD chromophore is embedded in a cleft between two α helices.[3,11] In contrast to LOV domains, the FAD cofactor of BLUF domains undergoes minimal conformational changes upon blue light absorption, and the signaling state is rapidly formed on the sub-nanosecond timescale. Light absorption at the ground state leads to an electron transfer from a conserved tyrosine residue to the flavin ring and gives rise to a short-lived radical pair. The side chain of a nearby, conserved glutamine residue is assumed to rotate, which is followed by a back transfer of an electron to the tyrosine to form the signaling state.[3] Upon conversion from the dark, inactive to the light-adapted, active state, the flavin absorption spectra of BLUF domains undergo a ~10 nm redshift which can persist from seconds up to minutes. This red-shifted spectrum results from the modulation of hydrogen bonds among the flavin and a tyrosine-glutamine-methionine-tryptophan tetrad.[11] It is known that in both the inactive and the signaling states, FAD maintains its fully oxidized state, but further details of the BLUF photocycle are still under debate.[3]

1.1.4 Xanthopsin

The xanthopsin photoreceptor class is represented by the photoactive yellow protein (PYP), which is a small, water-soluble, cytoplasmic photoreceptor of 126 amino acids that, upon absorption of blue light, undergoes a fully reversible photocycle that contains several intermediates.[3,21] PYP was first found in the extremely halophilic purple photosynthetic bacterium *Halorhodospira halophile*.[21,22] Although the protein has only been isolated from few sources, genomic and metagenomic analyses have identified more than 140 PYP genes that occur in a wide variety of bacteria and different metabolic niches.[21] In *Halorhodospira halophile*, PYP has been proposed to be involved in negative phototaxis triggered by blue light, while in *Rhodobacter* it is thought to be involved in the regulation of cell buoyancy. PYP serves as the structural paradigm for the PAS domain family of proteins, which is a key element in biological signal transfer also shared by LOV domains.[3] PYP uses a p-4-hydroxycinnamic acid (p-coumaric acid) as chromophore, which undergoes a trans-to-cis isomerization upon blue light illumination. In the dark state, the chromophore is stabilized by a thioester bond to a cysteine residue and by abnormally short hydrogen bonds to nearby glutamic acid and tyrosine side chains.[3] The blue-light-induced trans-to-cis isomerization of the p-coumaric acid is followed by several structurally distinct intermediates. The complete isomerization occurs within a few nanoseconds and introduces severe strain into the chromophore and the surrounding protein.[3] The relaxation of this strain initiates a long series of

changes in tertiary structure, such as rupture of a hydrogen bonds, ejection of the chromophore toward the solvent, partial unfolding of the Cα helix, and, ultimately, unfolding of N-terminal α helices packed on the distal side of the β sheet, which forms the structural core of all PAS and LOV domains including PYP.[3] By means of time-resolved crystallographic studies, high-resolution structures of PYP photocycle intermediates were obtained covering time scales from nano- to femtoseconds.[23,24]

1.1.5 Adenosylcobalamin-binding photoreceptors

Adenosylcobalamin-binding photoreceptors are a new class of photoreceptors that have only been recently characterized. These photoreceptors are members of the LitR/CarH family and sense ultraviolet, blue and green light using the vitamin B12 derivate adenosylcobalamine (AdoCbl) as a chromophore.[6,25] AdoCbl was originally identified as a cofactor for radical-based enzyme reactions, and only recently its biological function could be expanded to light sensing.[26] The LitR/CarH photoreceptors contain a C-terminal cobalamin-binding domain and are involved in light-induced transcriptional regulation.[25] Homologs of LitR/CarH exist widely in non-phototrophic bacteria and the best characterized photoreceptors are from *Myxococcus xanthus* (MxCarH) and *Thermus thermophilus* (TtCarH).[25-28] In these organisms, CarH controls the light-induced expression of carotenoids, which mediate protection against photo-oxidative damage.[26-28] In the dark, CarH-type photoreceptors form dimer-of-dimers type tetramers.[6,26] Each monomer of CarH consists of an N-terminal DNA binding domain and a C-terminal AdoCbl-binding and oligomerization domain that is responsible for light-sensing.[26] The flexible DNA-binding domain displays a canonical recognition helix and β-hairpin wing for DNA binding**.** The light-sensing, AdoCbl-binding domain is composed of a four-helix bundle and a Rossman-fold domain and is structurally rigid. In the tetramer, the four light-sensing domains together form a central core and the DNA-binding domains are displayed on the surface.[26] In the dark, the AdoCbl-bound CarH tetramer binds to the promoter region of target genes, such as the carotenoid synthesis operon, to block transcription.[6,26] Illumination with ultraviolet, blue, or green light causes photolysis of the cofactor, through rupture of the photosensitive Co-C bond in AdoCbl, resulting in rearranging of the four-helix bundle and subsequent tetramer disassembly (Figure 1.3 E). This consequently leads to loss of operator-binding and the activation of gene expression.[26]

1.1.6 Phytochromes

Phytochromes make up the diverse family of red/far-red responsive photoreceptors first discovered in plants, where they are one of the three major regulators of photomorphogenesis[3,29], but they are also found in the microbes such as cyanobacteria, proteobacteria and filamentous fungi.[30,31] In the last two decades a variety of new bacterial and cyanobacterial members of the phytochrome family have been identified, which has greatly facilitated the biochemical and structural characterization of this family.[29] All phytochromes are photoswitchable photosensors that utilize a covalently attached linear tetrapyrrole, a bilin chromophore, to photoconvert between a red-light-absorbing (Pr) biologically inactive state and far-red-light-absorbing (Pfr) biologically active state. Although dark reversion is an intrinsic property of all phytochromes, plant phytochromes have evolved a slower dark reversion. Plant phytochromes, bacteriophytochromes and cyanobacterial

phytochromes share a similar domain architecture and high sequence homology. They are homodimeric complexes that consist of an N-terminal photosensory region with 3 conserved domains, PAS, cGMP-specific phosphodiesterase adenylate cyclase FhlA (GAF) and phytochrome-specific GAF-related domain (PHY), and a C-terminal regulatory histidine kinase or histidine kinase-related domain.[3,29,30] The two N-terminal domains, PAS and GAF, together form a chromophore binding domain.[3] The full photocycle involves absorption of two photons, one to drive the forward transition *(*Pr to Pfr), and the other for the backward transition (Pfr to Pr).[32] All four pyrrole nitrogens in the bilin chromophore are protonated in both the Pr and Pfr states,[3] where the primary photochemical transition involves the isomerization of the bilin chromophore. In the traditional view, this cis-to-trans isomerization occurs around the C15 and C16 double bond between rings C and D in the prosthetic bilin chromophore, consequently leading to a flip of the D ring. However, recent studies suggest that in certain phytochromes isomerization occurs due to the linkage between the A and B rings.[32] The combined structural data on microbial phytochromes support a largely unifying post-isomerization mechanism for photoreceptor action. This mechanism involves the reorientation of the PHY domain relative to the GAF domain by altering the PHY hairpin contact, and motion within the GAF domain, resulting in an effect on the dimerization contact along the entire interface of the phytochrome dimer. Finally, the relative positions of the output modules are rearranged. While variations in the bilin photochemistry have been identified among various phytochrome types, many important key residues and structural motifs of the phytochrome assembly and photochemistry seem to be highly conserved, suggesting that most members of the phytochrome family employ a similar conformational signaling mechanism.[31] In plants, absorption of red light by the Pr form, which results in a transition to the Pfr form, subsequently leads to the recruitment of downstream signaling molecules such as phytochrome interacting factors (PIF) (Figure 1.3 C).[19]

1.1.7 Opsins

In contrast to the other five soluble photoreceptor classes, opsins are membrane proteins.[3,4] They are photoreceptors that serve as the primary light-sensitive proteins in vision and also in the entrainment of circadian rhythms in mammals, but related proteins, in particular rhodopsins, have also been identified as photoreceptors in microorganisms and algae.[3,33] Plant as well as bacterial rhodopsins belong to the large family of seven-helix transmembrane proteins. Light is sensed via a retinal chromophore that is covalently bound to a lysine residue as a protonated Schiff base. In plant and bacterial rhodopsin, the dark-adapted state binds a retinal chromophore in the *all-trans* conformation. Upon blue-light absorption around 470 nm, the retinal isomerizes to the 13-*cis* form, which initiates a cycle of structural changes.[3,4] A well-known example of plant rhodopsins is channelrhodopsin, which mediates phototaxis in flagellate algae, and was first identified in *Chlamydomonas reinhardtii* as light-gated cation channel.[34] Other algal rhodopsins function as light driven H+ pumps similar to bacteriorhodopsin, although their physiological role in photosynthetic organisms remains unclear.[3] Microbial rhodopsins mediating light-driven ion transport fall into two categories: actively transporting ion pumps and ion channels.[4]

In higher species, opsins are the light-sensitive proteins found in photoreceptor cells, but are also present in non-visual tissue. Like in microorganisms and plants, mammalian opsins are seven-transmembrane receptors which use retinal as a chromophore. In contrast to microbial rhodopsin, mammalian opsins preferentially bind 11-cis retinal as a chromophore in the dark instead of *all-trans* retinal. Upon light absorption by the opsin-chromophore complex, retinal isomerizes to the *all-trans* form. Retinal isomerization in turn causes conformational changes in the opsin, which allow coupling to distinct G-proteins and further activation of downstream signalling pathways.[33] Generally, mammalian opsins are divided into visual and non-visual opsins, with distinct functions and G-protein coupling specificity.[33,35]

1.1.7.1 Visual mammalian opsins

Visual opsins are found in the photoreceptor cells of the retina. Cone cells express cone opsins and are responsible for color vision, while rod cells express rhodopsin which regulates twilight vision. Humans have one rhodopsin, and three cone opsins: short-, medium-, and long-wave-sensitive opsin (OPN1SW, OPN1MW and OPN1LW, respectively). Mice, on the other hand, lack the red-light-sensing OPN1LW.[36] Vertebrate rod and cone opsins are bleaching photopigments, which means that the photoproduct of the opsins is unstable and dissociates from its activated chromophore.[35] Upon chromophore activation visual opsins couple to the heterotrimeric G-protein transducin (G_t) which consists of three polypeptide chains: Gα, Gβ and Gγ. The Gα subunit of G_t couples to phosphodiesterase 6 (PDE6), an enzyme that hydrolyses cyclic guanosine monophosphate (cGMP). Decreased levels of cGMP cause the closure of cyclic nucleotide gated channels (CNG channels), which in turn leads to the hyperpolarization of the cell (Figure 1.2).[35,37]

1.1.7.2 Non-visual mammalian opsins

In contrast to visual opsins, the function of non-visual opsins in general is less explored. They are thought to be involved in physiological mechanisms such as circadian rhythm, temperature regulation, pupillary constriction as well as body pigmentation.[35] However, the exact function depends on the opsin and for some, the function is still unclear.

Melanopsin, also called opsin 4 (OPN4), is the most studied and best understood of the non-visual mammalian opsins. Its expression is mainly restricted to a 3rd class of photoreceptor cells next to rods and cones, a small subset of intrinsically photosensitive retinal ganglion cells. Melanopsin was found to be involved in pupillary constriction, the regulation of sleep and circadian photoentrainment.[38] It is maximally sensitive to blue light (Table 1.1).[39] Human melanopsin couples to $G\alpha_q$ and $G\alpha_i$, whereas the coupling to $G\alpha_q$ seems much more efficient than to $G\alpha_i$. $G\alpha_q$ coupling of melanopsin leads to the activation phospholipase C (PLC). PLC in turn, hydrolyzes phosphatidylinositol 4,5-bisphosphate (PIP_2) to diacyl glycerol (DAG) and inositol trisphosphate (IP_3) , which results in an increase of the intracellular calcium concentration and consequently leads to cell depolarization (Figure1.2).[39,40]

Opsin 3 (OPN3) was initially called encephalopsin because it was first found in the brain[41], but was later renamed panopsin as it was found to be expressed in a wide range of tissues including brain, liver, and retina.[42] The function of OPN3 is still

unclear, even though there is some evidence that OPN3 can be linked to asthma susceptibility, pigmentation and pulmonary vasorelaxation.[43-45] The spectral properties of vertebrate (pufferfish) and invertebrate (mosquito) OPN3 homologs were identified, which both have an absorption maximum in the blue to green region (Table 1.1). Both OPN3 variants showed a bistable nature, which means that after cis-retinal isomerization, the pigment can photoisomerize *all-trans* retinal back to cis-retinal upon light stimulation. In the same study, it was found that OPN3 homologs couple to the $G\alpha_i$ signaling cascade, which consequently leads to an inhibition of adenylate cyclase activity and thus a decrease of the intracellular cAMP concentration (Figure 1.2).[46] Mammalian OPN3 could not be characterized to date.

Opsin 5 (OPN5) also known as neuropsin is the most recently identified mammalian opsin.[47] Human and mouse OPN5 exhibit an absorption maximum at 380 nm and they also display a bistable nature (Table 1.1). Upon UV light illumination, OPN5 is converted to a blue-absorbing state, with an absorption maximum of 470 nm, and activates the $G\alpha_i$ signaling cascade (Figure 1.2).[48,49] Recently it could be shown that OPN5 is involved in the mediation of photoentrainment of local circadian oscillators in mammalian retina and cornea.[50]

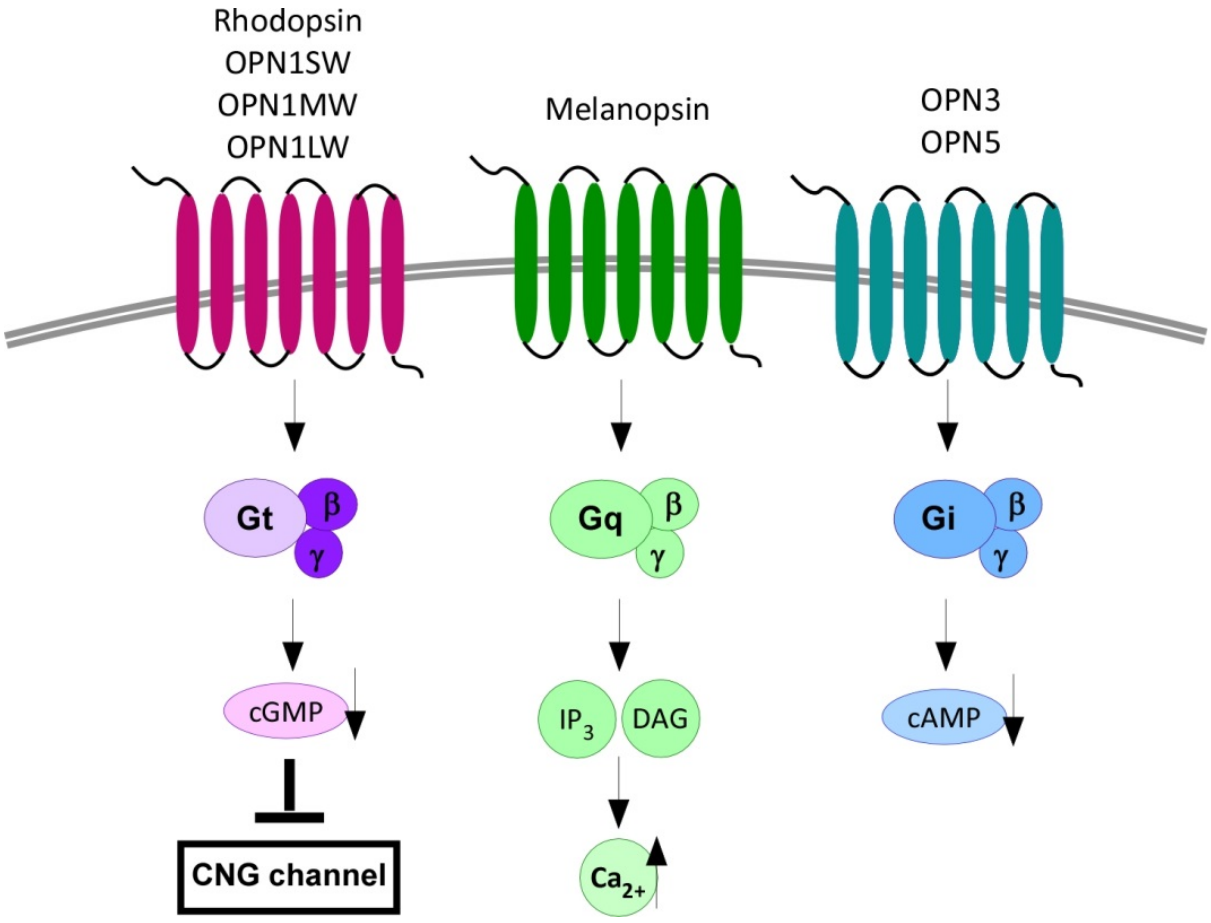

Figure 1.2 Opsin signaling via heterotrimeric G-proteins. Visual and non-visual opsins signal through different G-proteins. Visual opsins couple to the G_t pathway, which leads to a decrease in cGMP and closure of CNG channels. Melanopsin couples to $G\alpha_q$, which raises IP3 and DAG levels resulting in increased intracellular calcium concentration. OPN3 and OPN5 couple to $G\alpha_i$, which decreases cAMP levels.

Table 1.1 Spectral properties and photochemical characteristics of mammalian visual and non-visual opsins. Opsins can be classified into visual and non-visual opsins, with different absorbance maxima as well as different photopigment characteristics for each opsin. Absorbance is also species specific.

Name	Absorbance λ max [nm]	Photopigment Characteristics	References
Visual Opsins			
Rhodopsin	500	Bleaching	Imai et al. 2006[51]
OPN1SW (blue cone opsin)	358 (mouse) 420 (human)	Bleaching	Fasick et al. 2002[52] Deeb et al. 2005 [53]
OPN1MW (green cone opsin)	508 (mouse) 530 (human)	Bleaching	Sun et al. 1997[54] Deeb et al. 2005[53]
OPN1LW (red cone opsin)	560 (human)	Bleaching	Deeb et al. 2005 [53]
Non-visual Opsins			
Melanopsin	500 (mouse) 479 (human)	Bistable	Walker et al. 2008[55] Bailes et al. 2013[39]
OPN3	460/ 470 (pufferfish)	Bistable	Koyanagi et al. 2013 [46]
OPN5	380/470 (mouse and human)	Bistable	Kojima et al. 2011[48]

1.2 Optogenetic tools

Naturally-occurring photoreceptors and their light-sensing domains have been harnessed in recent years in the emerging field of optogenetics.[1,56-59] The development of optogenetics was motivated by the observation that light can be an ideal stimulus to control cell and animal behavior, as it can be applied and withdrawn remotely and therefore permits transient and local activation on very short time and length scales (e.g. milliseconds and micrometers).[1,60] Optogenetics flourished in the hands of neurobiologists that utilized microbial opsins to dissect neural circuits,[1,56] but more recently optogenetic approaches also started to have a big impact on cell biology, by regulating important cellular signaling pathways such as mitogen-activated protein kinases/extracellular signal-regulated kinase (MAPK/Erk) pathway and cell behaviors (e.g. cell fate) by light.[61] General advantages of optogenetics over pharmacology and genetics include the ease with which light can be applied and withdrawn and the possibility of transient and local light activation.[60]

However, a persisting challenge in cell signaling optogenetics is to couple photoreceptors or their domains to protein targets, resulting in functional chimeras. Success in tackling this challenge depends on two factors, first a profound understanding of the biochemical, biophysical and structural photoreceptor properties, and second the expansion of the photoreceptor repertoire.[62] By now there is a relatively broad spectrum of optogenetic tools available that use different photoreceptors or photoreceptor domains as a light sensing module to induce various cell behavioral outputs. In particular, CRY, LOV domains and phytochromes are frequently used as light sensing modules.[19] For example, the LOV2 domain from *Avena sativa* phototropin 1 was used to control actin-based contractility and directional cell movement in mammalian cells. In this setup, the LOV2 domain was fused to the N-terminus of the GTPase ras-related C3 botulinum toxin substrate 1 (Rac1), thereby sterically blocking the binding of Rac1 effectors. Upon blue light illumination the unfolding of Jα releases (Figure 1.3 B) the inhibition and induce Rac1-dependent actin assembly.[63] A second LOV domain based approach mimicked growth factor based mitogenic and morphogenic cell behavior by light-activated receptor tyrosine kinases (RTKs). This was achieved by fusing LOV domains from the *Vaucheria frigida* aureochrome photoreceptor to the C-terminus of RTKs, which led to blue-light-dependent receptor dimerization and activation (Figure 1.3 A).[64] Recently also a green-light-based RTK inactivation system was engineered by using the CarH domain.[65] An example for CRY based systems are tools where light-inducible heterodimeric interaction of CRY2 and CIB1 (Figure 1.3 C) from *Arabidopsis thaliana* was used to induce protein translocation, transcription, and Cre-mediated DNA recombination by light,[66] as well as a CRY2 based approach that allows light-induced, rapid, robust, and reversible protein oligomerization (Figure 1.3 D).[67] While blue-light-activated LOV domain- and CRY2-based systems return to their inactive state only by slow spontaneous decay in the dark, a major advantage of phytochrome-based red/far-red light-responsive systems is the possibility to actively switch between two states by illumination with either red or far-red light. Moreover, red light exhibits a much deeper tissue penetration compared to blue light, which is advantageous for *in vivo* applications. The natural chromophore of phytochromes, phytochromobilin, is not available in orthologous systems, but a

related tetrapyrrole, phycocyanobilin, is commercially available or can be easily extracted from the cyanobacterium *Spirulina,* and can be added to the culture media to substitute for the natural chromophore.[19] For example, a heterodimeric phytochrome system was used for regulating gene expression in mammalian cells (Figure 1.3 C). This was achieved by splitting a transcription factor consisting of the tetracycline repressor TetR fused to PIF6 and a nuclear-targeted phytochorme B fused to the VP16 transactivation domain. Red light illumination induced reversible reconstitution of the transcription factor, triggering reporter expression from a response construct that contained a TetR-specific operator upstream of a minimal promoter.[68]

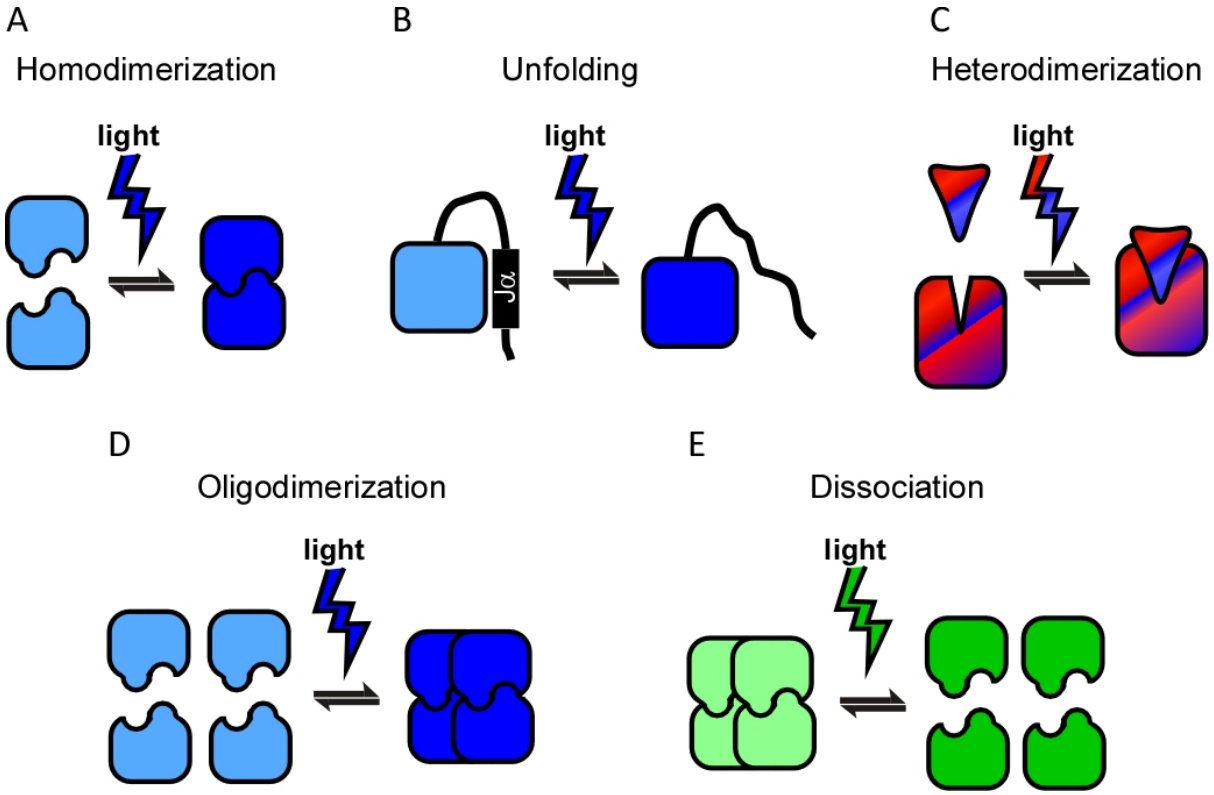

Figure 1.3 Light-induced structural changes of different photoreceptors. (A) Blue-light-induced homodimerization occurs for example in LOV domains, which were used for light-induced RTK activation. (B) Blue light illumination of some LOV domains leads to the unfolding of the C-terminal Jα helix. This mechanism can be used by fusing proteins to the Jα helix and thereby sterically inhibiting them in the dark and releasing them during illumination. (C) Light-induced heterodimerization of light-sensing domains with for example different transcription factors such as CIB or PIF occurs in blue-light-absorbing CRYs as well as in red-light-absorbing phytochrome domains. This mechanism was also already used in several optogenetic tools. (D) Blue-light-induced oligomerization occurs in blue-light-sensing CRY domains. (E) Green light-induced dissociation of CarH-type photoreceptors was already used for light-controlled inactivation of RTKs.

1.3 β-cells

1.3.1 Pancreas

The pancreas is an organ, which is essential for keeping the nutritional household in balance and it is critically involved in the regulation of glucose homeostasis.[69] The architecture of the rodent pancreas is often less defined in shape compared to the human pancreas, where designated regions are termed head, neck, body and tail. Also birds, reptiles and amphibians have a pancreas with a similar histological anatomy and developmental program as mammals.[70] The pancreas comprises two distinct tissue types, the exocrine tissue and the endocrine tissue. These two tissues have entirely different functions as well as distinct morphologies.[71] The exocrine cells secrete enzymes into the digestive tract, while the endocrine cells secrete hormones into the bloodstream to tightly regulate the circulating glucose levels.[70] The endocrine tissue represents ~2% of the pancreas and it is made up of cell clusters of endocrine cells called the "islets of Langerhans".[69] Each islet in turn is composed of five different types of cells, namely, insulin-producing β-cells, glucagon-releasing α-cells, somatostatin-producing δ-cells, pancreatic polypeptide-containing PP cells, and ghrelin-containing ε-cells. Together these cells are involved in the tight regulation of circulating glucose levels.[69] The exocrine portion is composed of ductal cells and acinar cells.[71] These form a branched, acinar gland with its secretory cells grouped into acini. They are secreting up to 22 different inactive precursor enzymes, including proteases, amylases, lipases and nucleases, which become active after they enter the duodenum.[70] Each of these disparate pancreatic cell types derive from the same endodermal origin of the upper duodenal region of the foregut, which later gives rise to the digestive system. The development of the pancreas starts with a dorsal and ventral protrusion of a region of the primitive gut epithelium, which later converges to form the pancreas.[70,72] Endocrine cells are the first to develop and differentiate, whereas exocrine and ductal cells develop from the same progenitors, but at a later stage. Another interesting aspect of the endocrine cell development is the remarkable similarity to neuronal cells regarding their expression of hormones and enzymes during their differentiation.[72]

1.3.1.1 Islets of Langerhans

Islets of Langerhans are highly vascularized micro-organs located in the pancreas. As described in the previous section, islets consist of a diverse cluster of endocrine cells that function together to control glucose homeostasis.[73] The size of rodent and human islets can vary, from a few cells up to thousands of cells and a diameter of ~50 µm up to ~500 µm.[73,74] In rodent islets, there is a clear segregation of cell types to different islets regions. β-cells are clustered in the central islet core and smaller numbers of α-cells, δ-cells, PP cells and ε-cells are located in the periphery surrounding the β-cells (Figure 1.4 A). In contrast, human islets have a more random organization of endocrine cells (Figure 1.4 B).[73,75] Another pancreatic islet property that displays species variability is the proportion of the different cell types. Murine islets are composed out of 70–80% β-cells and of a smaller portion of α-cells (~15%), δ-cells (less than 10%) and PP cells (less than 1%), whereas human islets contain only around 50% β-cells but much larger portions of α-cells (~40%) as well as δ-cells (~ 10%) and PP cells (less than 5%).[73,75]

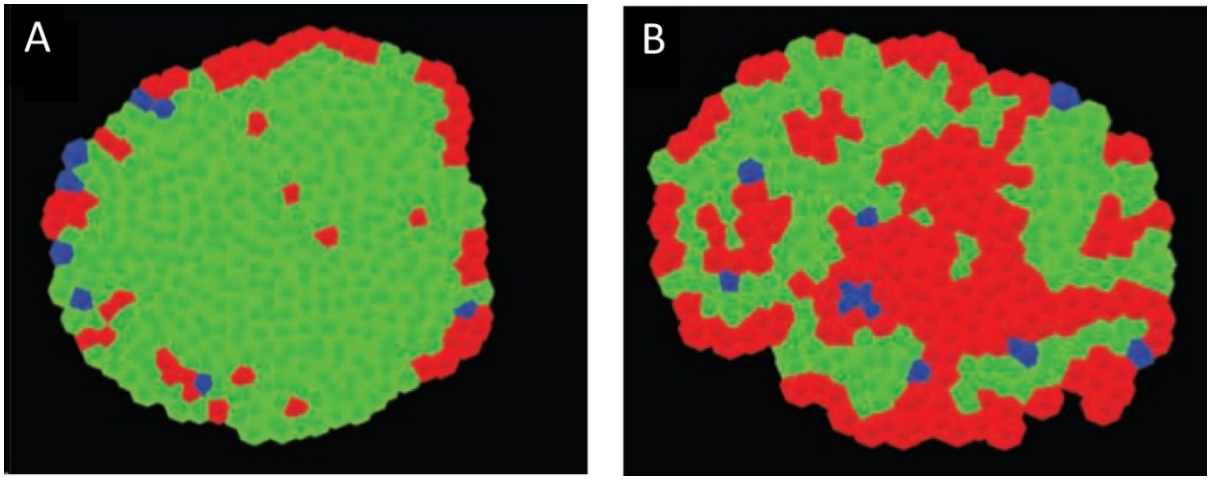

Figure 1.4 Comparison of architectural organization of (A) rodent and (B) human islets. Spatial distribution of β-cells (green), α-cells (red), and δ-cells (blue) are illustrated based on immunohistochemical images. (Modified image from Steiner et al. 2010)[73,75]

1.3.1.2 Maintenance of glucose homeostasis

Glucose is an important source of energy for many organs and tissues in the body. Especially the brain derives its metabolic energy almost exclusively from glucose. Glucose is also an important regulatory signal that controls the secretion of hormones by various endocrine cells.[76] The endocrine pancreas is the key actor in blood glucose homeostasis. β-cells in particular play a major role in the regulation of blood glucose levels, by functioning as glucose sensors as well as glucose-dependent insulin releasers.[77] Insulin is a 51 amino acids long protein polypeptide, composed of an A and a B chain, which are linked by disulfide bonds. Insulin is synthesized as proinsulin by ribosomes of the rough endoplasmic reticulum (RER). Secretory vesicles transport the proinsulin from the RER to the Golgi apparatus, where proinsulin forms hexamers. Enzymes acting outside of the Golgi finally convert proinsulin to insulin and C-peptide, which are secreted into the circulation by exocytosis.[78] The first step of glucose metabolism (Figure 1.5) is the uptake of glucose through the β-cell membrane by the low affinity glucose transporter-2 (GLUT-2).[77] After glucose has entered the β-cell, it is further processed by glucokinase (GK). GK belongs to the family of hexokinases and catalyzes the phosphorylation of glucose to glucose-6-phosphate (G6P), thus trapping glucose inside the cell. G6P is then further processed by glycolysis and finally enters the citric acid cycle, which consequently leads to an increase in adenosine triphosphate (ATP) to adenosine diphosphate (ADP) ratio, and the initiation of the first phase of insulin secretion. This first triggering phase (Figure 1.5) starts with the ATP-dependent closure of the K_{ATP} channel, which leads to the depolarization of the cell membrane, resulting in opening of voltage-dependent Ca^{2+} channels (VDCC) in the cell membrane, causing an influx of Ca^{2+}. The subsequent increase in intracellular Ca^{2+} concentration $[Ca^{2+}]_i$ triggers the exocytosis of insulin vesicles.[77,78] The sustained augmentation phase of insulin secretion is independent of K_{ATP} channels. While the triggering phase can be induced by any stimulus that results in increased $[Ca^{2+}]_i$, the sustained phase relies on other secretagogues and thus requires the metabolism of glucose. In the β-cell, different pools of insulin vesicles are present. These pools include the intracellular reserve pool (~90%), the morphologically docked vesicles (~10%) and the readily releasable pool (RRP; ~0.3-2.2%). In the

first triggering phase, the vesicles from the RRP and the docked pool are secreted. In contrast, the sustained augmentation phase of insulin secretion is dependent on vesicle mobilization and priming from the reserve pool.[77] The mechanisms underlying this phase are not well known. Current hypotheses include various factors playing a significant role in the sustained phase of glucose mediated insulin secretion, such as cytosolic long-chain acyl-CoA, the pyruvate-malate shuttle, glutamate export from mitochondria, and an increased ATP to ADP ratio as well as hormones, such as vasoactive intestinal peptide, glucagon-like peptide 1 (GLP-1), and glucose-dependent insulinotropic polypeptide (GIP).[78,79] The finally secreted insulin has various major effects on muscle and adipose tissue, the lipid metabolism as well as the protein metabolism. For example, insulin increases glucose uptake and glycolysis in muscle and adipose tissue, decreases the rate of lipolysis in adipose tissue and increases the rate of protein synthesis in muscle, adipose tissue and liver.[80]

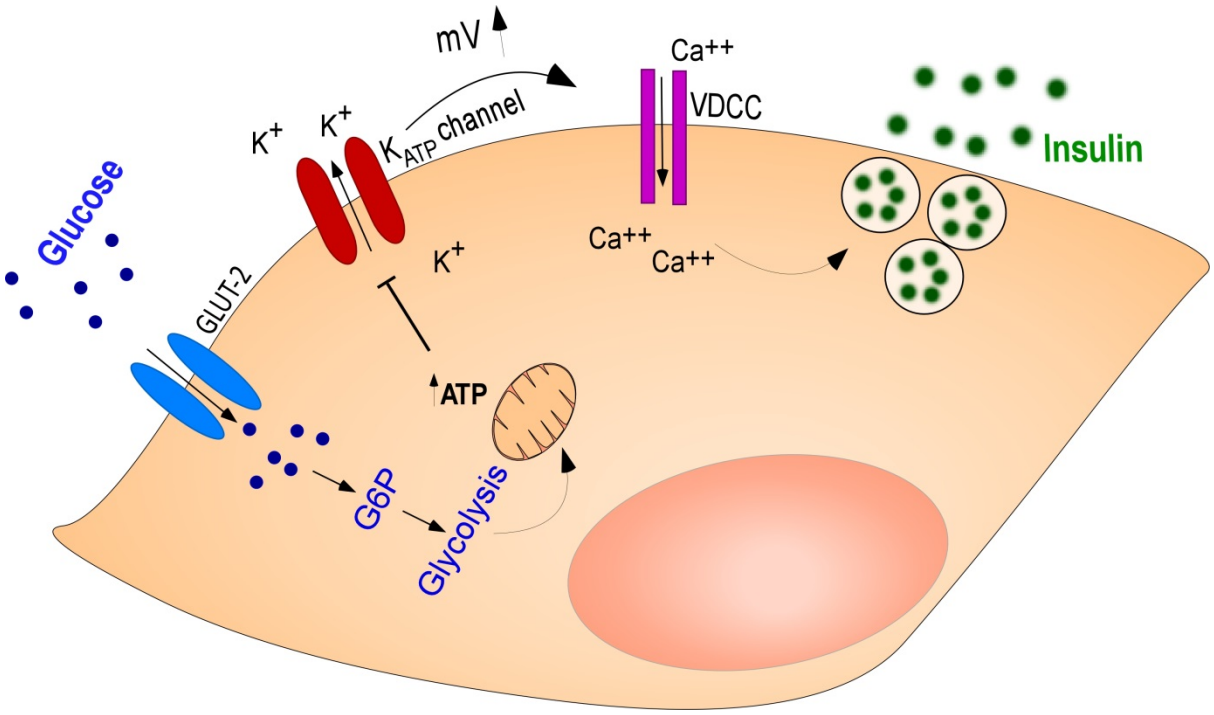

Figure 1.5 Glucose metabolism in pancreatic β-cells and the first phase of glucose-dependent insulin secretion. Glucose is entering the cell through GLUT-2, where it is further processed, which consequently leads to an increase in ATP resulting in closure of K_{ATP} channels. This leads to the depolarization of the cell membrane, resulting in opening of VDCC and subsequent increase in $[Ca^{2+}]_i$ triggering the secretion of insulin.

1.3.2 Diabetes

Diabetes, often termed diabetes mellitus, is a diseases with one of the highest and fastest increasing morbidities worldwide.[81] An estimated 422 million adults worldwide were suffering from diabetes in 2014, compared to 108 million in 1980. The global prevalence of diabetes was tremendously raised, and resulted in 1.5 million deaths in 2012, thus placing an enormous burden on today's healthcare system.[82] Therefore, it has become a priority in the field of medical research to find ways to treat and cure diabetes. There are various clinical forms of diabetes referred to as Type 1 (T1D), Type 2 (T2D), gestational diabetes (GD) and so-called maturity onset

diabetes of the young (MODY). The most common forms are T1D and T2D, whereas GD, occurring in 2-5% of pregnant women, and MODY, which is caused by mutations in transcription factors essential for β-cell development, are rare forms of diabetes.[69] However, β-cells are the focal point of disease development and progression of all forms of diabetes. A deficiency in functional pancreatic β-cells results in inadequate insulin supply and, consequently hyperglycemia, which in turn is connected to secondary disorders such as retinopathy[83] and neuropathy.[69,84]

1.3.2.1 Type 1 Diabetes

T1D is an autoimmune disease characterized by an absolute deficiency of insulin resulting from specific destruction of insulin producing β-cells.[69,85] T1D is prevalently diagnosed in children and adolescents, thus also termed juvenile-onset diabetes.[86] The onset of T1D is triggered by a combination of various factors, of which just a small portion is identified to date.[87] One factor increasing the susceptibility to T1D is the inheritance through a series of genes. Variations in the human leukocyte antigen class II-locus on chromosome 6 accounts for approximately 50% of the genetic risk that leads to T1D. Other loci, such as insulin, protein tyrosine phosphatase, non-receptor type 22, cytotoxic T-lymphocyte-associated protein 4, and interleukin-2 receptor alpha chain, exhibit a smaller contribution.[87,88] Most of the loci associated with T1D susceptibility are connected to immune responses, supporting the concept that genetic factors are involved in mechanisms that lead to abnormal immune responses.[88] Genetic components are essential, but insufficient in explaining the immune pathogenesis of T1D, because the majority of people with mutations in these susceptibility genes never develop the disease.[87] The second factor that plays a major role in the development of T1D is the exposure to different environmental factors, which, in combination with genetic susceptibility, trigger the onset of the disease. However, despite extensive research, the number of evaluated potential environmental influences is quite small. Investigated and correlated factors are, for example, a relative lack of vitamin D as well as viral infections.[86,87] The final autoimmune response results from a failure of the immune system to distinguish between self and non-self-antigens, which leads to the loss of self-tolerance.[69] T1D can be divided into two distinct stages, insulitis and diabetes. Insulitis is characterized by the infiltration of pancreatic islets by a heterogeneous population of leukocytes, where β-cell destruction is mostly mediated by CD4+ T helper and CD8+ T cells.[85] In addition to T cells, antigen presenting cells (APCs), like macrophages and dendritic cells are also required for the autoimmune response. All these various immune cells that infiltrate the pancreatic islets release different inflammatory mediators, including cytokines and free oxygen radicals that further contribute to β-cell destruction.[69,89] Two different mechanisms for the initiation of β-cell death and inflammatory response have been reported. In the recognition based model (cell-cell contact), CD8+ T cells are directly activated by recognizing β-cell antigens, including peptides derived from insulin or glutamic acid decarboxylase, presented by major histocompatibility complex (MHC) I molecules. In the recognition-independent (cytokine activation) mechanism, β-cell antigens are taken up by local APCs, probably mature dendritic cells, in pancreatic islets and transported to the pancreatic lymph nodes where the antigens are processed and presented by MHC II, and in turn activate CD4+ T helper cells. These activated CD4+ T helper cells return to the pancreatic islets and re-encounter cognate antigens to initiate an inflammatory response, subsequently resulting in the local production of highly concentrated

proinflammatory cytokines.[69,85] β-cells are finally destroyed by apoptosis induced through Fas receptor/Fas ligand and tumor necrosis factor receptor/ligand interactions, as well as by granzymes and perforin released from cytotoxic effector T cells. Thus, activated APCs and T cells, as well as cytokines secreted from these leukocytes, synergistically destroy β-cells in pancreatic islets.[69,89] Continuous insulitis finally results in the development of full-blown autoimmune mediated T1D, due to the significant loss in insulin secreting β-cells. Prior to the first clinical symptoms of T1D, β-cell mass of pancreatic islets has already been reduced by ~70%.[88] At this stage of the disease, exogenous insulin supply becomes imperative.

1.3.2.2 Type 2 Diabetes

In contrasts to T1D, T2D is mainly diagnosed in adults and its prevalence increases with age, which is why it was formerly also called adult-onset diabetes. Recent data, though, indicate that symptoms that characterize T2D are progressively being recognized in adolescents.[69,82] T2D is the most common form of diabetes accounting for 85–95% of all diabetes cases and it is characterized by β-cell failure due to insulin resistance in the canonical insulin sensitive tissues including adipose tissue, skeletal muscle and liver.[69,82,90,91] Symptoms are similar to those of T1D, but often less distinct. Thus the disease often remains undiagnosed for several years, until complications have already arisen.[82] The process of T2D development can be separated in three major stages: susceptibility, β-cell adaptation and β-cell failure.[91] The susceptibility of individuals to develop T2D originates due to the interplay of genetic predispositions and environmental and metabolic factors.[82,91] In general, the risk of developing T2D is influenced by factors such as ethnicity, family history of diabetes, and previous GD combined with increased age, overweight, unhealthy diet, lack of physical activity and smoking.[82] Despite many factors contributing to the development of T2D the major risks factor remain obesity and insufficient physical activity. A big portion of the obese population develops insulin resistance over the years, which subsequently leads to an increased insulin demand to maintain glucose homeostasis. After the susceptibility stage, the β-cell adaptation stage follows. In this stage, β-cells try to compensate the elevated insulin demand by expansion of β-cell mass and an increase in insulin secretion.[69,91] Ultimately, glucose homeostasis in these individuals can only be preserved at the expense of increased insulin levels by expanded insulin secretion and β-cell mass. The chronic exposure of β-cells to hyperglycemia (glycotoxicity) and elevated free fatty acids and lipid intermediates (lipotoxicity) triggered by obesity finally leads to β-cell failure. This stage is characterized by progressive loss of β-cell mass and function as well as possible dedifferentiation of β-cells, induced by a persistently harmful environment, eventually leading to the development of T2D.[91] Although the biological and physiological mechanisms during the adaptation to obesity and insulin resistance are not entirely clear, several studies established the concept that the nutrient-regulated mechanistic target of rapamycin/ribosomal protein S6 kinase beta-1 signaling pathway negatively regulates insulin signaling by acting on insulin receptor substrate proteins and could therefore contribute to and partly explain some of the abnormalities that ultimately result in β-cell failure and the development of T2D in conditions of nutrient overload.[91,92]

1.3.2.3 Treatment options for diabetes

The main treatment for T1D is currently the administration of exogenous insulin. This treatment mostly protects patients from nephropathy and retinopathy, but unfortunately it is not efficient in preventing the recurrence of hypoglycemic events, seizures, and coma. To date, one of the therapeutic approaches that have been reported to have the potential to cure T1D is pancreas transplantation.[69] Pancreas transplantations in diabetic patients are divided into three categories (i) those performed simultaneously with kidney transplantation (75%), (ii) those transplanted after a previous kidney transplantation (18%), and (iii) pancreas transplantation alone (7%). The total number of pancreas transplantations steadily increased until 2004, but although graft function improved significantly over the years since 2004, the number of transplantation has declined. Pancreas transplantation is mainly performed in patients suffering from a terminal stage of diabetes, including nephropathy and, making dialysis a necessity.[93] Although whole pancreas transplantation can prolong and improve the quality of life of patients suffering from terminal diabetes, is the procedure controversial due to the need of major surgery and long-term immunosuppression. Thus, pancreatic islet transplantation is considered a less invasive and, consequently, safer alternative to both major surgery and lifelong insulin injections.[69] The introduction of the Edmonton Protocol in 2000 led to an enormous improvement in the procedure of islets transplantation. James Shapiro and colleagues demonstrated that all seven treated subjects were insulin independent for at least one year following pancreatic islet transplantation using the Edmonton Protocol, which includes the use a special sirolimus-based and steroid-free immunosuppressive cocktail.[94] Between 2000 and 2005 more than 470 patients with T1D have received islet transplants following the Edmonton Protocol, at 43 institutions worldwide.[95] Only a small portion of recipients became insulin independent after one transplant, while the majority needed two to three transplants in order to become fully insulin independent.[96] On average, repeated infusions of islets obtained from two to four donors are needed until normoglycemia is achieved. In order to establish islet transplantation as a widely accepted treatment, it is essential that the donor to recipient ratio is brought down to 1:1.[97] Another major concern about this procedure is the loss of insulin independence within five years after the procedure in the majority of the patients, as well as the risks of immunosuppressant side effects.[95] The success of this approach is dependent on finding new ways to improve long-term islets functionality, the development of better and safer immunosuppressants, and the discovery of new approaches to overcome the non-proliferative status of β-cells *ex vivo,* in order to expand islets *ex vivo* prior to transplantation.[95,98] In addition to research focusing on improving islets transplantation, such as finding new methods and sites of transplantation in the body,[99,100] substantial research has been done to tackle T1D in different ways. These approaches include, for example, viral targeting of islet cells to express growth factors and growth factor receptors in order to increase islet survival and proliferation.[101-103]

In contrast to T1D, for T2D very effective approaches are available to prevent the disease and to prevent complications and premature death that can result from all types of diabetes. These strategies include regular physical activity, wholesome food, avoiding overweigth, avoiding smoking, and the control of blood pressure and lipids.[82] In addition to preventive actions, several drugs are on the market for T2D

that help to maintain glucose homeostasis. There are different classes of drugs available, some of them have been widely availabe for more than a decade, such as sulphonylureas, biguanides and thiazolidinediones.[104]

Sulphonylureas act directly by triggering insulin release from the pancreatic β-cell. They occupy a specific site (SUR site) on the K_{ATP} channel, which leads to blockage of the channel, membrane depolarization and subsequent opening of calcium channels. This further results in exocytosis of insulin. Glibenclamide, gliclazide, glipizide and glimepiride are the primary sulphonylureas in current clinical use for T2D. Unfortunaetly, sulphonylureas show a progressive reduction in their effectivity during long-term use. This decline in effect is the result of a decrease in the insulin-producing capacity of pancreatic β-cell. Another adverse effect of sulphonylureas is the occurance of hypoglycaemic events. Sulphonylureas can be combined with a basal insulin injection to provide enhanced endogenous insulin secretion after meals. In addition to sulphonylureas, there are now many other choices for initial therapy of T2D, such as metformin and thiazolidinediones that affect insulin sensitivity by independent mechanisms.[105]

Metformin is the most well-known representative of the biguanide family and is the drug that is most commonly administered as a first instance drug in T2D patients. In contrast to sulphonylureas, metformin does not directly act on insulin secretion. Mechanistically, metformin inhibits the mitochondrial complex I, thus reducing ATP and increasing AMP levels. Elevated AMP concentrations in the cell inhibit adenylyl cyclase activity, especially in response to glucagon binding to its receptors, which in turn downregulates the effects of glucagon.[106,107]

Thiazolidinediones, such as rosiglitazone and pioglitazone are peroxisome proliferator-activated receptors γ (PPARγ) agonists and have been widely used to treat T2D for almost 20 years. PPARγ was the first gene identified to be related to T2D. PPARγ is a member of the nuclear hormone receptor superfamily and is expressed in adipose tissues and in low levels also in the liver and muscle.[108,109] Thiazolidinediones are classical insulin sensitizers and act to restore blood glucose to normal levels by increasing the insulin sensitivity of target tissues without the risk of causing hypoglycemia, thereby potentially rescuing the pancreatic islets from the burden of synthesizing and secreting more insulin and the consequent functional depletion.[108] Mechanistically, thiazolidinediones regulate the expression of a panel of PPARγ downstream target genes associated with glucose and lipid metabolism, adipokine secretion, and inflammatory reactions in target tissues.[109] Despite those major advantages of thiazolidinediones, rosiglitazone was removed from the market after 6 years because of successive detection of adverse events, such as increased cardiovascular risk, fluid retention, bone fractures, hepatotoxicity and body weight gain.[110] Pioglitazone is still on the market but is marked for potentially increased risk for cardiovascular complications and bladder cancer. Thus, the clinical use of first-generation full PPARγ agonists has been greatly restricted.[108]

Incretin-related products are another approved treatment of hyperglycemia in T2D. They are designed to mimic or strengthen the action of GLP-1.[104] GLP-1 acts through binding and activating the human GLP-1 receptor on both β- and α-cells to enhance glucose-dependent insulin and suppress glucagon secretion, respectively. It also slows gastric emptying, reduces food intake, increases β-cell mass, maintains β-cell function and improves insulin sensitivity.[111] Incretin-based drugs act either on

the GLP-1 receptor directly, or the enzyme responsible for the degradation of GLP-1, dipeptidyl peptidase-4 (DPP-4.) DDP-4 inhibitors protect GLP-1 from rapid degradation resulting in potent and efficient glucose control and moreover they show protective actions against diabetic complications.[112]

There is progressive research in various directions, for both T1D and T2D, to improve or to find new treatment options for T1D and T2D, including some less conventional methods. Some of these approaches employ optogenetic methods to overcome certain drawbacks of conventional methods. These approaches include light-controlled insulin secretion through the usage of channelrhodopsin[113,114], light activated transgene (incretin) expression[115] as well as light switchable incretin mimetics.[116]

1.3.2.4 Growth factors and their cognate receptors as treatment options for diabetes

Growth factors and their cognate receptors, growth factor receptors (GFRs), many of which are members of the RTK protein family, play a central role in the normal physiology as well as in the development and progression of various diseases.[117] RTKs are single-pass transmembrane proteins with an extracellular ligand-binding domain and an intracellular kinase domain. The human genome encodes more than 50 RTKs that are grouped into 20 different families according to structural and sequence similarity.[117] For many RTKs, binding of a polypeptide ligand to the extracellular domain leads to receptor dimerization and subsequent autophosphorylation of intracellular tyrosine residues, which act as docking sites for adaptor proteins and 'hubs' to downstream signaling mediators. In this way, RTKs link extracellular stimuli to major intracellular signaling cascades such as the MAPK/Erk and the phosphatidylinositol-3 kinase/Akt (PI3K/Akt) pathway. Through these pathways RTKs control cell proliferation, survival, migration and invasive capacity.[118] Numerous studies performed in cell and animal models have unequivocally demonstrated the contribution of growth factors, their cognate receptors and various associated signaling pathways (e.g. MAPK/Erk, PI3K/Akt) in the regulation of β-cell growth, survival, function and differentiation.[119-122] Growth factors, such as hepatocyte growth factor (HGF), β-cellulin, fibroblast growth factor 21, and glial cell line-derived neurotrophic factor, are efficacious in different models of diabetes and candidates for β-cell regeneration.[119,120,123-126] As each of these factors is secreted, and can exogenously implement its action through their cognate receptors, they have the potential to be administered for treatment. Unfortunately there are some major drawbacks to this method. One is the non-specific effect of growth factors on other organs where receptors are present.[120] Another one is the short half-life of exogenous growth factors in the blood circulation.[119,127] However, the major disadvantage, of growth factors as therapeutic agents for diabetes is their frequent characterization as oncogene and their tumorigenic properties as a consequence of prolonged activation.[119,128] For instance, HGF regulates intercellular mechanisms essential for beneficial effects in β-cells, but ubiquitously elevated HGF levels display tumorigenicity in a broad array of tissues in mouse models, suggesting that prolonged high levels of HGF, although therapeutically important, may have adverse consequences. In conclusion, temporary, local expression of growth factors or their receptors in β-cells may be a preferable therapeutic option.[119]

CHAPTER 2: AIM

The potential of optogenetic techniques as therapeutic options is currently limited by various factors. First, the wavelengths used to activate the most common optogenetic tools make non-invasive light delivery to target tissues difficult. At the moment, mostly blue and green light is used to control optogenetic tools and these wavelengths have very limited tissue penetration.[64,115,129,130] Second, optogenetics requires gene transfer, restricting its use as therapeutics as gene therapy is still associated with many risks.[131-134]

The overall goal of this thesis is the development of new strategies to overcome the limitations of optogenetic approaches, with regard to light delivery to tissues and feasibility as therapeutic approach with a specific focus on cell regeneration. The overall goal can be divided into two parts. First, to overcome the limited light delivery to target tissues by engineering and characterizing red-light-activated growth factor receptors. Red light exhibits a much higher tissue penetration than other wavelengths of the visible spectrum. Second, to eliminate the necessity of gene therapy to make target tissues light sensitive, by identifying and investigating endogenous light-sensitive mechanisms and their potential to promote proliferative and pro-survival signals.

A special focus lies on implementing these new light-based approaches in pancreatic β-cell systems, as pancreatic β-cells are the key players of diabetes. Diabetes is one of the most frequent and fastest growing diseases worldwide. Therefore, it has become a priority in the health-care field to find ways to treat and cure this disease.[82] Numerous studies performed in cell and animal models have unequivocally demonstrated the contribution of growth factors, their cognate receptors and various associated signaling pathways in the regulation of β-cell proliferation and survival.[120,121,124,125,135] However, there are several drawbacks to growth factor therapies that have remained a theoretical exercise, such as the non-specific effects of growth factors as well as their tumorigenic properties.[120,128,135] An optogenetic or optical approach of promoting the activation of proliferative and pro-survival signaling cascades can overcome these disadvantages of growth factors as therapeutic agents for diabetes by providing the required spatio-temporal precise activation.[135] The strategies established in this thesis additionally decrease optogenetic limitations such as non-invasive light delivery and gene transfer.

CHAPTER 3: MATERIALS AND METHODS

3.1 Materials

3.1.1 Animals

CD-1 mice were purchased from Charles River at an age of 6 to 8 weeks and were used for primary islet isolation at an age of 7 to 12 weeks. C57BL/6J mice were bred within the breeding facility of IST Austria and were used at an age of 8 weeks only for primary islet isolation for OPN3$^{-/-}$ control experiments. OPN3$^{-/-}$ mice were generated in a C57BL/6J genetic background and were a gift from the laboratory of King-Wai Yau at the Johns Hopkins University School of Medicine. The Opn3$^{-/-}$ mouse line was generated by crossing an Opn3$^{flox/flox}$ mouse line, derived from embryonic stem cell clones, with a Sox2-Cre transgenic line, in which Cre recombinase was expressed globally in early embryos. The Opn3$^{flox/flox}$ construct included a targeting construct for inserting both a flippase recognition target (FRT) flanked-lacZ cassette upstream of exon 2 of the Opn3 gene, which was additionally flanked by a pair of loxP sites (Figure 3.1). A set of three primers was used to genotype the Opn3$^{-/-}$ mice: OPN3WT_F, OPN3$^{-/-}$_F and OPN3_R (Table A1). A combination of OPN3WT_F and OPN3_R gave a 530 bp band for the WT allele, whereas a combination of OPN3$^{-/-}$_F and OPN3_R gave a 670 bp band for the Opn3$^{-/-}$ allele.[50]

All animals were housed within the breeding facility of IST Austria, which has been approved by the Austrian Federal Ministry of Science, Research and Economy. All animals were housed in commercially available individually ventilated cages–Type II (500 cm^2) made of polysulfone under standard laboratory conditions (room temperature 22 ± 1°C; relative humidity 55 ± 10%; day/night rhythm of 12 hours) and supplied with standard diet (Altromin.1324 maintenance diet or Altr.1314 breeding diet) and autoclaved water *ad libidum*.

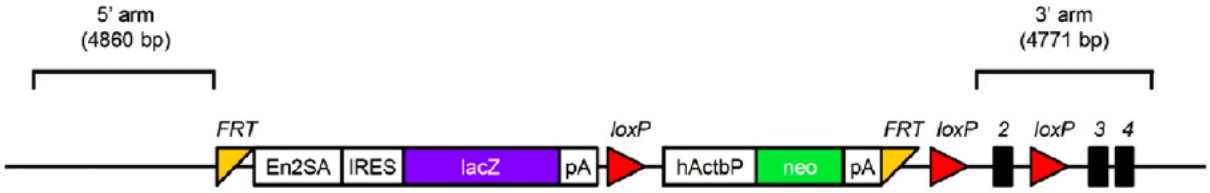

Figure 3.1 Schematic representation of the Opn3$^{flox/flox}$ targeting construct.

Through homologous recombination at the 5′ and 3′ arms, a FRT-lacZ cassette was inserted before exon 2 of the Opn3 gene. The exon is additionally flanked by loxP sites. Cre-dependent recombination at these sites leads to the deletion of exon 2, which encodes almost three entire transmembrane domains of OPN3. Dark bars indicate exons. En2SA: mouse Engrailed2 intron splice acceptor; hActbP: human β-actin promoter; IRES: internal ribosome entry site; lacZ: β-galactosidase cDNA; neo: neomycin-resistance gene; pA: SV40 polyadenylation site (illustration adapted from Buhr *et al.* 2015).[50]

3.1.2 Tissue culture

Dulbecco's modified eagle medium (DMEM, Gibco/Thermo Fisher Scientific)

Roswell park memorial institute 1640 medium (RPMI 1640, Gibco/Thermo Fisher Scientific)

Connaught medical research laboratories medium, no glutamine (CMRL, Gibco/Thermo Fisher Scientific)

CO_2-independent medium (Gibco/Thermo Fisher Scientific)

Leibovitz's L-15 Medium (Gibco/Thermo Fisher Scientific)

Opti-MEM I® (Gibco/Thermo Fisher Scientific)

Phosphate-buffered saline 1x (PBS, Gibco/Thermo Fisher Scientific)

Polyethylenimine (PEI, Polysciences); PEI was dissolved in Milli-Q H_2O at a concentration of 1mg/ml followed by sterile filtration through a 0.22 µm membrane.

Lipofectamine® 2000 (Invitrogen/ Thermo Fisher Scientific)

Fetal Bovine Serum (FBS, Gibco/Thermo Fisher Scientific); FBS was heat inactivated at 56°C for 35 minutes and stored at -20°C.

Trypsin-ethylenediaminetetraacetic acid (0.25%), phenol red (Trypsin-EDTA) Gibco/Thermo Fisher Scientific)

Acutase (Sigma)

Penicillin-Streptomycin (Gibco/Thermo Fisher Scientific)

4-(2-hydroxyethyl)-1-piperazineethanesulfonic acid (HEPES, Sigma)

Sodium pyruvate (Gibco/Thermo Fisher Scientific)

L-Glutamine (Gibco/Thermo Fisher Scientific)

β-Mercaptoethanol (Sigma)

Poly-L-ornithine (PLO, Sigma); The working dilution was 1:25 in Milli-Q® H_2O.

Cryotubes Nunc™, sterile (A. Hartenstein)

35 mm cell culture dishes, Nunc™ (for HEK293 cells and HeLa cells, Nunc/Thermo Fisher Scientific)

35 mm cell culture dishes, Falcon® (for INS-1E cells, BD Falcon)

96-well clear bottom plates (Greiner Bio-One)

T-75cm^2 tissue culture flask (for HEK293 cells and HeLa cells, TPP)

T-25cm^2 tissue culture flask (for HEK293 cells and HeLa cells, TPP)

T-75cm^2 tissue culture flask (for INS-1E cells, BD Falcon)

T-25cm^2 tissue culture flask (for INS-1E cells, BD Falcon)

4',6-Diamidino-2-phenylindole dihydrochloride (DAPI, Life technologies/ Thermo Fisher Scientific); The working dilution was 1:4000 in PBS.

Mowiol® 4-88 (Sigma)

3.1.3 Molecular biology

pGL4.33 vector (Promega)

RNase Away Reagent (Sigma)

Ultrapure nuclease-free water (Gibco/Thermo Fisher Scientific)

DNAseI and DNAseI buffer (Sigma)

Random hexamer primer (Thermo Fisher Scientific)

5x RevertAid reaction buffer (Thermo Fisher Scientific)

Deoxyribonucleotide triphosphates (dNTPs, New England Biolabs)

RiboLock RNAse inhibitor (Thermo Fisher Scientific)

RevertAid reverse transcriptase (RT, Thermo Fisher Scientific)

DpnI (New England Biolabs)

Alkaline Phosphatase, Calf Intestinal (CIP, New England Biolabs)

PfuX polymerase and 10x PfuX buffer (Jena Bioscience)

Dimethylsulfoxid (DMSO, Sigma)

NEB restriction enzymes and corresponding buffers (New England Biolabs)

T4 ligase and corresponding 10x T4 buffer (New England Biolabs)

1 kbp DNA ladder (New England Biolabs)

100 bp DNA ladder (New England Biolabs)

Clarity Western ECL Substrate (Bio Rad)

Agarose Standard (Carl Roth)

Agarose NEEO Ultra-Qualität (Carl Roth); only used for gel purification

6x loading dye Orange G (Sigma); 0.15% Orange G in 30% glycerol

LB ampicillin agar plates (Media kitchen IST Austria)

50x Tris-acetate-EDTA buffer (TAE buffer, Media kitchen IST Austria)

XL10-Gold® Ultracompetent *E. coli* cells (Agilent Technologies)

3.1.4 Antibodies

3.1.4.1 Primary antibodies

Anti phospho-p44/42 MAPK (Erk1/2) (Thr202/Tyr204) (Cell Signaling)

Anti phosph-Akt (Ser473)(D9E)XP rabbit mAB (Cell Signaling)

Anti Erk2 antibody (K-23) (Santa Cruz Biotechnology)

Anti Akt antibody (Cell Signaling)

Anti calnexin antibody (H-70) (Santa Cruz Biotechnology)

Anti vinculin antibody (Abcam)

Anti insulin antibody (R&D Systems)

3.1.4.2 Secondary antibodies

Goat *anti* rabbit IgG(H+L)-HRP conjugated (1706515, Bio Rad)

Alexa Fluor555 goat *anti* rat IgG (A-21434, Thermo Fisher Scientific)

3.1.5 Miscellaneous

Altromin1314 and 1324 diet (Altromin Spezialfutter GmbH&Co.KG)

Beetle luciferin (Promega)

Bovine Serum Albumin (BSA; Sigma)

Bromophenol blue (Sigma)

Calciumchlorid-dihydrate ($CaCl_2$-$2H_2O$, Sigma)

Clarity Western ECL Substrate (Bio Rad)

Collagenase P (Sigma)

Complete™, EDTA-free Protease Inhibitor Cocktail (Sigma)

Ethanol 99.9% (Sigma)

Ethylenediaminetetraacetic acid (EDTA, Roche)

Fibroblast growth factor 2 (FGF2, Sigma)

Glucose D(+) (Sigma)

Glycine (Sigma)

Guanidine hydrochloride (Guanidine-HCl, Sigma)

Glycerol (Sigma)

Phycocyanobilin (PCB, Livchem Logistics)

9-*cis* retinal (Sigma)

Isopropanol (Sigma)

Magnesium chloride hexahydrate ($MgCl_2 \cdot 6H_2O$, Sigma)

Milli-Q® H_2O (Media kitchen IST Austria)

Methanol 99.9% (Sigma)

Paraformaldehyde (PFA, Sigma)

Potassium chloride (KCl, Sigma)

Precision PLUS protein WesternC standard (Bio Rad)

Precision protein StrepTactin-HRP conjugated (Bio Rad)

Sodium hydroxide (NaOH, Sigma)

Sodium dodecyl sulphate (SDS, Sigma)

Sodium deoxycholate (Sigma)

Sodium chloride (NaCl, Sigma)

Synthetic genes (CPH1So, GloSensor-22F, Epoch Life Science, Inc.)

Trametinib (GSK1120212, Selleckchem/Absource Diagnostics GmbH)

Thiazolyl blue tetrazolium bromide (Sigma)

Triton X-100 (Sigma)

Trizma hydrochloride (Tris-HCl, Sigma)

Trizma base (Sigma)

4–20% Mini-PROTEAN® TGX™ Precast Protein Gels, 10-well (Bio Rad)

15 ml falcon tube (BD Falcon)

1.5 ml microcentrifuge tube (Eppendorf)

3.1.6 Buffers and solutions

DMEM complete medium
DMEM
10% FBS
100 U/ml Penicillin
0.1 mg/ml Streptomycin

INS-1E complete medium
RPMI-1640
10% FBS
100 U/ml Penicillin
0.1 mg/ml Streptomycin
10 mM HEPES
1 mM Sodium pyruvate
2 mM L-Glutamine
50 µM β-Mercaptoethanol

Murine islets complete culture medium
RPMI-1640
10% FBS
100 U/ml Penicillin
0.1 mg/ml Streptomycin

Human islets complete culture medium
CMRL
10% FBS
100 U/ml Penicillin
0.1 mg/ml Streptomycin
2 mM L-Glutamine

DMEM transfection medium
DMEM
5% FBS

INS-1E transfection medium
RPMI-1640
5% FBS
10 mM HEPES
1 mM Sodium pyruvate
2 mM L-Glutamine
50 μM β-Mercaptoethanol

DMEM reduced serum medium
DMEM
0.5% FBS
100 U/ml Penicillin
0.1 mg/ml Streptomycin

INS-1E reduced serum medium
RPMI-1640
0.1% FBS
100 U/ml Penicillin
0.1 mg/ml Streptomycin
10 mM HEPES
1 mM Sodium pyruvate
2 mM L-Glutamine
50 μM β-Mercaptoethanol

CO_2-independent reduced serum starve medium
CO_2-independent medium
0.5% FBS
2 mM L-Glutamine
100 U/ml Penicillin
0.1 mg/ml Streptomycin

Leibovitz's L-15 complete medium
Leibovitz's L-15 Medium
10% FBS
100 U/ml Penicillin
0.1 mg/ml Streptomycin

RIPA buffer
150 mM NaCl
1.0% Triton X-100
0.1% SDS
50 mM Tris-HCl, pH 8.0
0.5% Sodium deoxycholate
Complete™, EDTA-free Protease Inhibitor Cocktail (one tablet for 50ml)

Loading buffer (Laemmli 4X)
40% Glycerol
240 mM Tris-HCl pH 6.8
8% SDS
0-04% Bromophenol blue
5% β-Mercaptoethanol

SDS-running buffer (10x)
30,3 g/L Tris-HCl
144 g/L Glycine
1% SDS
pH 8.3
Diluted to 1x before final use.

Transfer buffer (20x)
58.6 g Glycine
116.2 g Tris-HCl
37.5 ml 20% SDS
Milli-Q® H_2O to 1 L

Transfer buffer (1x)
50 ml 20x Transfer Buffer
200 ml Methanol
750 ml Milli-Q® H_2O

Tris-buffered saline (TBS, 10x)
80 g/L NaCl
2 g/L KCl
30 g/L Trizma base
pH to 7,4
Milli-Q® H_2O to 1 L

TBST
999 ml TBS (1x)
1 ml Tween

PBST
999 ml PBS (1x)
1 ml Tween

Blocking buffer for immunoblotting
5 g Skinny milk powder or BSA
100 ml TBST

Blocking buffer for Click-iT® Plus EdU Alexa Fluor® 488 Imaging
0.1 g BSA
10 ml PBST

Krebs buffer (KRB)
7.13 g/L NaCl
0.35 g/L KCl
0.224 g/L $MgCl_2$-$6H_2O$
0.37 g/L $CaCl_2$-$2H_2O$
2.38 g/L HEPES
pH adjust pH to 7.4 with NaOH
Sterile filtered through a 0.22-µm membrane.

Sterile 1.65 M Glucose D(+) solution
29.73 g/L Glucose D(+)
Milli-Q® H_2O to 100 ml
Autoclaved

Stimulation buffer (16.7 mM glucose in KRB)
25 ml KRB
0.5% BSA
0.250 ml sterile 1.65 M Glucose D(+) solution

Basal buffer (3.3 mM glucose in KRB)
75 ml KRB
0.5% BSA
0.150 ml sterile 1.65 M Glucose D(+) solution

Acidic isopropanol
1 ml 1 M HCL
9 ml Isopropanol

Acidic ethanol
75 ml Ethanol 100%
23.5 ml Milli-Q® H_2O
1.5 ml concentrated HCl

4% Paraformaldehyde fixation solution
90 ml Milli-Q® H_2O
4 g PFA
10 ml PBS (10x)
Water was heated to 60°C and PFA was added. NaOH was added dropwise until the solution became clear. pH was adjusted to 7.4 with HCl. Finally 10 ml PBS (10x) were added.

A+AB buffer
135 mM NaCl
5.6 mM KCl
1.2 mM $MgCl_2$-$6H_2O$
1.28 mM $CaCl_2$-$2H_2O$
10 mM HEPES
3 mM Glucose D(+)
1% (V/V) Penicillin/Streptomycin
0.1 mg/ml BSA
Before adding Penicillin/Streptomycin and BSA the pH of the solution was adjusted with NaOH to pH 7.4.
Sterile filtered through a 0.22 µm membrane.

Collagenase solution
2 mg Collagenase P (1.9 U/mg)
2 ml A+AB buffer

Extraction buffer
100 mM Tris-HCl
4 mM EDTA
6 M Guanidine-HCl
pH7.8

3.1.7 Kits

Total RNA Purification Kit (Jena Bioscience)

QIAquick Gel Extraction Kit (Qiagen)

PCR Purification Kit (Jena Bioscience)

Plasmid MiniPrep Kit (Jena Bioscience)

PathDetect Elk1 trans-Reporting System (Agilent Technologies)

One-Glo Assay System (Promega)

Click-iT® Plus EdU Alexa Fluor® 488 Imaging Kit (Life Technologies)

Human Insulin ELISA Kit-80-INSHU-E01.1-AL (ALPCO/BioCat)

Pierce™ BCA Protein Assay Kit (Fisher Thermo Scientific)

ATP Determination Kit (Invitrogen/ Fisher Thermo Scientific)

3.1.8 Equipment

Hemocytometer-Neubauer chamber improved (Marienfeld-Superior)

Molecular Imager® VersaDoc™MP Substrate (Bio Rad)

Gel Doc™ XR

Thermocycler C1000^{TM} (BioRad)

High intensity LEDs HLMP-CE35 (Broadcom)

X4-Life RGB LED-stripes SMD5050 (12 V, 1 m and 5 m, RGB X4, Conrad)

BioTek Synergy H1 microplate reader (BioTek)

Power meter (PM120VA, Thorlabs).

Lamp illuminator with rapid filter exchange (DG4plus, Sutter instruments)

Microscope Olympus SZ51 (Olympus)

Water bath TW 8 (Julabo)

Thermomixer comfort (Eppendorf)

Eppendorf centrifuge 5424R (Eppendorf)

Multifuge X3R (Fisher Thermo Scientific)

EVOS® fluorescence microscope (Fisher Thermo Scientific)

LSM 700 inverted (Zeiss)

Standard scissors-straight sharp/blunt (Fine Science Tools)

Tungsten-carbide iris scissors (Fine Science Tools)

Narrow pattern forceps (Fine Science Tools)

Small straight clamp (Fine Science Tools)

Large curved clamp (Fine Science Tools)

3.2 Molecular biology methods

3.2.1 RNA extraction and DNase I digest

The extraction of total RNA was performed using the Total RNA Purification Kit according to the manufacturer's instructions. The RNA was eluted in 30 µl nuclease-free water, placed immediately on ice and further processed by DNase I digest. For the digest, 30 µl of eluted RNA (not more than 1 µg) was mixed with 4 µl 10x DNaseI buffer, 1 µl DNAseI and 5 µl nuclease-free water. The reaction was incubated for 30 minutes at 37°C followed by the addition of 2 µl 50 mM EDTA and 10 minutes incubation at 65°C to inactivate the DNaseI. After inactivation, the RNA was immediately placed on ice. For RNA extraction from islets, 70 to 100 murine islets or human islet equivalents (IEQs) were used. For cell lines, RNA was extracted from $1x10^6$ cells.

3.2.2 cDNA synthesis

All steps of the cDNA synthesis were prepared on ice. 3 µL of random hexamer primer were added to the inactivated DNAseI reaction and incubated for 5 minutes at 70°C. For a minus RT control (-RT), an additional reaction was prepared. After the random hexamer primer incubation, 13 µL of 5x RevertAid reaction buffer, 5 µL of 10 mM dNTPs and 2 µL of RiboLock RNAse inhibitor were added to the reactions and incubated for 5 minutes at 25°C. After 5 minutes, 1 µL RT was added to the reaction, but not to the -RT control, and incubated for 10 minutes at 25°C. Then the reactions were incubated for 1 hour at 42°C followed by 10 minutes at 70°C. Afterwards the cDNA was immediately placed on ice or frozen at -20°C.

3.2.3 Polymerase chain reaction

Polymerase chain reaction (PCR) was carried out using a thermocycler. The PCR mix was prepared as outlined in Table 3.1. Primers were designed to have a melting temperature (T_m) of ~72°C according to Equation 3.1. Details of primers are given in appendix Table A2. Standard PCRs were performed with the conditions outlined in Table 3.2, for RT-PCR the conditions are outlined in Table 3.3 and primers are listed in Table A3. After completion of a standard PCR, the DNA template of the PCR was eliminated by enzymatic digest with 1 µl of DpnI for 1.5 hours at 37°C followed by a purification using the PCR Purification Kit according to the manufacturer's instructions. The products of a RT-PCR were analyzed by agarose gel electrophoreses, followed by sequencing.

Equation 3.1 Calculation of T_m of PCR primer

$$T_m = 81.5+0.41 \times ((\text{GC units}/ \text{length}) \times 100)-(675/ \text{length})-((\text{mismatches}/ \text{length}) \times 100)$$

Table 3.1 Reagents for PCR

Reagents	Volume
PfuX polymerase	0.5 µl
PfuX buffer (10x)	5 µl
Forward primer (10 µM)	1 µl
Reverse primer (10 µM)	1 µl
DMSO	1 µl
Plasmid DNA (20 ng/µl)/cDNA	1 µl/3 µl
dNTPs (10 mM)	1 µl
Nuclease-free water	Fill up to 50 µl

Table 3.2 Standard PCR conditions

Steps	Temperature (°C)	Duration (min:sec)	Number of cycles
Pre-denaturation	95	2:00	1
Denaturation	95	0:20	
Annealing	56	0:20	34
Elongation	68	1:00/kb	
Extension	68	1:00/kb	1

Table 3.3 RT-PCR conditions

Steps	Temperature (°C)	Duration (min)	Number of cycles
Pre-denaturation	95	2:00	1
Denaturation	95	0:20	
Annealing	58	0:20	34
Elongation	68	0:30	
Extension	68	1:00	1

3.2.4 Site-directed mutagenesis

To perform a site-directed mutagenesis, a pair of complementary mutagenic primers was designed to amplify the entire plasmid resulting in a recircularized product. Primers were designed as for a standard PCR using Equation 3.1 and the details of used primers are in appendix Table A2. The reagents of the reaction mix were identical to those of a standard PCR (Table 3.1) and the reaction conditions mentioned in Table 3.4 were used. After completion of the reaction, the DNA template was eliminated by enzymatic digest with 1 µl of DpnI per reaction for 1.5 hours at 37°C. After DpnI digest, the circular product was directly inserted into competent *Escherichia coli* (*E. coli,* XL-10 Gold) by incubating 1.2 µl of the reaction product with the cells for 30 minutes on ice. After 30 minutes the transformed cells were plated on a prewarmed LB-ampicillin plate and incubated overnight at 37°C. The workflow of a site-directed mutagenesis is outlined in Figure 3.2.

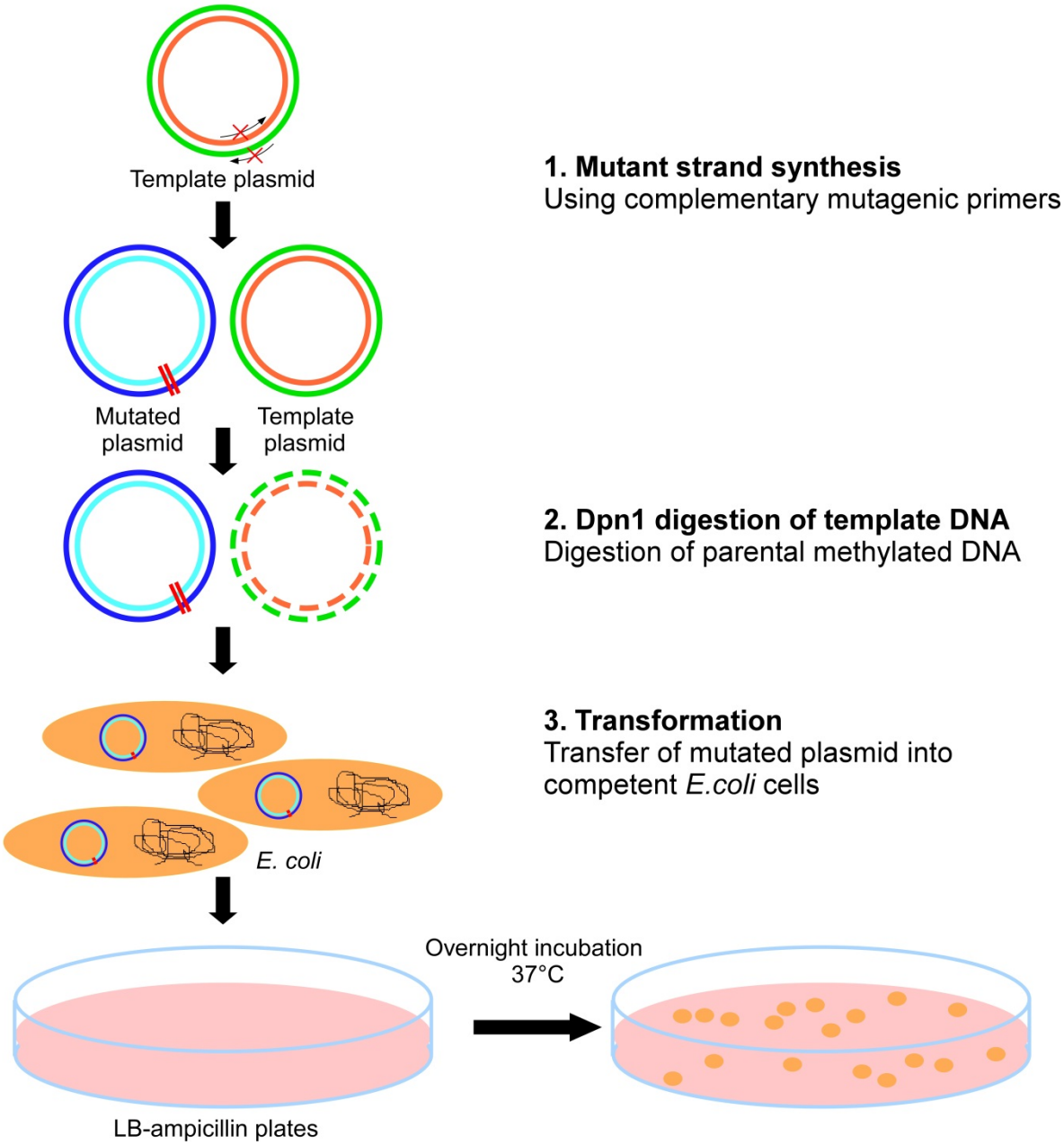

Figure 3.2 Work flow of site-directed mutagenesis. First, mutant strand synthesis is carried out by performing thermal cycling to denature the DNA template, anneal mutagenic primers, containing the desired mutation, and elongation using a high-fidelity DNA polymerase. Second, the template plasmid is enzymatically digested by DpnI. Third, competent *E.coli* cells were transformed with the mutated plasmid and finally transferred on LB-ampicillin plates and incubated overnight at 37°C.

Table 3.4 Site-directed mutagenesis reaction conditions

	Temperature (°C)	Duration (min:sec)	Number of cycles
Pre-denaturation	95	2:00	1
Denaturation	95	0:20	21
Annealing	56	0:20	
Elongation	68	1:00/kb	
Extension	68	1:00/kb	1

3.2.5 DNA digest using restriction enzymes

PCR products flanked with restriction sites or plasmids were digested using restriction enzymes for 1 hour at 37°C and further purified with the PCR Purification Kit according to the manufacturer's instructions. Exceptionally, DNA digests with the restriction enzyme SgrAI were performed for 30 minutes at 37°C, followed by a gel purification step using the QIAquick Gel Extraction Kit according to the manufacturer's instructions. For enzymatic digests, restriction enzymes and the corresponding buffers from New England Biolabs were used. The reaction was prepared as outlined in Table 3.5. Digested backbone plasmids were additionally treated with 1 µl CIP for 1.5 hours at 37°C. The CIP treatment catalyzed the removal of the 5´ phosphate groups from DNA, in order to avoid self-ligation and therefore decrease the vector background. Digested products were further processed in ligations.

Table 3.5 Composition of digest reactions

Reagents	Amount
Nuclease-free water	Fill up 30 µl
10x NEB buffer (corresponding to restriction enzyme)	3 µl
Restriction enzyme	1 µl
DNA	1500 ng

3.2.6 Ligation

Enzymatically digested plasmids and PCR products were ligated at a plasmid to insert ratio of 1:4 using T4 ligase. The ligation reaction was prepared as outlined in Table 3.6. As a control an additional reaction without insert was prepared. The ligation reactions were incubated for 3 hours at room temperature or 18 hours at 4°C. Transformation, after ligation, was performed as described in section 3.2.4.

Table 3.6 Reagents of ligation

Reagents	Amount
Nuclease-free water	Fill up to 20 µl
T4 ligase buffer (10x)	2 µl
T4 ligase	1 µl
Plasmid	50 ng
Insert	4 times plasmid amount

3.2.7 Agarose gel electrophoresis

A 1% gel was prepared for checking PCR products and for gel extraction, for RT-PCR analysis a 2% agarose gel was prepared. For gel extraction, the PCR product was mixed with 10 µl 6x loading dye and loaded onto the gel. For standard PCR products and RT-PCR products, 5 µl of the product was mixed with 4 µl 6x loading dye and 16 µl H_2O. For the DNA ladder, 1 µl was mixed with 4 µl 6x loading dye and 20 µl H_2O. Twenty µl of each sample was loaded onto the gel and all samples were run at 100 volt (V) for 15 minutes. Gels were visualized using Gel Doc.

3.3 Genetic engineering

3.3.1 Engineering of expression plasmids of phytochrome sensory domains

The gene fragment coding for the sensory domain of the phytochrome, CPH1 from Synechocystis PCC6803 (CPH1S) was amplified from a genomic DNA library using PCR (oligonucleotides 1 and 2, Table A1). In addition, the gene fragment for CPH1S was synthesized with mammalian codon optimization (CPH1So) according to the supplier's recommendation and amplified using a PCR (oligonucleotides 3 and 4, Table A1). In order to perform expression as well as cytotoxicity tests in mammalian cells, an expression plasmid based on pcDNA3.1(-) was used in which a BspEI restriction site was placed after the fluorescent protein mVenus and a glycine- and serine-rich linker.[136] CPH1S and CPH1So were inserted into this plasmid after PCR amplification by using the restriction enzyme XmaI (Figure 3.3 A).

3.3.2 Engineering of red-light-activated RTKs

To generate a red-light-activated murine fibroblast growth factor receptor 1 (mFGFR1-CPH1So, Figure 3.3 B), the codon optimized phytochrome sensory domain, CPH1So, was inserted into a mFGFR1 construct that was described previously in Grusch et al. 2014[136] using a PCR and the restriction enzyme XmaI (oligonucleotides 3 and 4, Table A2). This construct contained the complete intracellular domain of mFGFR1, a myristoylation membrane anchor and a HA-epitope (Figure 3.2 B). For multi-color fluorescent reporter assays, the CMV promoter of the mFGFR1-CPH1So expression vector was truncated for lower expression[137] using an inverse PCR with phosphorylated primers (oligonucleotides 5 and 6, Table A1) followed by blunt end ligation. Point substitutions in mFGFR1-CPH1So (Y271F, Y272F and R195E; numbered relative to start methionine of red-light-activated mFGFR1) were introduced using site-directed mutagenesis (oligonucleotides 11-14, Table A1). The red-light-activated rat tropomyosin receptor kinase B (rtrkB-CPH1So, Figure 3.3 B) was generated using an inverse PCR on mFGFR1-CPH1So (oligonucleotides 7 and 8, Table A1). By using PCR amplification the mFGFR1 intracellular domain was replaced and a linear double-stranded DNA product with terminal SgrAI restriction sites was generated. The PCR product was digested with SgrAI, ligated and propagated in *E. coli* cells. The rtrkB intracellular domain was then inserted using a PCR and the restriction enzyme BspEI and AgeI (oligonucleotides 9 and 10, Table A1). A point substitution in rtrkB-CPH1So (K131A, numbered relative to start methionine of red-light-activated rtrkB) were introduced using a site-directed mutagenesis (oligonucleotides 15 and 16, Table A1).

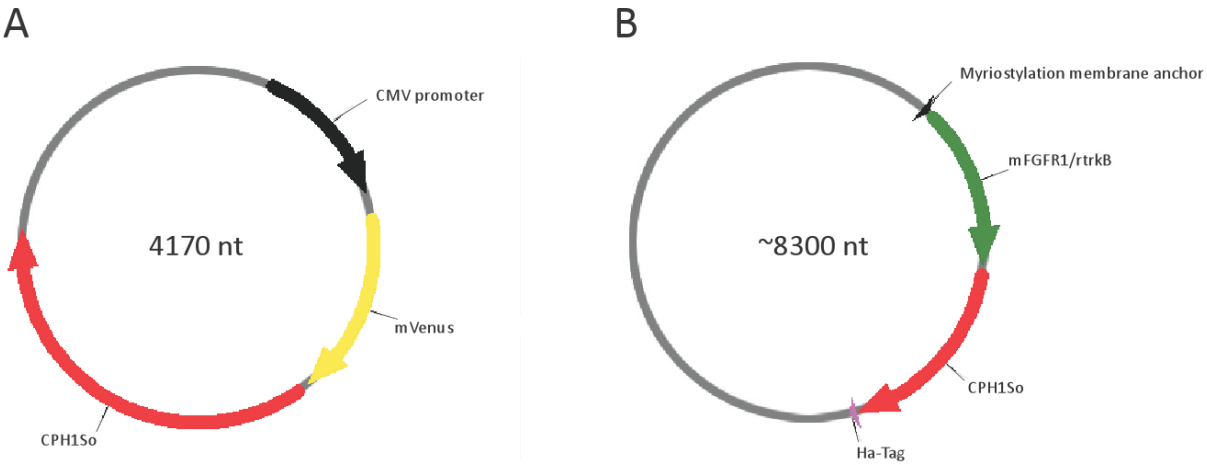

Figure 3.3 Expression plasmids (A) Example of expression plasmid used for expression and cytotoxicity tests of phytochrome sensory domains. The plasmid is based on pcDNA3.1(-) including mV followed by CPH1So under the control of a CMV promoter. (B) Expression plasmid of mFGFR1/rtrkB-CPH1So containing the intracellular RTK domain, a myristoylation membrane anchor, the CPH1So domain and a Ha-Tag

3.3.3 Engineering of fluorescence reporters

Fluorescence transcriptional reporters were generated by Alexandra-Madelaine Tichy (IST Austria), by first removing the luciferase gene from the pGL4.33 vector using an inverse PCR and the restriction enzyme AscI (oligonucleotides 17 and 18, Table A1). Then mCherry was inserted using PCR, followed by an enzymatic digest with AscI (oligonucleotides 19 and 20, Table A1). The mCerulean3-N1 expression vector (Addgene # 54730) was used as a fluorescence viability reporter in multi-color fluorescent reporter assays.

3.3.4 Engineering of real-time cAMP sensor

A genetically-encoded real-time cAMP sensor (GloSensor-22F)[138] was obtained as a synthetic gene and subcloned into pcDNA3.1(-) using NheI and KpnI restriction enzymes by Catherine McKenzie (IST Austria).

3.4 Tissue culture methods

3.4.1 Description of cell lines

Three different cell lines were used as cellular models for different experimental approaches. I) Human Embryonic Kidney (HEK) 293 cells were derived in 1971, from a healthy human embryonic kidney transformed by sheared adenovirus 5 DNA.[139] HEK293 cells were used as model system for various studies of this thesis; especially in experiments were transfection was necessary, because of their reliable growth and propensity for transfection. II) HeLa cells are human epithelial cells derived from cervical cancer cells, 1951. HeLa cells are the oldest and most commonly used human cell line.[140] The cell line was used as an additional cell line to study light effects on mammalian cells. III) INS-1E cells have the characteristics of pancreatic β-cells, including a high insulin content and responsiveness to glucose. This cell line was clonal isolated from INS-1 cells, which are derived from a rat insulinoma induced by X-ray.[141] INS-1E cells were used in this project as a model of pancreatic β-cells to study red-light-dependent signaling activation through mammalian tissue and to study the general effect of light on mammalian tissues.

3.4.2 Maintenance and storage of cell lines

HEK293 cells and HeLa cells were cultured in DMEM complete medium. INS-1E cells were cultured in INS-1E complete medium. All cells were cultured in a humidified incubator with 5% CO_2 atmosphere at 37°C and they were subcultured two to three times a week depending when they reached 90-100% confluency. For subculturing, the medium was removed and the cells were washed once with PBS. Then cells were detached by 1 ml trypsin/EDTA for 3 minutes at 37°C, followed by the addition of 5 ml complete medium and the transfer of the cell suspension into a 15 ml falcon tube, which was centrifuged for 5 minutes at 700 rpm. The supernatant was removed and the cell pellet was resuspended in 5 ml complete medium. 0.5 ml of the cell suspension was transferred to a new T-75cm^2 tissue culture flask containing 10 ml complete medium.

For cryopreservation and storage of cells, the same procedure as for subculturing was implemented, but the cell pellets were resuspended in freezing medium (complete culture medium supplemented with 10% DMSO) instead of complete medium. For HEK293 and HeLa cells 1 ml of cell suspension was transferred to a cryotube which was placed for 24 hours at -80°C and subsequently transferred to a liquid nitrogen storage vessel. For INS-1E cells, the cryotube containing 1 ml of cell suspension was first placed for 6 hour at -20°C, then for 24 hours at -80°C and subsequently transferred to a liquid nitrogen storage vessel for long-term storage. Cell lines were thawed by placing them in a 37°C water bath until the cell suspension was completely thawed. Cells were further transferred to a 15 ml falcon tube containing 10 ml pre-warmed complete medium, which was centrifuged for 5 minutes at 700 rpm. Cell pellets were resuspended in 5 ml complete medium and transferred to a T-25cm^2 tissue culture flask.

3.4.3 Cell quantification

Before cell quantification, the same procedure as for subculturing was followed. After resuspending the cell pellet in 5 ml complete medium, a 1:10 dilution of the cell

suspension was prepared and 10 µl of this dilution were transferred to one side of a hemocytometer. The number of cells was determined by counting four 1 mm^2 squares of a hemocytometer and using Equation 3.2.

Equation 3.2 Cell concentration per ml

Cells/ml = Average number of cells per 4 squares counted x the dilution factor x 10^4

3.4.4 Transfection of cell lines

Cells were either transfected using PEI or Lipofectamine® 2000 as transfection reagent following the same protocol. Cells were either seeded 16 hours before transfection or directly before transfection. First, transfection reagent was mixed with Opti-MEM I® to a total volume of 25 µl/96-well or 125 µl/35 mm dish and incubated for 5 minutes at room temperature. During incubation, DNA was mixed with Opti-MEM I® to a total volume of 25 µl/96-well or 125 µl/35 mm dish (Table 3.7). After 5 minutes the transfection reagent/Opti-MEM I® mixture was combined with the DNA/Opti-MEM I® sample and incubated for 20 minutes at room temperature. After 20 minutes the mixture was added to the cells seeded in appropriate transfection medium. Six hours after transfection medium was replaced with appropriate medium.

Table 3.7 Reagents for transfection

Reagents	96-well	35 mm dish
DNA	~200 ng	~2500 ng
PEI (1 µg/µl) / Lipofectamine® 2000 (1mg/ml)	1 µl / 0.5 µl	20 µl / 10 µl
Opti-MEM I® (fill up to)	50 µl	250 µl

3.4.5 Expression and cytotoxicity test of phytochrome sensory domains in HEK293 cells

To test expression and cytotoxicity of phytochrome sensory domains 5 x 10^4 HEK293 cells were seeded in 100 µl DMEM transfection medium in each well of a PLO-coated 96-well clear bottom plate. HEK293 cells were transfected with 200 ng total plasmid (5-10 ng expression plasmid filled up with empty vector to 200 ng). The investigated expression plasmids were mV-CPH1S, mV-CPH1So and previously described mV-FKBP.[136] Six hours after transfection the medium was replaced with DMEM complete medium. Thirty hours after transfection expression was assessed by replacing medium with PBS and measuring fluorescence (mV: $\lambda_{Ex/Em}$ = 495/528 nm) in a microplate reader. After fluorescence measurement, cytotoxicity of phytochrome sensory domains was assessed in HEK293 cells expressing mV-CPH1S, mV-CPH1So and mV-FKBP using a colorimetric-based assay to detect cellular metabolic activity (MTT assay). In detail, after fluorescence measurement cells were incubated for 2 hours with 0.5 mg/ml thiazolyl blue tetrazolium bromide dissolved in PBS followed by lysis with 70 µl acidic isopropanol. Finally, absorbance at 570 nm and 690 nm was measured in the microplate reader and cell viability was determined by Equation 3.3.

Equation 3.3 Cell viability

Cell viability = Absorbance 570nm – Absorbance 690nm (background)

3.5 Tissue preparations

3.5.1 Preparation of synthetic tissues

To pretest whether red-light-activated RTKs allowed non-invasive signaling activation in mammalian tissues, agarose gels stained with different dyes termed synthetic tissues, whose spectral properties matched those of human skin, skull and muscle, were prepared.[142-144] Synthetic tissues were prepared by supplementing high purity 2% agarose gels with dyes depending on the tissue type (Table 3.8). The dyes were added to the liquid gel and mixed thoroughly until the dyes were homogenously distributed. The dye supplemented gel was poured into a transparent container having the same dimensions as a 96-well plate and was allowed to solidify. The walls of the container were covered with light-impermeable tape in order to allow light transmission just through the synthetic tissue. Synthetic skin and muscle were generated by supplementing 104.5 ml gel with different amounts of tartrazine and amaranth. Synthetic skull was generated by supplementing 31.4 ml gel with tartrazine, amaranth, allura red AC, prussian blue and brilliant blue (Table 3.8). 10 mm of synthetic tissue corresponded to 10 mm of animal tissue, except for skin which has 20-fold higher absorption; in this case, 10 mm of synthetic tissue corresponded to 0.5 mm of mammalian skin.

Table 3.8 Dye composition of synthetic tissues mimicking absorption spectrum of different mammalian tissues.

Tissue type	Tartrazine (µg)	Amaranth (µg)	Allura red AC (µg)	Prussian blue (µg)	Brilliant blue (µg)
Skin	50	3	-	-	-
Muscle	15	15	-	-	-
Skull	75	10	55	25	50

3.5.2 Determination of light transmission through mouse tissue

To determine light transmission properties of different light wavelengths (λ = 470 nm, 545 nm, 640 nm) through mammalian tissue, light penetration through murine head and abdomen was determined (Figure 3.4 A). For measuring light penetration through head, the lower jaw and the palate bone of shaved mouse heads were removed to create an opening. Light that penetrated through the shaved scalp, the skull and the whole brain was measured. For mouse abdomen, the shaved mouse torsos were opened and light that penetrated through shaved skin, fat, muscle, spine and organs was measured. A DG4plus lamp was used as illumination source for these experiments. A dish covered with light-impermeable tape excluding a defined window was placed above a sensor connected to a power meter (Figure 3.4 B). Three measurements were acquired each first without sample to determine the initial light intensity, I_0, in µW/cm^2 and then with the sample to determine transmission, I, in µW/cm^2. Percentage of light transmission was calculated by Equation 3.4.

Equation 3.4 Percentage light transmission (% Transmission)

$$\%\text{Transmission} = (I / I_0) \times 100$$

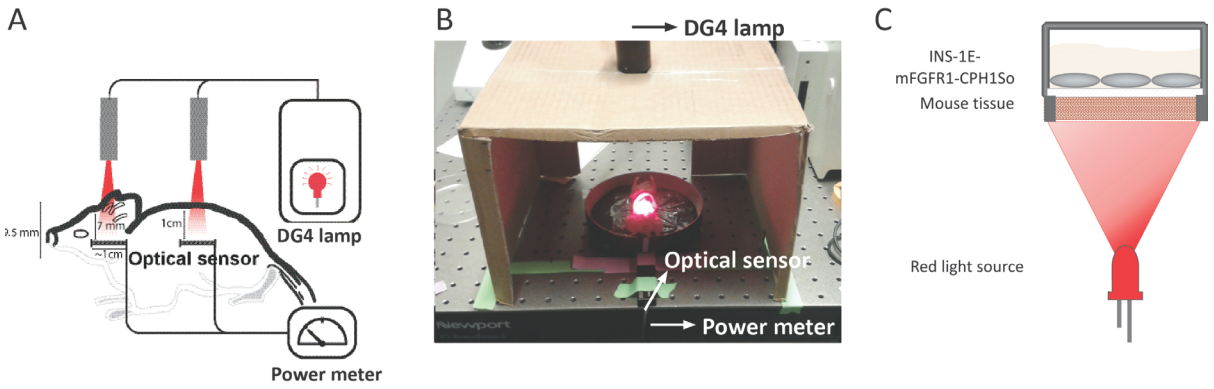

Figure 3.4 Setup of different light penetration experiments. (A) Setup for measuring light penetration through the head and the abdomen of a mouse. Light was aimed above the shaved mouse head (thickness ~7 mm) or above the opened mouse abdomen (thickness ~10 mm). An optical sensor (diameter ~10 mm) connected to a power meter was placed directly under the ventral part of the brain or under the shaved abdomen of the mouse. (B) Picture of measuring red light penetration through the mouse abdomen. (C) INS-1E cells transfected with mFGFR1-CPH1So were illuminated with red light from the bottom through ~10 mm of mouse tissue (the sides of the plates were covered with black tape).

3.6 Islets methods

3.6.1 Murine islet isolation

Pancreatic islets were isolated from 8 to 12 weeks old mice. The experimental animals were sacrificed by cervical dislocation. The animals were laid with the abdominal side facing up and sterilized with 70% ethanol and fixed with rubber bands on a board in order to allow the opening of the abdominal cavity with scissors (Figure 3.5 B). The exposed organs were placed on one side and the liver was fold back in order to make the common bile duct visible. The ending of the common bile duct into the duodenum is closed through a constrictor, sphincter of Oddi, which is marked by a white point. A large curved clamp was placed at the common bile duct close to the liver. Two additional small clamps are placed at the small intestine, in order to prevent the uncontrolled reflux of the collagenase solution (Figure 3.5 A). At the end of the common bile duct (the white point) the cannula was inserted into the pancreatic duct and 2 ml ice-cold collagenase solution was injected until the pancreas was fully bloated (Figure 3.5 C). Afterwards the clamps were removed the pancreas was carefully detached from the gut, stomach and spleen and put into a cooled 15 ml falcon. The pancreatic tissue was vortexed for 5 seconds and put into a shaking water bath at 37°C for 6 minutes, while vortexed every 2 minutes. The collagenase digest was stopped by adding 10 ml ice-cold A+AB buffer. The digested tissue was centrifuged for 20 seconds at 2000 rpm at 4°C. Afterwards the supernatant was removed and the pellet was dissolved in 12 ml of ice-cold A+AB buffer and again centrifuged for 20 seconds at 2000 rpm at 4°C. This whole step was repeated once more. The resulting pellet was resuspended in 5 ml A+AB. Further on, islets were selected from the cell suspension under the microscope with a 1.2 times magnification and transferred into a fresh petri dish containing A+AB buffer (Figure 3.5 D and E). The selected islets were transferred twice into a fresh petri dish to remove remaining tissue debris (Figure 3.5 F). Finally the collected islets were counted and transferred into a microcentrifuge tube. After the islets were deposited to the bottom of the tube, the supernatant was carefully removed and murine islets complete culture medium was added to the islets, which were then transferred to an appropriate cell culture dish depending on the planed experiment.

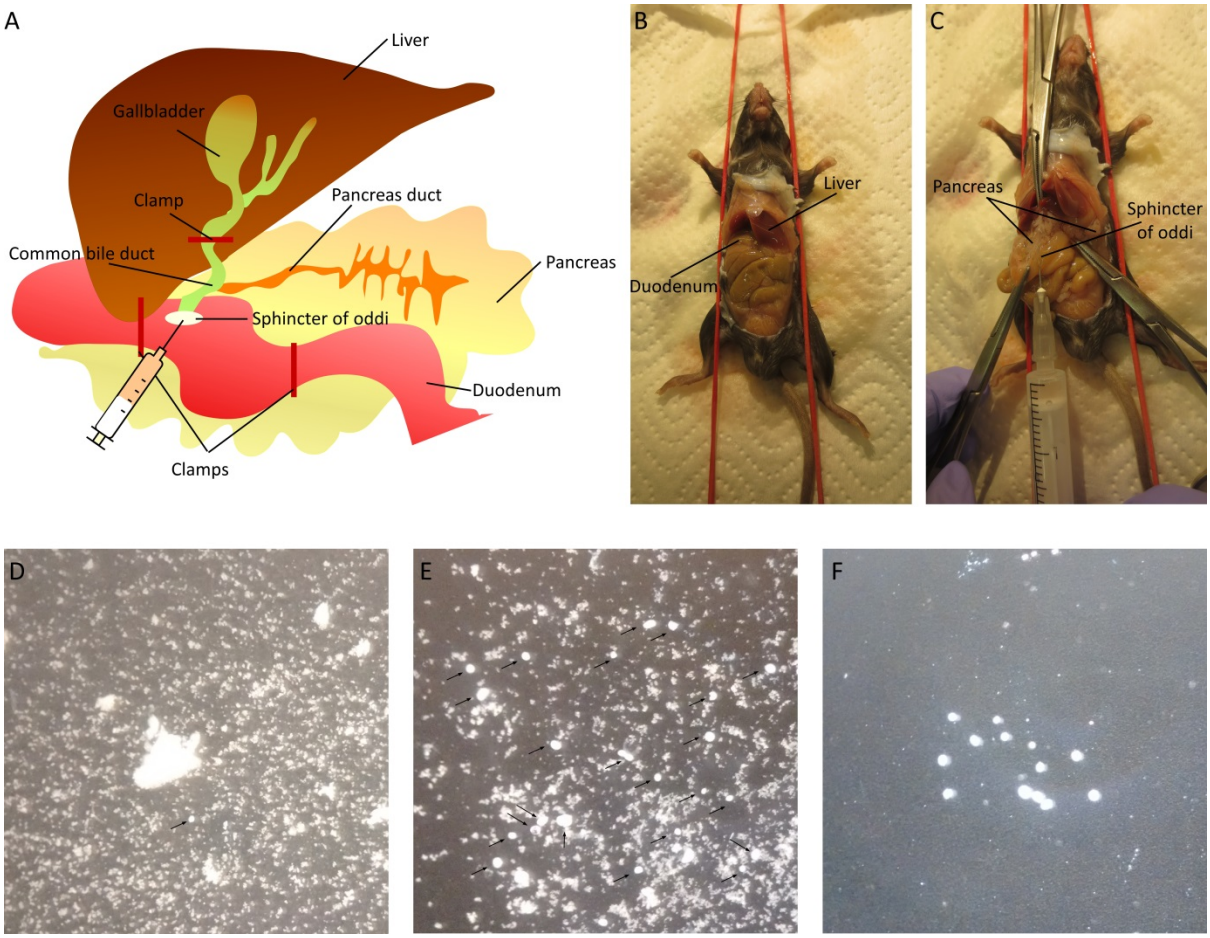

Figure 3.5 Different steps of murine islets isolation and selection. (A) Illustration of the liver, gallbladder, the common bile duct, the sphincter of Oddi, the pancreas, the pancreatic duct and the duodenum. The end of the common bile duct into the duodenum is closed by the sphincter of Oddi, marked by a white point. Collagenase was injected through the sphincter of Oddi to the pancreatic duct. (B) To open the abdominal cavity and to get access to the duodenum, the pancreas and the common bile duct, the moues was fixed with rubber bands on a board. (C) To perfuse only the pancreas and to prevent the collagenase solution from flowing into the liver and the duodenum, a curved clamp was placed on the common bile duct close to the liver, and two small clamps on the duodenum on each side of the sphincter of Oddi. (D) Unselected cell suspension containing islets (black arrow). (E) Selected islets (black arrow) transferred once into a fresh dish. (F) Final select islets.

3.6.2 Culture conditions for murine islets

Murine islets were maintained in murine islets complete culture medium. After isolation murine islets were cultured overnight in complete culture medium at 37°C and 5% CO_2 for regeneration after isolation. After ~16 hours medium was changed and islets were further processed for different experiments.

3.6.3 Culture conditions for human islets

Human adult pancreatic islets were obtained from a local collaborator (S. Kubicek, CeMM Research Center for Molecular Medicine, Austrian Academy of Sciences) and the European Consortium for Islet Transplantation (Geneva) and the Integrated Islet Distribution Program (IIDP). For different experiments, islets from 4 different donors

with a mean age of 46 years ranging from 34 to 59 years were used. Donor details are given in appendix Table A4. The islet purity was ranging between 85% and 95%, based on reports from the islet providers. Upon their receipt, human pancreatic islets were maintained in human islets complete culture medium at 37°C and 5% CO_2. Every other day medium was changed or fresh medium was added.

3.6.4 Islets dissociation

Murine and human islets were dissociated according to a slightly different protocol. All murine islets from one condition were collected in a microcentrifuge tube and were centrifuged for 5 minutes at 200 RCF. Medium was carefully removed and islets were resuspended in 150 µl trypsin/EDTA and incubated for 5 minutes at 37°C. After 5 minutes islets were further mechanically dissociated by repeated up and down pipetting. After all islets were dissociated, 1 ml of murine islets complete culture medium was added followed by 5 minutes centrifugation at 200 RCF. Supernatant was carefully removed and cell pellet was resuspended in 100 µl PBS/50 islets. 100 µl of cell suspension was transferred to one yellow pipette of the cytospin device (Figure 3.6 B). All human islets from one condition were collected in a 15 ml falcon tube and were centrifuge for 5 minutes at 200 RCF. Medium was carefully removed and the islets were resuspended in 200 µl PBS and transferred to a microcentrifuge tube and again centrifuged for 5 minutes at 200 RCF. Supernatant was removed and islets were resuspended in 25-100 µl Acutase (5000 islets/ml) and incubate for 20 minutes at 37°C. After 20 minutes, islets were dispersed by pipetting up and down 5 times, and then 1 ml of human islets complete culture medium was added followed by 5 minutes centrifugation at 200 RCF. Supernatant was carefully removed and cell pellet was resuspended in 100 µl PBS/50 islets. 100 µl of cell suspension was transferred to a yellow pipette tip of a cytospin device (Figure 3.6 B). The custom-build cytospin device[145] was composed out of filter paper, a cut plastic tip box inlet, shortened 10 µl pipette tips, a glass slide, foldback clips and 200 µl pipette tips (Figure 3.6 A). The punched filter paper was placed between a glass slide and the cut plastic tip box inlet. Shortened 10 µl pipette tips were put in the holes of the filter paper and the plastic inlet. Every cell sample was applied to a yellow pipette tip, which was connected to the shortened 10 µl pipette tip (Figure 3.6 B). The whole apparatus was finally placed into the plate holder of a centrifuge to spin down the cells onto the glass slide for 5 minutes at 750 RCF (Figure 3.6 C).

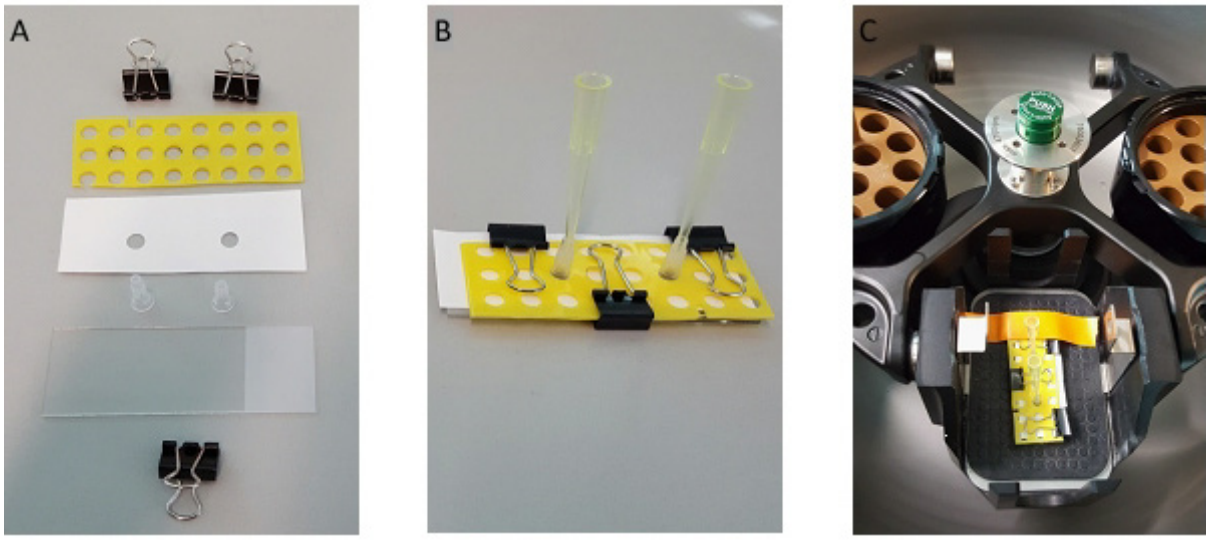

Figure 3.6 Custom-build cytospin device. (A -B) The cytospin was built out of filter paper, a cut plastic tip box inlet, shortened 10 µl pipette tips, a glass slide, foldback clips and 200 µl pipette tips. Yellow pipette tips were filled with cell suspension and (C) the whole apparatus was placed into the plate holder of a centrifuge to spin down the cells onto the glass slide.

3.7 Signaling detection methods

3.7.1 PathDetect Elk1 trans-Reporting System

Activation of the MAPK/Erk pathway was assayed with the PathDetect Elk1 trans-Reporting System also termed luciferase assay. 5 x 10^4 HEK293 cells were seeded in 100 µl DMEM transfection medium in each well of PLO-coated 96-well clear bottom plates and simultaneously transfected with 210.3 ng total plasmid (0,3 ng receptor, 10 ng trans-activator and 200 ng trans-reporter). 6 hours after transfection, medium was replaced with 100 µl CO_2-independent reduced serum starve medium supplemented with 10 µM PCB in the dark. After overnight incubation at 37°C and 5% CO_2, cells were either stimulated with red light (λ = 630 $\pm$ 5 nm, *I* = 6.2 µW/cm^2) for 8 hours or protected from light at 37°C. For control experiment, cells were stimulated with blue (λ = 470 $\pm$ 5 nm, *I* = 150 µW/cm^2) or green (λ = 530 $\pm$ 5 nm, *I*= 6.2 µW/cm^2) light instead of red light. Light intensities in an incubator equipped with 300 light emitting diodes was controlled with a dimmer and measured with a power meter. After 8 hours incubation, plates were processed with Luciferase One-Glo Assay System according to the manufacturer's instructions. Luminescence was detected with the microplate reader.

3.7.2 Signaling activation by rtrkB/mFGFR1-CPH1So through synthetic tissue

5 x 10^4 HEK293 cells were seeded in 100 µl DMEM transfection medium in each well of PLO-coated 96-well clear bottom plates and simultaneously transfected with 210.3 ng total plasmid (0,3 ng receptor, 10 ng trans-activator and 200 ng trans-reporter). 6 hours after transfection, medium was replaced in the dark with 100 µl CO_2-independent reduced serum starve medium supplemented with 10 µM PCB. After overnight incubation at 37°C and 5% CO_2, the 96-well plate containing the transfected HEK293 cells was placed on top of the container containing the synthetic tissue. The two plates were taped to each other with light-impermeable tape as well as all transparent parts of the plates were covered with tape to ensure that cells were only stimulated by light that passed through synthetic tissue. Cells were stimulated with red light (λ = 630 $\pm$ 5 nm, *I* = 6.2-17.5 µW/cm^2) for 8 hours at 37°C. Control cells were kept on the same plate but wells were fully covered with light-impermeable tape. After 8 hours incubation, plates were processed as described in section 3.7.1.

3.7.3 Multi-color fluorescence reporter assay

In order to assess MAPK/Erk pathway activation and cell viability simultaneously a multi-color fluorescence reporter assay was performed by using novel engineered fluorescence transcriptional reporters (described in section 3.3.3). For the multi-color fluorescence reporter assay, 5 x 10^4 HEK293 cells were seeded in 100 µl DMEM transfection medium, in each well of PLO-coated 96-well clear bottom plates. HEK293 cells were incubated for 16 hours at 37°C and 5% CO_2, followed by transfection with 251 ng total plasmid (1 ng viability reporter, 100 ng transcriptional reporter and 150 ng receptor). Sixteen hours after transfection, medium was replaced with 90 µl CO_2-independent reduced serum starve medium and incubated in the dark at 37°C at 5% CO_2. After 5 hours, 10 µM PCB and, where required, 0.1 µM Trametinib or 10% DMSO were added in the dark to each well and cells were

incubated for further 4 hours in the dark at 37°C at 5% CO_2. Cells were then stimulated either with red light (λ = 630 ± 5 nm, I = 6.2 μW/cm^2) or kept in the dark for 18 hours at 37°C. After red light illumination, medium was replaced by 50 µl PBS and fluorescence was measured with the microplate reader (mCerulean3: $\lambda_{Ex/Em}$ = 433/475 nm, mCherry: $\lambda_{Ex/Em}$ = 588/630 nm).

3.7.4 Immunoblotting

3.7.4.1 Temporal precise signaling activation by rtrkB-CPH1So

To prove the temporal precision of red-light-dependent activation of MAPK/Erk and PI3K/Akt pathways by rtrkB-CPH1So immunoblotting was used. 1 x 10^6 HEK293 cells were seeded in 2 ml DMEM transfection medium in PLO-coated 35 mm dishes and simultaneously transfected with 4.02 µg total plasmid per dish (0.2 µg receptor and 4 µg empty vector). 6 hours after transfection, medium was replaced with 1.5 ml DMEM reduced serum starve medium supplemented with 10 µM PCB. After 20 hours, cells were illuminated for 3 minutes with red light (λ = 630 ± 5 nm, I = 6.2 μW/cm^2). Cells were then either immediately, or after additional 5, 15 or 30 minutes in the dark washed with ice-cold PBS and lysed on ice in 250 µl RIPA buffer per dish. Dark control cells, control cells without PCB treatment and mock transfected cells were not illuminated and washed and lysed immediately. The lysates were shaken for 30 minutes at 4°C and centrifuged for 20 minutes at 12000 rpm at 4°C. Twenty µl lysate mixed with loading buffer per lane were separated by SDS-PAGE (60 minutes, 140 V) and electro-blotted onto PVDF membranes (100 minutes, 100 V). After 1 hour incubation in blocking buffer at room temperature, blots were further incubated with primary antibodies *anti* phospho-p44/42 MAPK (Erk1/2) (Thr202/Tyr204) and *anti* Akt, or *anti* phosph-Akt (Ser473)(D9E) and *anti* Erk2 (K-23) overnight at 4°C. Primary antibodies were applied as a 1:1000 dilution in blocking buffer. The secondary antibody, goat *anti* rabbit IgG(H+L)-HRP conjugated, was applied at a dilution of 1:10000 for 2 hours at room temperature. Chemiluminescence was developed with Clarity Western ECL Substrate and signals recorded with Molecular Imager® VersaDoc™MP.

3.7.4.2 Light-dependent signaling activation in different cell lines

To investigate signaling responses of different cell lines to visible light stimulation MAPK/Erk activation was assessed using immunoblotting. 1 x 10^6 HEK293, HeLa or INS-1E cells were seeded in 2 ml cell line appropriate complete medium in PLO-coated 35 mm dishes. 16 hours after seeding medium was replaced with 1.5 ml cell line appropriate reduced serum starve medium. After 20 hours of starvation, cells were illuminated for 5 minutes with blue-green light (λ = 470 nm, I = 240 µW/cm^2, λ = 535 nm, I = 240 µW/cm^2). After illumination cells were immediately washed with ice-cold PBS and lysed on ice in 130 µl RIPA buffer per dish. Dark control cells were not illuminated and washed and lysed immediately. Samples were further processed as described in section 3.7.4.1. Blots were incubated with primary antibodies *anti* phospho-p44/42 MAPK (Erk1/2) (Thr202/Tyr204) and *anti* calnexin.

3.7.4.3 MAPK/Erk activation in INS-1E cells through mouse abdomen by mFGFR1-CPH1So

1.5 x 10^6 INS-1E cells were seeded in 2 ml INS-1E transfection medium in a PLO-coated 35 mm dish that was covered with light-impermeable tape except for the bottom. After 16 hours of incubation at 37°C and 5% CO_2 cells were transfected with 2.5 µg total DNA per dish (0.05 µg receptor and 2.45 µg empty vector). 9.5 hours after transfection, medium was replaced with 1.5 ml INS-1E reduced serum starve medium supplemented 10 µM PCB and incubated for 18 hours in the dark. Ten mm of mouse tissue including shaved skin, fat, muscle, and spine was placed in a 35 mm dish. The dish was covered with black tape, except for a defined window (~1 cm^2) at its bottom and top where the light could penetrate. The dish containing the cells was placed on top of the tissue-containing dish and were illuminated for 15 minutes with red light (λ = 647 ± 35 nm, I = 3.0 mW/cm^2) from the bottom through the mouse abdomen (Figure 3.4 C). Cells were then immediately washed with ice-cold PBS, lysed, and processed as described in section 3.7.4.1. Dark and mock transfection controls as well as further steps were also performed as described in section 3.7.4.1. The blot was incubated with primary antibody *anti* phospho-p44/42 MAPK (Erk1/2) (Thr202/Tyr204).

3.7.4.4 Light-dependent signaling activation in pancreatic islets

Immunoblots were performed to investigate downstream signaling activation in primary pancreatic islets upon light illumination. In particular, the activation of the proliferative MAPK/Erk and PI3K/Akt pathway was analyzed. 100 murine islets or 600 human IEQ were seeded in a 60 mm dish in appropriate complete culture medium. After overnight incubation, islets were collected in a 15 ml falcon tube, centrifuged for 5 minutes at 200 rpm and resuspended in A+AB buffer. 50 murine islets or 300 human IEQs per condition were transferred into separate microcentrifuge tubes and incubated for 2 hours in the dark. After 2 hours of starvation in the dark islets were illuminated with blue-green light (λ = 470 nm, I = 64 µW/cm^2, λ = 535 nm, I = 64 µW/cm^2) for 5 minutes followed by lysing in 30 µl ice-cold RIPA buffer for murine islets and 90 µl RIPA buffer for human IEQs. Dark controls were immediately put on ice and lysed after 2 hours of dark incubation. For an additional temperature control cells were wrapped in foil, to avoid light exposure, and placed for 5 minutes in the light incubator, followed by immediate lysis. The positive control was treated with 33 ng/µl FGF2 and 10% FBS for 5 minutes followed by lysis. Cell lysates were shaken for 30 minutes at 4°C and centrifuged for 15 minutes at 12,000 rpm at 4°C. 30 µl of lysate mixed with loading buffer per lane were separated by SDS-PAGE (60 minutes, 140 V) and electro-blotted onto PVDF membranes (100 minutes, 100 V). After 1 hour blocking at room temperature, blots were further incubated with primary antibodies *anti* phospho-p44/42 MAPK (Erk1/2) (Thr202/Tyr204) and *anti* Akt, or *anti* phosph-Akt (Ser473)(D9E), *anti* Erk2 (K-23) and *anti* vinculin overnight at 4°C. Primary antibodies were applied as a 1:1000 dilution in blocking buffer, except *anti* vinculin, which was applied 1:10000. Secondary antibody, goat *anti* rabbit IgG(H+L)-HRP conjugated, was applied as 1:10000 dilution for 2 hours at room temperature. Chemiluminescence was developed as described in section 3.7.4.1.

3.7.4.5 Wavelength- and intensity-dependent signaling activation of pancreatic islets

To prove wavelength- and intensity-dependency of the light-dependent proliferative effect in pancreatic islets, immunoblotting was performed. In detail murine islets were first handled as described before in section 3.7.4.4. For wavelength-dependency the islets were illuminated for 5 minutes with white light and different wavelengths, blue, green and red (light (λ = 469 ± 35 nm, λ = 545 ± 25 nm, λ = 647 ± 70 nm, I = 64 µW/cm^2) by placing bandpass filters in front of a white LED. Blue-green illumination was achieved by using two LEDs (λ = 470 nm, λ = 535 nm, I = 64 µW/cm^2) at the same time. For intensity dependency they were illuminated with blue-green light for 5 minutes at different intensities (λ = 470 nm, λ = 535 nm, I = 0.05 µW/cm^2, I = 64 µW/cm^2, I = 255 µW/cm^2). Intensity was adjusted using a power meter. After illumination samples were further handled as described in section 3.7.4.4.

3.7.5 Light-dependent cAMP level changes in different cell lines

The change in cAMP levels in different cell lines (HEK293, HeLa, INS-1E) upon illumination was assessed using a real-time cAMP sensor (section 3.3.4). 1.5 x 10^4 cells were seeded in 100 µl appropriate complete medium in each well of PLO-coated 96-well clear bottom plate and incubated overnight at 37°C and 5% CO_2. After overnight incubation medium was changed to 100 µl appropriate transfection medium and cells were transfected with 200 ng total plasmid (100 ng cAMP sensor, 100 empty vector). 6 hours after transfection, medium was replaced by 100 µl Leibovitz's L15 complete medium. Twentyfour hours after transfection, cells were supplemented with 10 µM 9-*cis* retinal in the dark and incubated overnight at 37°C and 5% CO_2. After overnight incubation cells were supplemented with 2 mM beetle luciferin which was reconstituted in 10 mM HEPES and equilibrated in the dark at 37°C followed by luminescence recording for 30 minutes every 60 seconds. Illumination was performed using a custom-build, external array of high-intensity LEDs (λ = 505 ± 15 nm, I = 9.6 mW/cm^2), followed by another 15 minutes every 60 seconds luminescence recording. Recordings were analyzed by averaging the last ten data points of pre-illumination and locating the maximum value after illumination.

3.8 Physiological methods

3.8.1 Proliferation assay of primary pancreatic islets

To determine an increase of proliferation in primary pancreatic islets, islets were illuminated for 72 hours (murine islets) or 96 hours (human islets) with blue, green and blue-green light (λ = 470 nm, I = 64 µW/cm^2; λ = 535 nm, I = 64 µW/cm^2) and cell proliferation was assessed by performing an nucleotide incorporation assay using the Click-iT® Plus EdU Alexa Fluor® 488 Imaging Kit. 25 to 50 murine islets or 125 to 250 human IEQs per condition were cultured in either a well of a 96-well plate or a 35 mm dish in appropriate complete culture medium for 16 hours at 37°C in 5% CO_2. After 16 hours, medium was changed to fresh complete culture medium supplemented with 5 µM EdU followed by blue-green light illumination for 72 hours or 96 hours (the control dishes were kept in the dark). After 48 hours, 1 ml fresh complete culture medium supplemented with 5 µM EdU was added to each dish containing human IEQs. After 72 hours or 96 hours of illumination islets were collected and dissociated as described in section 3.6.4. Cells were fixed with 4% paraformaldehyde fixation solution for 8 minutes, followed by washing them three times with blocking buffer. Subsequently, newly synthesized DNA was stained by using the Click-iT® Plus EdU Alexa Fluor® 488 Imaging Kit following the manufacturer's instructions. Human islets were additionally stained with an *anti* insulin antibody to determine β-cell specific proliferation and total β-cell mass. For *anti* insulin staining, cells (after nucleotide incorporation assay) were incubated for at least 6 hours in blocking buffer at 4°C followed by overnight incubation with the primary antibody (*anti* insulin, 1:100) at 4°C. After primary antibody incubation cells were washed with PBST and the secondary antibody (Alexa Fluor555 goat anti rat IgG, 1:200) was applied for 1 hour at room temperature. For visualizing cell nuclei, the slides were stained with DAPI for 5 minutes at room temperature. After washing with PBST, the slides were mounted with Mowiol® 4-88. Images of dispersed murine islets were taken with an EVOS® fluorescence microscope and images of human dispersed islets were taken with LSM700. Percentage of proliferation in islets was defined by counting total number of cells (DAPI) and proliferating cells (EdU positive). Percentage of insulin positive proliferating cells was defined by counting total number of cells and cells that were EdU positive and insulin positive. The total β-cell mass was defined by determining the total number of insulin positive cells in ratio to total cell number.

3.8.2 Glucose-stimulated insulin secretion of human pancreatic islets

To prove functionality of human islets after 96 hours, of illumination a glucose-stimulated insulin secretion assay was performed. For every independent experiment at least duplicates for each condition were made and 200 to 500 human IEQs per condition were used. Human islets were illuminated with continuous blue-green light (λ = 470 nm, I = 64 µW/cm^2, λ = 535 nm, I = 64 µW/cm^2) and control dishes were kept in the dark. After 48 hours 1 ml fresh medium was added to each well containing. Human IEQs were collected after 96 hours of illumination and centrifuged for 5 minutes at 300 rpm. The supernatant was removed and human IEQs were resuspended in 1 ml basal buffer and transferred to a microcentrifuge tube followed by another 5 minutes centrifugation step at 300 rpm. The supernatant was again

removed and the pellet was resuspended in 500 µl basal buffer. IEQs were incubated for 30 minutes at 37°C in a shaking thermomixer at 300 rpm. After 30 minutes samples were centrifuged for 2 minutes at 300 rpm and 300 µl of the supernatant were collected and frozen at -80°C for further processing with the Human Insulin ELISA Kit. The remaining supernatant was removed and the IEQs were resuspended in 500 µl stimulation buffer followed by 1 hour incubation at 37°C in a shaking thermomixer at 300 rpm. After 1 hour the reaction was stopped by placing the tubes on ice followed by centrifugation for 1 minute at 300 rpm at 4°C and collection of 300 µl of the supernatant, which was frozen at -80°C for further processing with the Human Insulin ELISA Kit. In order to determine the internal insulin amount, the remaining supernatant was removed and 500 µl of acidic ethanol was added to each tube and IEQs were lysed for 1 hour in an ultrasonic bath. After 1 hour samples were vortexed for a few seconds followed by a 5 minutes centrifugation at 300 rpm. 300 µl of the supernatant were collected and frozen at -80°C for further processing with the Human Insulin ELISA Kit. The Human Insulin ELISA was performed according to the manufacturer's instructions. For normalizing insulin levels to the number of human IEQ, the total protein amount of each sample was determined from the cell lysate, by using the Pierce™ BCA Protein Assay Kit according to the manufacturer's instructions.

3.8.3 ATP quantification after blue-green light illumination in murine pancreatic islets

ATP levels were determined after different time points (2 minutes, 10 minutes, and 24 hours) of blue-green light illumination. Two hundred murine islets (100 islets per condition) were seeded in a 35 mm dish in murine islet complete culture medium and incubated overnight at 37°C and 5% CO_2 in the dark. For the 2 minutes and 10 minutes setup, islets were split in two tubes after overnight incubation and incubated for 2 hours in the dark before illumination. For the 24 hours setup, islets were split into two 35 mm dishes and were immediately illuminated after overnight incubation. Murine islets were illuminated with blue-green light for either 2 minutes, 10 minutes or 24 hours (λ = 470 nm, I = 64 µW/cm^2, λ = 535 nm, I = 64 µW/cm^2), followed by lysis in 60 µl ice-cold extraction buffer. Dark controls were immediately put on ice and lysed. The lysates were shaken for 30 minutes at 4°C, then boiled for 3 minutes at 95°C and finally centrifuged for 2 minutes at 20000 RCF at 4°C. ATP levels were determined by using the ATP Determination Kit according to the manufacturer's instructions. For normalizing ATP levels to the number of islets, the total protein amount of each sample was determined by using the Pierce™ BCA Protein Assay Kit according to the manufacturer's instructions.

3.8.4 Light-dependent cell viability variations of different cell lines

To assess cell viability upon illumination a MTT assay was performed. 3 x 10^4 cells were seeded in 100 µl cell line appropriate complete medium in each well of PLO-coated 96-well clear bottom plate and incubated overnight at 37°C and 5% CO_2. After overnight incubation medium was replaced with 100 µl cell line appropriate reduced serum starve medium and incubate for 24 hours at 37°C and 5% CO_2 in the dark. After 24 hours, cells were illuminated with blue light (λ = 470 nm, I = 64 µW/cm^2) for 24 hours at 37°C and 5% CO_2. Control cells were kept in the dark. After 24 hours illumination, medium was removed and cells were incubated for 1.5 hours

with 0.5 mg/ml thiazolyl blue tetrazolium bromide dissolved in PBS, followed by lysis with 70 µl acidic isopropanol. Finally absorbance measurements were taken at 570 nm and 690 nm in the microplate reader and cell viability was determined as described in section 3.4.5.

3.9 Statistics

Values are given as mean ± standard error of the mean (SEM) or standard deviation (SD), as indicated in the figure caption. Statistical significance was assessed by a two-tailed, paired Student's-t test. A value of $p \leq 0.05$ was considered to be significant.

CHAPTER 4: ENGINEERING AND CHARACTERIZATION OF RED-LIGHT-ACTIVATED RTKS

4.1 Introduction

The protection and regeneration of cell populations, for instance by inducing cell proliferation and by augmenting cell survival, is a key target in the development of new treatments for a variety of disorders as diabetes or Parkinson's disease. Currently, very few methods are available to precisely regulate cell proliferation and cell survival *in vivo*. Growth factors are capable of activating proliferative and pro-survival signaling cascades, particularly the MAPK/Erk and PI3K/Akt signaling pathways.[120,125,127,146,147] However, as described in section 1.3.2.4 the use of growth factors to activate their cognate receptors and subsequently proliferative and pro-survival signaling cascades as therapeutical approach has several major limitations such as non-specific effects and increased risk of cancer. An optogenetic approach may overcome these limitations of growth factors as therapeutic agents by providing temporal and local activation. In a joint effort the groups of Harlad Janovjak and Michael Grusch have succeeded in creating optogenetic GFRs, particularly opto-receptor tyrosine kinases (called "Opto-RTKs").[64] Opto-RTKs were generated following the approach of chimeric receptor design by fusing a blue-light-sensitive protein domain, the LOV domain of aureochrome 1 from *Vaucheria frigida* to the kinase domain of the receptor. Moreover, the extracellular ligand-binding modules of RTKs were removed to obtain chimeras that are only responsive to light but not to native ligands (Figure 4.1 A and B). Based on these blue-light-activated Opto-RTKs, red-light-activated RTKs were designed and engineered (Figure 4.1 C). Red light, instead of blue light, as an activation signal, was chosen because red light has compared to blue light an increased tissue penetration that allows additional to temporal and spatial precise signaling activation also a non-invasive remote control of the system. Additionally to deep tissue penetration, red light also offers minimal phototoxicity and it is not overlapping with the absorbance spectrum of many fluorescent proteins (e.g. typical blue, green, and red fluorescent proteins are excited at $\lambda \approx 440$, 490, and 560 nm, respectively). A codon optimized sensory domain of the cyanobacterial phytochrome 1, CPH1So, was fused to the kinase domain of the receptor. CPH1So was chosen as a light sensing domain because previous *in vitro* studies have shown that this N-terminal light sensing module of CPH1 homodimerizes reversibly upon red light illumination.[148]

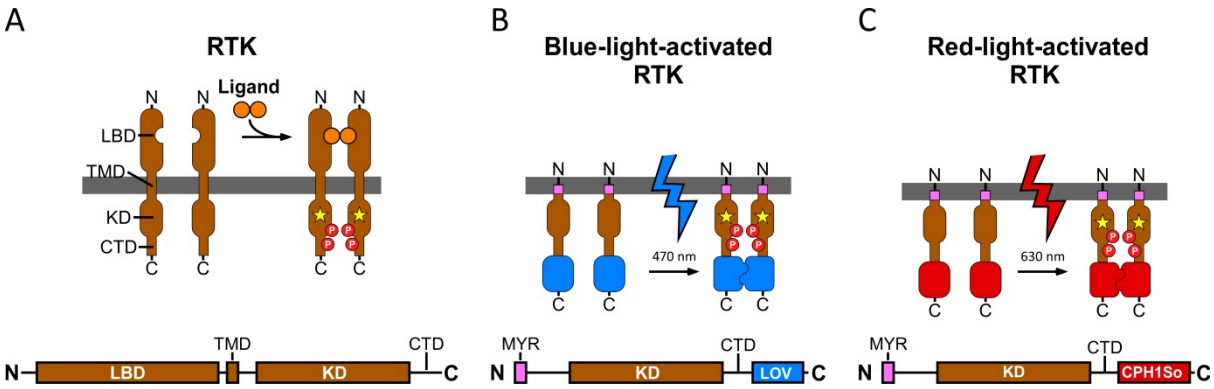

Figure 4.1 Structure and design of light-activated RTKs (A) RTKs consist of the extracellular ligand-binding domain (LBD), single-span transmembrane domain (TMD) and intracellular kinase domain (KD) and a C-terminal tail domain (CTD). (B) In blue-light-activated RTKs, only the intracellular domain is retained to generate a protein insensitive to its endogenous ligand. The chimeric receptor is attached to the membrane using a myristoylation membrane anchor (MYR) and a LOV domain is incorporated at the CTD to gain light sensitivity. (C) In red-light-activated RTKs, CPH1So was attached to the kinase domain of the receptors instead of the LOV domain.

4.2 Results

4.2.1 Expression and cytotoxicity assessment of a phytochrome sensory domain

Because of the homodimerizing feature of the phytochrome sensory domain, CPH1S, the domain was used to control protein–protein interactions in mammalian cells in response to red light. As CPH1S was previously never transferred to mammalian cells, expression in HEK293 cells, was tested and if expression would cause cytotoxicity in mammalian cells. CPH1S was first fused to the bright yellow fluorescent protein mVenus (mV), which allowed quantification of CPH1S expression. As a control a chemical homodimerization domain, the engineered FK506 binding protein (FKBP), was applied. The FKBP domain was previously robustly expressed in mammalian cells without measurable cytotoxicity.[149] Weak fluorescence was observed in HEK293 cells transfected with mV-CPH1S (Figure 4.2 A), which was indicative of poor protein expression and which may be limiting its further use as a red-light-sensing domain in chimeric receptors. To examine if the limited expression might originate from divergent codon usage of the cyanobacterial gene and the mammalian host cells, a codon-optimized variant of the gene (CPH1So) was synthesized. Indeed, CPH1So showed an increased expression in HEK293 cells without measurable cytotoxicity (Figure 4.2 B). Hence, CPH1So was further used for engineering red-light-activated RTKs.

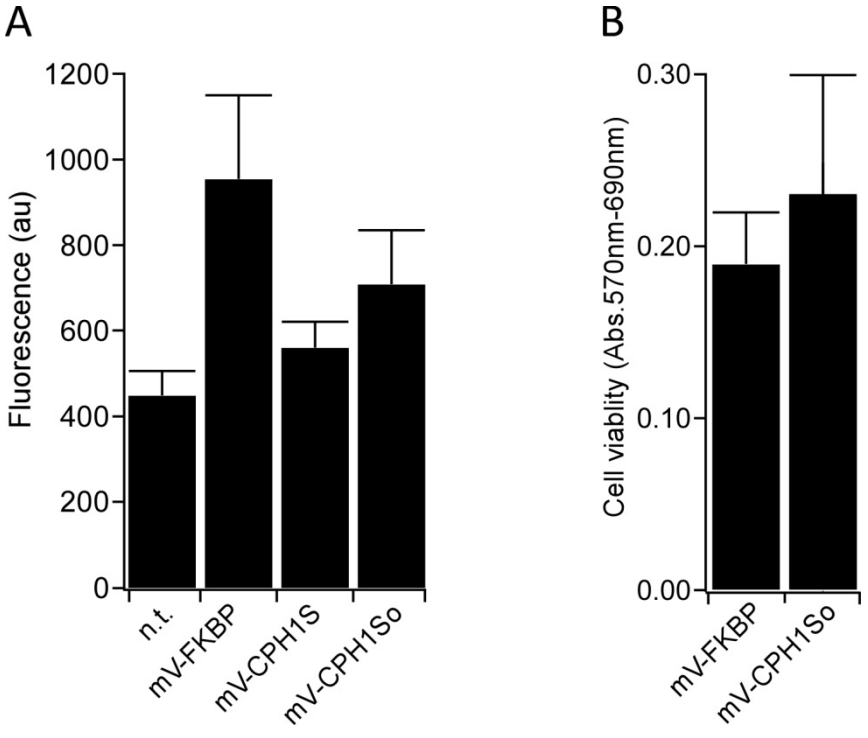

Figure 4.2 Expression and cytotoxicity assessment of a phytochrome sensory domain (A) Fluorescence intensity of HEK293 cells expressing CPH1S, CPH1So, and FKBP tagged with mV and non-transfected cells (n.t.). (B) Cell viability of HEK293 cells transfected with mV-FKBP or mV-CPH1So. Mean values ± SD are shown for three independent experiments each performed in triplicates.

4.2.2 Signaling activation by chimeric red-light-activated RTKs

Two red-light-activated RTKs were created by fusing CPH1So to the C-terminus of mFGFR1 and rtrkB, respectively (see section 3.2.2). After engineering these two red-light-activated RTKs, their ability to activate certain signaling pathways, characteristic for RTKs, was assessed using different read-outs.

4.2.2.1 MAPK/Erk pathway activation by red-light-activated RTKs

The ability of red-light-activated RTKs to activate the MAPK/Erk pathway, a key signaling pathway of RTKs, was examined. MAPK/Erk pathway activation in HEK293 cells expressing the chimeras, in response to red light was examined using Elk1 trans-Reporting System. In this assay, luciferase is produced under the control of an engineered Elk1 transcriptional activator and pathway activation is represented as raw light units (RLU). HEK293 cells expressing one of the two chimeric receptors (mFGFR1-mCPH1So or rtrkB-CPH1So) and supplemented with PCB responded to dim red light with strong MAPK/Erk pathway activation (Figure 4.3). Control experiments showed that (i) blue as well as green light illumination of cells expressing mFGFR1-mCPH1So did not result in pathway activation, (ii) red light had no effect on cells transfected with mFGFR1-FKBP fusion protein[149], and (iii) red light illumination of cells expressing rtrkB-CPH1So, but not supplemented with PCB, did not result in pathway activation (Figure 4.3). To prove kinase dependent activation of the MAPK/Erk pathway by red-light-activated RTKs, kinase activity was eliminated by introducing specific point mutations in each chimera. Y271F and Y272F mutations were introduced in mFGFR1-CPH1So and a K131A mutation was introduced in rtrkB-CPH1So.[150,151] In both chimeras these mutations abolished the red-light-dependent signaling activity, proving the kinase dependent signaling activation by red-light-activated RTKs (Figure 4.3). Finally, substituting R195 with glutamic acid in mFGFR1-CPH1So, which prevents the formation of a functionally essential, asymmetric kinase domain dimer in mFGFR1[152], abolished pathway activation (Figure 4.3), indicating that receptor dimerization is also required for receptor activation by CPH1So.

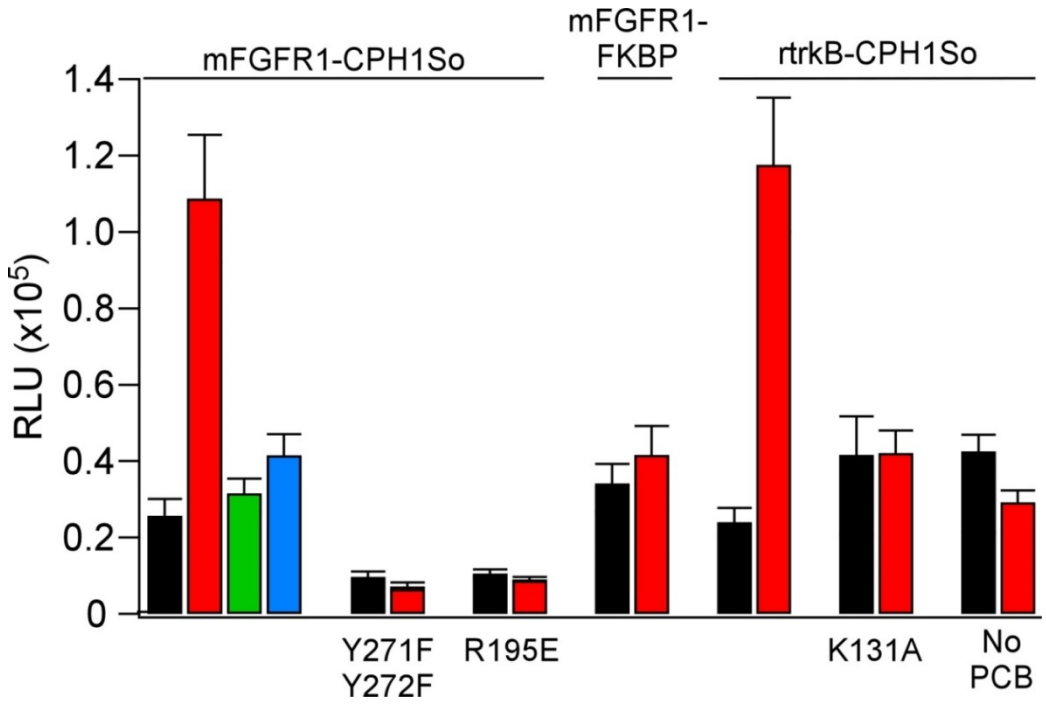

Figure 4.3 Activation of the MAPK/Erk pathway by mFGFR1-CPH1So and rtrkB-CPH1So in response to red light. Additional control experiments for mFGFR1-CPH1So show MAPK/Erk pathway activation upon green or blue light illumination or after the introduction of different mutations to mFGFR1-CPH1So (Y271F/Y272F and R195E). Control experiments for rtrkB-CPH1So sow MAPK/Erk pathway activation after the introduction of a point mutation (K131A) and without the supplementation of PCB. No MAPK/Erk activation was detected upon red light illumination in cells expressing mFGFR1-FKBP. MAPK/Erk pathway activation is expressed as RLU in HEK293 cells. Mean values ± SEM for technical replicates of 2–17 independent experiments, each performed in triplicate, are shown. Except "No PCB", mean value ± SEM for three technical replicates of one independent experiment is shown. Light intensity: 6.2 μW/cm^2 (red and green), 150 μW/cm^2 (blue); duration of illumination: 8 hours

4.2.2.2 Temporal precise signaling activation by rtrkB-CPH1So

To prove additionally to the signaling functionality also the ability of rtrkB-CPH1So to control signalling with high temporal precision, a time course experiment in HEK293 was performed. In this experiment the phosphorylation levels of Erk and Akt upon red light illumination were determined by immunoblotting in a time-dependent manner. The results demonstrated that 3 minutes of red light illumination were sufficient for activating the MAPK/Erk and PI3K/Akt pathways, detected as increased levels of phosphorylated Erk and Akt. After termination of the red light illumination, pErk levels returned to basal levels after 30 minutes, and pAkt levels already after 15 minutes (Figure 4.4). Overall, these results demonstrated that rtrkB-CPH1So allowed the activation of key intracellular signaling pathways with a high temporal resolution and in a reversible manner in response to red light.

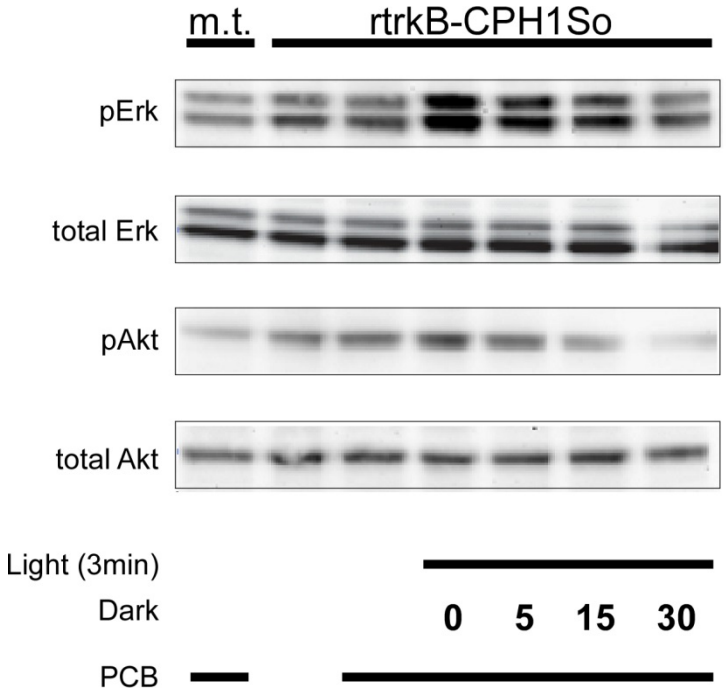

Figure 4.4 Time-dependent phosphorylation of Erk (pErk) and Akt (pAkt) in HEK293 cells transfected with rtrkB-CPH1So. Cells were illuminated for 3 minutes with red light (λ 630 ± 5 nm) followed by indicated duration (minutes) of darkness. Light intensity: 6.2 µW/cm^2

4.2.3 Activation of red-light-activated RTKs through various tissues

4.2.3.1 MAPK/Erk pathway activation through synthetic tissue

An important feature of red light is its ability to penetrate tissue more deeply than blue or green light.[143] To validate the ability of red-light-activated RTKs to be activated non-invasively through mammalian tissues, synthetic tissues mimicking the absorption spectrum of different mammalian tissue, such as muscle, skin and skull were generated by spiking agarose gels with different organic chemical dyes and comparing the absorption spectrum to published spectrums (Figure 4.5 A-C). HEK293 cells transfected with one of the two chimeric receptors (mFGFR1-CPH1So or rtrkB–CPH1So) were then stimulated through synthetic muscle, skin, and skull or combinations of two different synthetic tissues. Activation of the receptors was assessed by MAPK/Erk pathway activation using an Elk1 trans-Reporting System. Red light illumination through various synthetic tissues and combinations of synthetic tissues resulted in a potent induction of MAPK/Erk signaling (Figure 4.5 D and E). These results were the first indication that red-light-activated RTKs may allow non-invasive signaling activation *in vivo*.

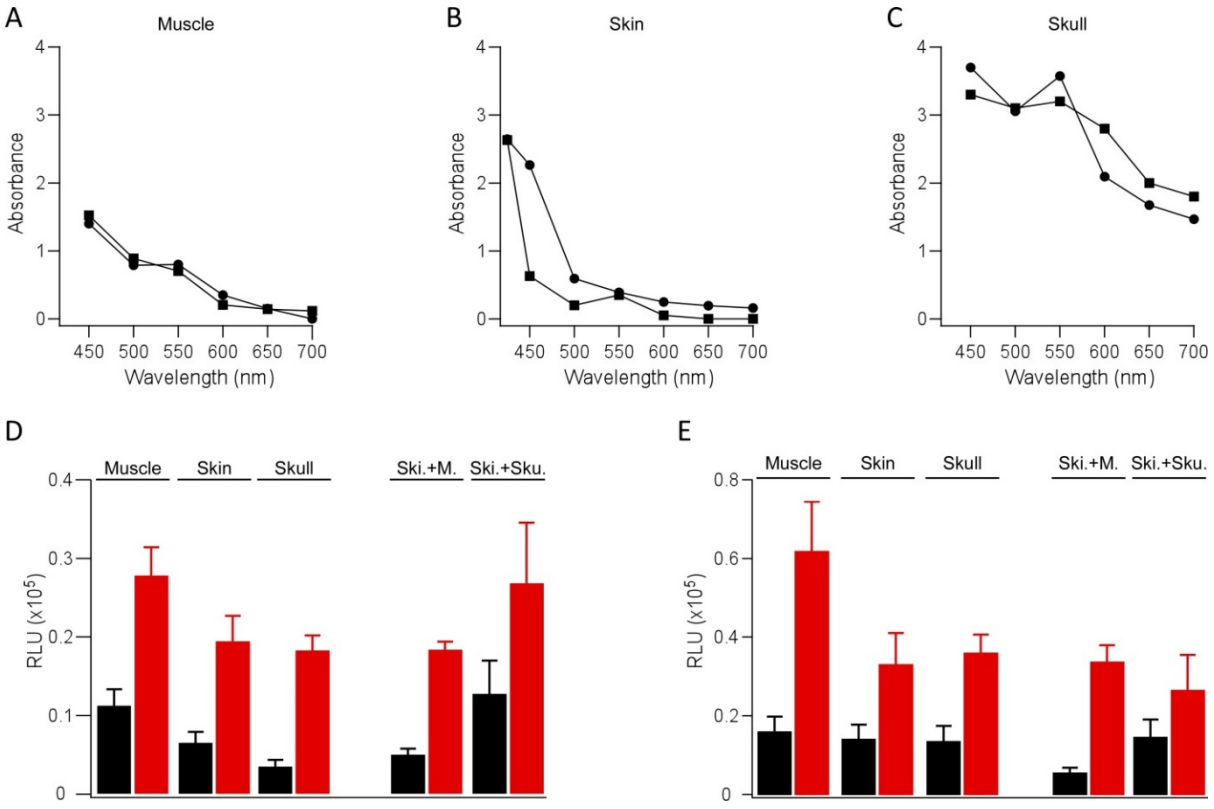

Figure 4.5 Absorption properties of synthetic tissues and MAPK/Erk pathway activation through synthetic tissues. (A-B) Absorption properties of mammalian 10 mm muscle (A), 0.5 mm skin (B) and 10 mm skull (C) (circles; data taken from literature)[142-144] and of the corresponding synthetic tissues produced by spiking agarose gel with various dyes (squares). (D-E) Activation of MAPK/Erk pathway in HEK293 cells transfected with mFGFR1-CPH1So (D) or rtrkB-CPH1So (E) illuminated through synthetic tissues mimicking 10 mm muscle, 0.5 mm skin, 3 mm skull, a combination of 0.5 mm skin and 10 mm muscle and a combination of 0.5 mm skin and 1.5 mm skull. Mean values ± SEM for one to three independent experiments performed in triplicates are shown. Light intensity: 6.2-17.5 µW/cm^2; duration of illumination: 8 hours

4.2.3.2 MAPK/Erk pathway activation in INS-1E cells through mouse abdomen

Synthetic tissues were mimicking the absorption, but not scattering properties of mammalian tissues.[153] Therefore an additional experiment using real mouse abdomen was performed. In initial experiments, the deeper tissue penetration of red light compared to other wavelength was verified by a light transmission experiment with blue, green and red light in mouse abdomen and skull. The results demonstrated that ~0.034% of red light penetrates through one centimeter of mouse abdomen and ~0.44% through 0.67 centimeter of the mouse head, whereas blue showed and penetration of around 0.004% through mouse abdomen and 0.002% through mouse head and green light less than 0.001% transmission through mouse abdomen and almost no transmission through mouse head (Figure 4.6 A and B).These results proved that red light had more than a 8 fold higher transmission through mouse abdomen and more than 220 fold higher penetration rate through mouse head than blue and green light. Based on this experimentally determined transmission of blue, green and red light through one centimeter of mouse abdomen and referring to the Kubleka-Munk theory (Equation 4.1), the transmitted light intensity through different depths of mouse abdomen was calculated (Equation 4.2). As an input intensity 5 W/cm^2 was chosen as this is representative for maximum intensities used in photodynamic therapy.[154] As presented in Figure 4.6 (C) the required light intensity of ~6 µW/cm^2 of red light to activate red-light-activated RTKs can be achieved up to a depth of 1.8 centimeter by applying a maximum input power of 5 W/cm^2. In contrast blue-light-activated RTKs can only be activated up to a tissue thickness of one centimeter due to the reduced tissue penetration of blue light and the increased activation intensity needed by blue-light-activated RTKs. These results indicated the possibility of activating red-light-activated RTKs transdermally without the need of an implant in mice.

Equation 4.1 Kubelka-Munk theory[155]

$$\text{Transmittance (T)} = \exp\left[-(K^2 + 2KS)^{1/2}\, d\right]$$

where K is the absorption coeffcient(cm^{-1}), S is the scattering coefficient (cm^{-1}) and d is depth from the surface (cm)

Equation 4.2 Output intensity through mouse abdomen

$$\text{Output intensity (µW/cm}^2\text{)} = \text{T(experimentally determined)}^{\text{Depth}} \times \text{input intensity (µW/cm}^2\text{)}$$

To validate this prediction, INS-1E cells were transfected with mFGFR1-CPH1So, illuminated with red light through one centimeter of mouse abdomen and MAPK/Erk activation was assessed by immunoblotting. INS-1E cells are an insulinoma cell line; they are frequently used in studies of pancreatic β-cell also in the context of diabetes.[141] INS-1E cells were chosen as a model system for this experiment because it was previously shown that decreased FGF signaling contributes to diabetes and that FGF signaling improves β-cell function in diabetic mice.[121,126] Furthermore β-cells (located in the pancreas) are located ~0.5 – 1 centimeter away from the mouse skin. We found that the MAPK/Erk pathway can be activated in INS-1E cells transfect with mFGFR1-CPH1So by red light illumination through ~1 centimeter of mouse abdomen (Figure 4.6 D). Notably, the applied light intensity (*I* =

3.0 mW/cm^2) was easily attained with standard light emitting diodes and were even lower than those used in photodynamic therapy[154], demonstrating the ability of non-invasive activation of red-light-activated RTK through mammalian tissue.

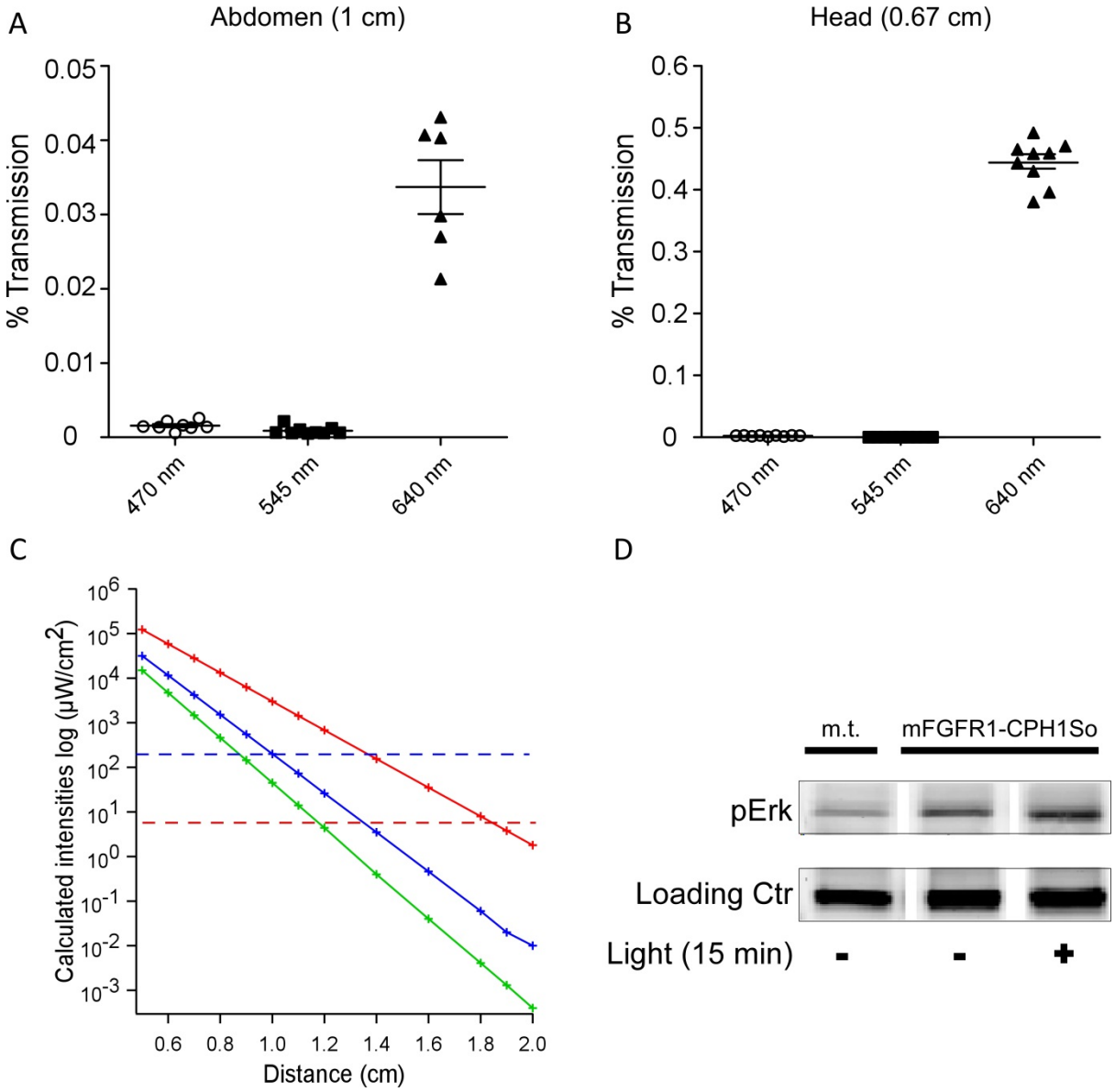

Figure 4.6 Light penetration and MAPK/Erk activation in INS-1E cells through mouse tissue. (A and B) Light penetration measurements of blue (470nm), green (545nm) and red (640nm) light through one centimeter of mouse abdomen (A) and 0.67 centimeter of intact mouse head (B). Percentages of transmitted light are presented. Error bars represent ± SEM. (C) Calculated transmitted light intensities (µW/cm^2) of red, blue and green light through different depths of moues abdomen. The applied input intensity was 5 W/cm^2. Dashed lines indicate minimal intensity need to activate Opto-RTKs (blue; 150 µW/cm^2) or red-light-activated RTKs (red; 6 µW/cm^2). (D) MAPK/Erk activation indicated by pErk levels in INS-1E cells transfected with mFGFR1-CPH1So and stimulated through one centimeter of mouse tissue with red light (λ = 647 ± 35 nm). Light intensity: 3 mW/cm^2; duration of illumination: 15 minutes

4.3 Discussion

There is a consensus in the field of regenerative medicine that a tightly spatial and temporal controlled growth factor signaling would be an efficient approach for tissue regeneration in diseases as diabetes.[135] Because light displays three major advantages over conventional pharmacological means as high temporal and spatial resolution and the possibility of remote application, light is the perfect stimulus for activating growth factor signals. The engineering of red-light-activated RTKs, which are activated with a wavelength of 630 nm, can overcome the drawback of blue-light-activated receptors that would also be candidates for light-dependent restoration, their limited tissue penetration, which is resulting in the use of invasive implants or powerful light sources.[129,130] The increased tissue penetration of red light over blue and green light was verified by a light penetration experiment through mouse abdomen and head (Figure 4.6). To achieve red light control of growth factor signaling, the sensory domain of phytochrome CPH1 was chosen as a red-light-sensing domain, because it was shown by *in vitro* assays that the sensory module of CPH1 undergoes light-dependent changes into a dimerization state.[148] First expression experiments showed that a mammalian codon optimization was necessary to increase protein expression to an acceptable level. In the past, several studies have already shown that modifying the coding sequence of a gene is an expedient way to increase protein expression, because it is known that the choice of synonymous codons in many species is strongly biased and that there is a correlation between high protein expression and the use of certain codons in a specific organism.[156,157] Efficient expression of codon-optimized genes can be related not only to the abundance of isoacceptor tRNAs in a specific organism, but also to the formation of a favorable secondary structure of the transcripts for translation. Hence, mammalian codon optimization can result in stable mRNA secondary structures because of stronger GC base pairing.[156,158] The mammalian codon-optimized version of CPH1S further allowed the engineering of red-light-activated RTKs. It was shown that red-light-activated RTKs are able to activate major growth factor signaling pathways with high temporal resolution, which cannot be achieved by growth factors or chemical activators.[135,149] Additionally the ability of red light to penetrate through different synthetic tissues and one centimeter of real mouse tissue, in order to activate red-light-activated RTKs and subsequently the MAPK/Erk pathway, was demonstrated. It was additionally proven that red-light-activated RTKs enable light-activated signaling *in situ* without invasive implants. These results verified that red-light-activated RTKs may be a very attractive tool for light-controlled cellular signaling *in vivo,* especially due to the potential for precise signaling activation to ensure a save application without side effects due to prolonged and systemic activation. Nevertheless red-light-activated RTKs also have to deal with some potential drawbacks, in particular for its translation into humans. Although it was proven that red light penetrates deep enough to activate red-light-activated RTKs remotely in mouse abdomen and head, for therapeutical applications in humans the tissue penetration of red light is probably not sufficient for applications deeper than subcutaneous layers. Light transmittance is affect by both the thickness and the optical properties of human tissue. The optical properties such as absorption and scattering depend on the composition of the tissue and are distinct, for instance, for skin, muscle, fat or bone.[143] In order to present the relevant factors for transmittance, according to previous studies, it can be roughly considered that a human body wall is composed of absorbing and

scattering particles and the Kubelka-Munk theory can be applied to estimate its optical properties.[143,155] The different levels of light transmittance through head and abdomen can be explained by the different optical properties based on different tissue composition. While abdominal tissue includes skin, blood, fat and muscle, the head is composed mainly out of skin skull and brain (Figure 4.6 A and B). The transmittance at a certain wavelength decreases exponentially with an increase in depth, based on this fact the transmitted light intensity transmitted through different depths of mouse abdomen was calculated (Figure 4.6 C). Based on these calculations it can be stated that red-light-activated RTKs can be controlled remotely in mice, but they are not suitable for an implant-free therapeutical approach in humans for disease like diabetes or Parkinson's disease as not enough light is reaching the tissue of interest.[143]

A contentious point of red-light-activated RTKs is the essential administration of the chromophore PCB to mice and humans. PCB is necessary for the ability of CPH1S to sense light, but mice as well as humans are lacking this chromophore. PCB is structurally closely related to the human bile pigments biliverdin and bilirubin.[159] Bilirubin is one of the most potent endogenous antioxidant substrates.[160] In relation to this characteristic of PCB, previous studies showed several positive effects of PCB relating to atheroprotection, liver regeneration and diabetic neuropathy.[160-162] PCB from *Spirulina* can be orally administrated to mice. Because *Spirulina* is used as a nutritional supplement for human and animals in many countries, as natural dye in cosmetics as well as supplement in pharmaceutical productions, it may be feasible to produce commercial quantities of PCB for human administration.[162] By assuming that humans and rodents digest and absorb *Spirulina*-bound PCB in a comparable manner, it can be concluded that an intake of 2 heaping tablespoons daily would be likely to have antioxidant activity in humans, but it is not known how much intake would be sufficient for red-light-activated RTKs.[159] Because a possible future application of red-light-activated RTK could be the regeneration of pancreatic β-cells, the positive effect of PCB on diabetic neuropathy is an attractive aspect and would allow a therapeutic approach against diabetes focusing on both the causal event (loss of functional β-cells) as well as a secondary disease (neuropathy) simultaneously. However, the necessity of PCB administration are on the one hand very favorable because of its additional positive antioxidant effect and it is ease to administer, on the other hand the routinely regular administration of PCB in human is not yet studied in detail and the assumptions on positive effects are based on animal studies. To exclude any severe side effects due to long-term PCB administration or incorrect dosage further animal studies as well as clinical studies are necessary to guarantee safety.

Additional to the required light implant and the administration of PCB for a therapeutical use in humans, red-light-activated RTKs also entail the necessity of gene therapy. Gene therapy is a fascinating and innovative technology due to its potential to treat diseases at their genetic roots.[131,163,164] In gene therapy a malfunctioning gene is counteracted or replaced within the adversely affected cells. As simple as the concept of gene therapy sounds, the manner to put it into practice is quite challenging. To deliver new genetic information to target cells, complex cellular and tissue barriers have to be overcome without disrupting essential cellular regulatory mechanisms.[132] In the last 25 years, remarkable progress has been made and a number of gene therapy applications have provided benefit to patients in

clinical trials. For example the successful transduction of bone marrow stem cells with lentiviral vectors to treat early-onset metachromatic leukodystrophy as well as the successful treatment of patients with inherited retinopathies and hemophilia B by local or systemic injection of adenovirus-associated viral vectors.[131,163-165] Nevertheless every now and then severe side effects occur after viral based gene therapy as the development of leukemia after treating severe combined immune deficiency patients with murine leukemia virus gene delivery vectors.[131] Although there are promising numbers of successful gene therapy approaches there are remaining challenges in providing a quantitative prediction of actual oncogenic risk in clinical setting as well as further improvements in safety, efficacy and manufacturing of gene delivery vectors are still required.[131,132] Therefore the option to apply red-light-activated RTKs to regenerate disease affected cells as in diabetes or other degenerative disease is of course an option, but probably also because of the necessity of a light implant and PCB administration, a last therapeutical approach and not as a state of the art therapy.

However, red-light-activated RTKs are attractive for optogenetic applications in animal models, given that red light offers deeper tissue penetration than other wavelengths, transdermal control and the fact that PCB can be easily orally administered. Gene deliveries via lentiviral vectors or adeno–associated viral vectors in mice are well-established methods.[101,102,166] Red-light-activated RTKs are an innovative tool for studying the spatial and temporal involvement of growth factor signaling events in degenerative disease, but also for developmental and behavioral studies. In developmental research a key aspect is the manipulation of cellular signaling processes, to understand the complex and acutely orchestrated signaling cascades of multiple interacting pathways that finally give rise to complex tissues and organs. Traditional methods are often limited to understand these temporal and spatial coordinated signaling events because of less specificity or lethality of full knockouts. By now methods to completely silence signals are well established, but applying signal control with high spatial and temporal precision is still challenging. Light-controlled tools can help to unravel these complex mechanisms due to their unprecedented precise control, allowing the investigation of specific cell types or signaling pathways and their local and temporal regulation during development.[65,167] Moreover the field of behavioral research, also in combination with degenerative disorders as Parkinson's disease, is an attractive field for applying red-light-activated RTKs, because no implants are needed for receptor activation a higher throughput of animals is enabled and animals are not influenced and disabled by additional hardware. Remote receptor control allows free moving and normal behavior of the animals during the study, which will lead to more robust and reliable outcomes of behavioral studies. Because of all these facts red-light-activated RTKs probably will not be the first choice of treatment for degenerative diseases, but a very attractive tool for a broad variation of research fields.

CHAPTER 5: LIGHT INDUCED β-CELL PROLIFERATION

5.1 Introduction

Optogenetic tools can only be used as therapeutic agents by using gene therapy, which is accompanied by risk factors that are difficult to predict such as described in section 4.3. Therefore, a new light-based strategy was investigated, that does not require gene transfer, to achieve promotion of cell proliferation and increase of cell survival, the key goal in the treatment of various diseases. As model cells, murine and human pancreatic islets/β-cells were used, since the lack of functional β-cells is the main cause of diabetes mellitus, induced by various genetic and environmental factors. This new light-based approach does not require gene transfer, it has the potential to be fully reversible, unlike in the case of conventional optogenetics and growth factor therapy, and in contrast to pharmacological approaches, offers tissue specificity. As it will be described in the following chapter, it is based on endogenous light-sensitive mechanisms, which lead to the activation of proliferative and pro-survival cellular signaling mechanisms.

Various studies in a broad spectrum of research fields have already investigated the influence of visible light on cell behavior. For example, Buscone and colleagues showed that rhodopsin as well as OPN3 is expressed in human hair follicle cells and that blue light illumination exerts a positive effect on their growth *ex vivo*, this effect could be reduced after silencing OPN3 by siRNA transfection, indicating the potentially involvement of OPN3 in this effect.[168] Another study showed that green light illumination directed the migration of human orbital fat stem cells (OFSC) through the activation of the MAPK/Erk/p38 signaling pathway. In this study, it was hypothesized, based on gene expression analysis, that the retinal pigment epithelium-derived rhodopsin homolog and also OPN3 are responsible for the green-light-induced OFSC migration.[169] In chicken embryos, it was demonstrated that *in ovo* illumination with green light resulted in enhanced body and muscle weight, a significant increase in the number of skeletal muscle cells as well as an enhanced number of proliferating cells in the intact muscle.[170] In addition to these blue- and green-light-based studies, there is also an extensive number of studies that investigate the positive effect of red and near-infrared light on cell behavior in various cell and disease models, ranging from neurodegenerative disorders, over wound healing to skeletal muscle regeneration.[171] For instance, several studies showed the therapeutic effect of red and near-infrared light on MPTP- and MPP+ -induced Parkinson's disease models.[172,173] There is now a growing consensus that red and near-infrared light is acting on cells through cytochrome c oxidase (CcO), as primary photoacceptor. CcO is the terminal enzyme of the mitochondrial electron transport chain, mediating the transfer of electrons from cytochrome c to molecular oxygen.[171,174] CcO has an absorption maximum around 430 nm and a secondary peak the red/near-infrared wavelength range.[175] Absorption of light by CcO can increase the levels of ATP and reactive oxygen species, leading to enhanced energy availability and signal transduction.[171,174] Although in some of these studies, the detailed molecular mechanisms of the light-induced cellular effects were partially unraveled, in many cases they are still unresolved.

5.2 Results

5.2.1 Characterization of light-induced cell behavioral effects

5.2.1.1 Light-induced proliferation of murine and human islet cells

The influence of visible light on islet cell proliferation was determined by a nucleotide incorporation assay. Murine islets were illuminated with different wavelengths of visible light (blue: λ = 470 nm, green: λ = 535 nm, blue-green: λ = 470 nm and λ = 535 nm) to determine light dependent proliferative effects. Blue or green light alone was not sufficient to increase proliferation in murine islets (Figure 5.1 A and B), but the combination of blue and green light (blue-green light) led to a significant increase in proliferation in murine islets after 72 hours of illumination (Figure 5.1 C). 96 hours of combined blue-green light illumination also led to a significant increase in proliferation in human islets (Figure 5.1 D). Except for two outliers in the human data set, murine islets showed a higher level of basal proliferation with around 2%, compared to human islets with an average basal proliferation of less than 1% (excluding the two outliers that exhibited high levels of proliferation in the dark). However, human islets as well as mouse islets showed a very reproducible increase in proliferation upon blue-green light illumination (1.6- and 1.4-fold, respectively).

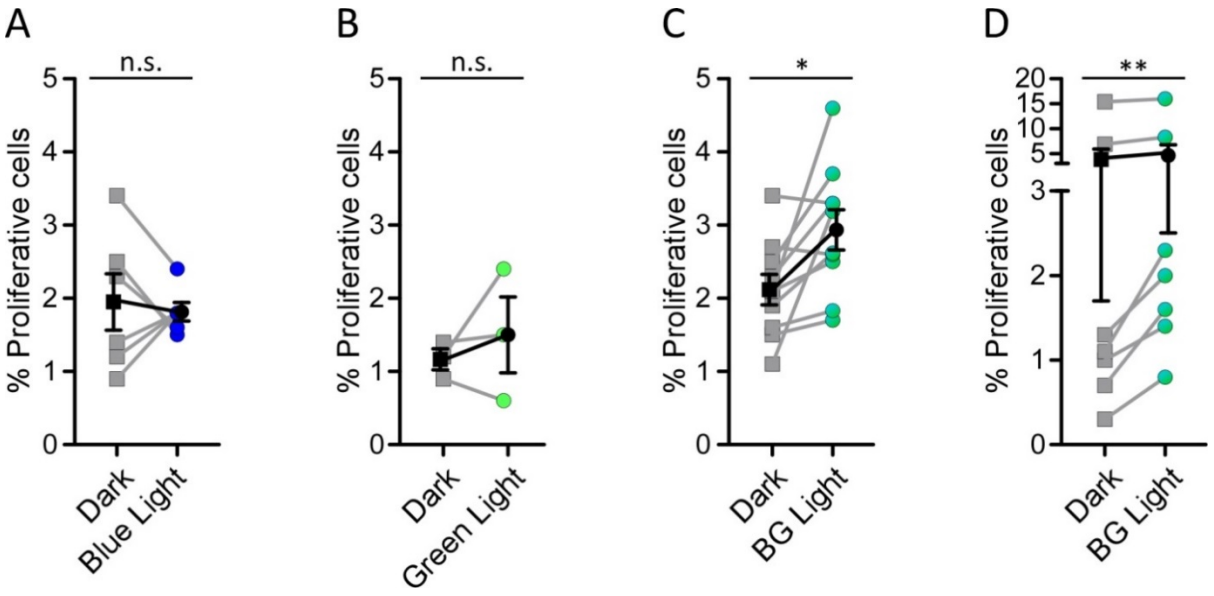

Figure 5.1 Light-induced proliferation of murine (A-C) and human (D) islet cells. (A) Murine islets: Percentage of proliferative cells upon blue light illumination, compared to non-illuminated cells (Dark). Individual experimental values (grey, blue) and mean (black) ± SEM are shown for six independent experiments (light intensity: 14 µW/cm^2; duration of illumination: 72 hours). (B) Murine islets: Percentage of proliferative cells upon green light illumination, compared to non-illuminated cells. Individual experimental values (grey, green) and mean (black) ± SEM are shown for three independent experiments (light intensity: 14 µW/cm^2; duration of illumination: 72 hours). (C) Murine islets: Percentage of proliferative cells upon blue-green (BG) light illumination, compared to non-illuminated cells. Individual experimental values (grey, blue-green) and mean (black) ± SEM are shown for ten independent experiments (light intensity: 14 µW/cm^2 each wavelength; duration of illumination: 72 hours). (D) Human islets: Percentage of proliferative cells upon BG light illumination, compared to non-illuminated cells. Individual experimental values (grey, blue-green) and mean (black) ± SEM are shown for seven independent experiments (light

intensity: 64 µW/cm^2 each wavelength; duration of illumination: 96 hours) (A-D) two-tailed, paired Student's t–test, a value of $p \leq 0.05$ was considered to be significant (*$p \leq 0.05$, **$p \leq 0.01$, n.s.: not significant)

5.2.1.2 Influence of blue-green light on β-cell specific proliferation and total β-cell mass in human islets

The β-cell specificity of the proliferative effect as well as the influence of illumination on total β-cell mass was determined by *anti*-insulin antibody staining. Because the percentage of β-cells in murine islets is up to 80%, no specific analysis of β-cells was performed in the mouse tissue. As human islets are more heterogeneous in regard to cell type distribution than murine islets, it was investigated whether the proliferative effect in human islets is β-cell specific. A very clear trend of increased β-cells proliferation upon blue-green light illumination can be observed. The results are not significant due to the inclusion of one dataset that shows an extreme increase in proliferation. In the dark, 0.5% of all cells are proliferative β-cells (~27% of all proliferative cells), whereas 96 hours of blue-green light illumination led to an almost 4 fold increase of proliferative β-cells (Figure 5.2 A), proving that at least a substantial part of the light induced proliferation is β-cells specific (~40% of all proliferative cells). Shown previously, proliferative agents often displayed concomitant de-differentiating effects,[103,176] therefore the overall composition of illuminated islets was monitored by determining the total number of β-cells. Insulin staining revealed no reduction, but rather a small overall increase of the total β-cell mass after illumination (Figure 5.2 B), indicating that blue-green light illumination of 96 hours did not induce any de-differentiation.

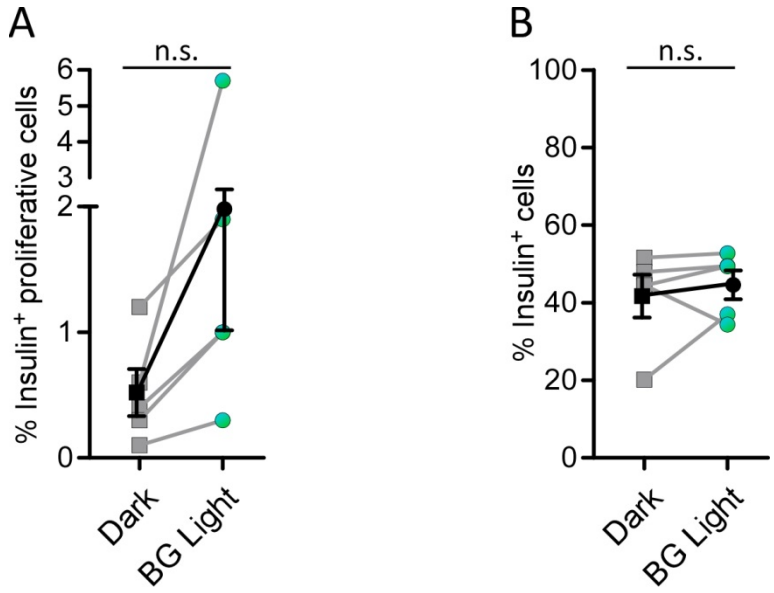

Figure 5.2 Determination of β-cell specific proliferation and total β-cell mass in human islets. (A) Percentage of insulin positive ($^+$) proliferative cells after BG light illumination, compared to non-illuminated cells. Individual experimental values (grey, blue-green) and mean (black) ± SEM are shown for five independent experiments. (B) Percentage of total insulin$^+$ cells after BG light illumination, compared to non-illuminated cells. Individual experimental values (grey, blue-green) and mean (black) ± SEM are shown for five independent experiments. (A-B) Light intensity: 64 µW/cm^2 each wavelength; duration of illumination: 96 hours; two-tailed, paired Student's t–test, a value of $p \leq 0.05$ was considered to be significant (n.s.: not significant)

5.2.1.3 Preserved islet functionality upon blue-green light illumination

To investigate the effect of prolonged illumination on islet functionality, in particular on their ability to secrete insulin in response to high glucose, a glucose-stimulated insulin secretion assay was performed. After 96 hours of blue-green light illumination, basal insulin secretion (3.3 mM glucose) as well as high glucose (16.7 mM glucose) stimulated insulin secretion of human islets was assessed. While donor to donor variability of the overall insulin secretion ability was observed, blue-green light illumination did not have a negative effect on islet functionality. On the contrary, blue-green light illumination rather led to an increase of islet insulin secretion potential. While blue-green light illumination had no or only a small effect on insulin secretion under basal glucose conditions, islets from two donors (donor 1 and donor 3) secreted more insulin after illumination compared to untreated islets, when challenged with high-glucose (Figure 5.3 A). Moreover, the amount of intracellular insulin was investigated to evaluate for conserved β-cell properties after illumination. Except for donor 3, blue-green light illuminated human islets contained similar amounts of intracellular insulin compared to untreated islets from the same donor, further demonstrating that blue-green light illumination had no negative effect on β-cell properties (Figure 5.3 B). The unexpected high intracellular insulin level of the untreated sample of donor 3 arises from one outlier of the sample replicates and is therefore not a representative data point.

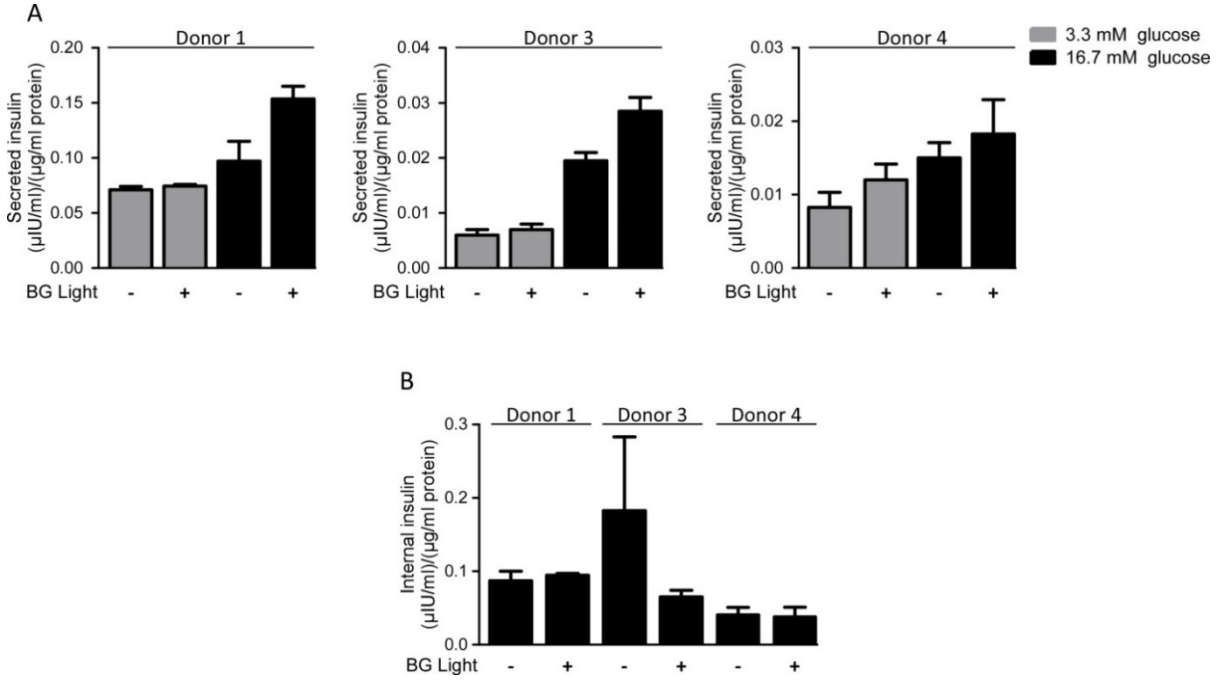

Figure 5.3 Influence of blue-green light illumination on insulin secretion (A) and internal insulin levels (B) in human islets (A) Measurement of glucose-stimulated insulin secretion in human islets kept in the dark or illuminated with blue-green light. Secreted insulin values were normalized to total protein amount of each sample. (B) Measurement of internal insulin of human islets kept in the dark or illuminated with blue-green light. Secreted insulin values were normalized to total protein amount of each sample. (A-B) Light intensity: 64 µW/cm^2; duration of illumination: 96 hours; values were assessed in two (donor 1 and 3) or four replicates (donor 4) for each donor and mean values ± SEM are shown.

5.2.2 Signaling activation in murine and human islets cells

5.2.2.1 MAPK/Erk signaling activation in murine and human islets

The MAPK/Erk pathway was previously associated with positive proliferative effects in pancreatic islets and β-cells, which can for example be activated by various growth factors.[120,126,177,178] The ability of blue-green light illumination to activate the pro-proliferative MAPK/Erk pathway was assessed by determining the levels of pErk by immunoblotting. Five minutes of illumination was sufficient to activate the MAPK/Erk pathway, both in murine (Figure 5.4 A and C) and human islets (Figure 5.4 B and D). pErk levels were increased by a factor of 2.5 in murine islets and a factor of 2.3 in human islets after light treatment. As a positive control the fibroblast growth factor 2 (FGF2) combined with 10% FBS, acting on multiple GFRs, was used. Previous studies have proven the ability of FGFs to activate the MAPK/Erk pathway in β-cells, as well as their significant role in β-cell function.[121,122,126]

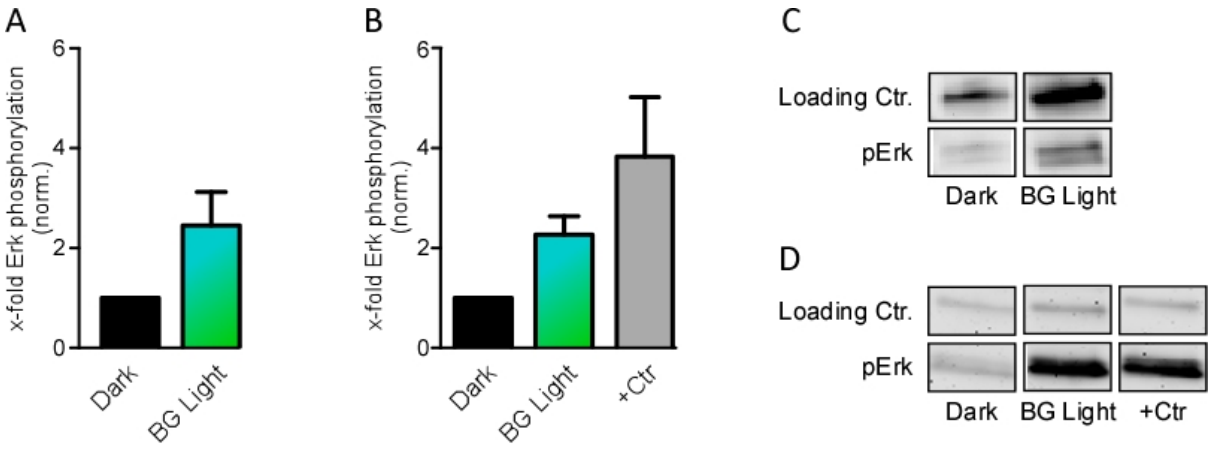

Figure 5.4 MAPK/Erk signaling activation in murine (A, C) and human islets (B, D). (A) Murine islets: Quantification of blue-green-(BG) light-induced pErk increase from immunoblott analysis. Mean values ± SEM are shown for four independent experiments. (B) Human islets: Quantification of BG-light-induced pErk increase from immunoblott analysis. +Ctr: positive control stimulation with 10% FBS and 33 ng/ml FGF2. Mean values ± SEM are shown for three independent experiments. (C) Murine islets: Representative immunoblot of BG-light-induced pErk increase. (D) Human islets: Representative immunoblot of BG-light-induced pErk increase. (C-D) Loading Ctr: (C) total Akt or (D) vinculin; light intensity: 64 μW/cm^2; duration of illumination: 5 minutes

5.2.2.2 PI3K/Akt signaling activation in murine and human islets

The PI3K/Akt pathway was previously associated with pro-survival effects in pancreatic islets and β-cells, which can be activated, similar to the MAPK/Erk pathway, by various growth factors.[120,126,177,178] The ability of blue-green light illumination to activate the pro-survival PI3K/Akt pathway was assessed by determining the levels of pAkt by immunoblotting. Again, 5 minutes of illumination was sufficient to activate the PI3K/Akt pathway, both in murine (Figure 5.5 A and C) and human islets (Figure 5.5 B and D). pAkt levels were increased by a factor of ~2 in murine and human islets. FGF2 combined with 10% FBS was again used as a positive control for pathway activation.[122,126] The level of pAkt increase upon blue-green light in human islets was comparable with that of the positive control (Figure 5.5 B and D).

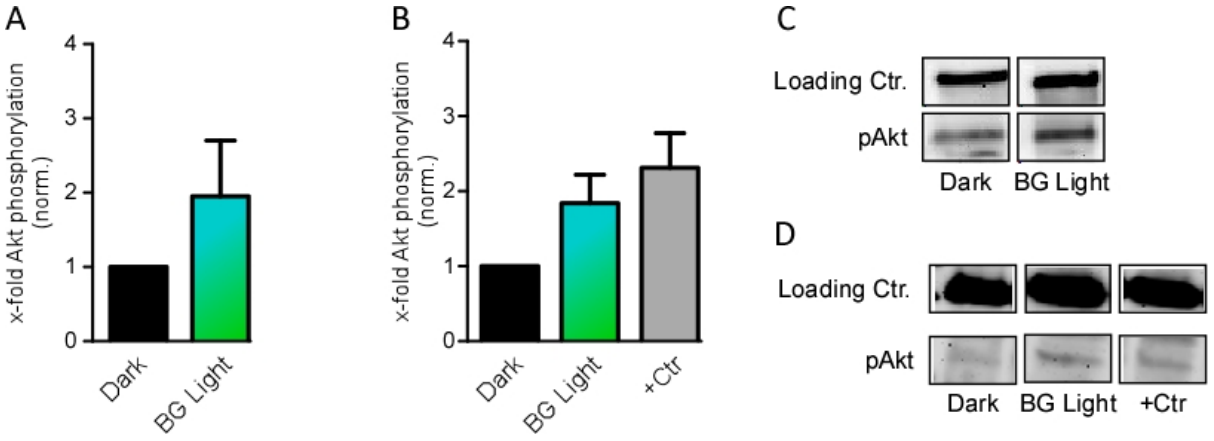

Figure 5.5 PI3K/Akt signaling activation in murine (A, C) and human islets (B, D) (A) Murine islets: Quantification of BG-light-induced pAkt increase from immunoblott analysis. Mean values ± SEM are shown for two independent experiments. (B) Human islets: Quantification of BG-light-induced pAkt increase from immunoblott analysis. +Ctr: positive control stimulation with 10% FBS and 33 ng/ml FGF2. Mean values ± SEM are shown for three independent experiments. (C) Murine islets: Representative immunoblot of BG-light-induced pAkt increase. (D) Human islets: Representative immunoblot of BG-light-induced pAkt increase. (C-D) Loading Ctr: (C) vinculin or (D) total Erk; light intensity: 64 μW/cm^2; duration of illumination: 5 minutes

5.2.3 Characterization of the endogenous light-sensing mechanism

5.2.3.1 Wavelength dependency of MAPK/Erk activation by visible light

To determine the wavelength dependency of the light-based effects in murine islets, MAPK/Erk pathway activation upon illumination with different wavelengths (blue: λ = 469/35 nm, green: 545/25 nm, red 647/70nm, blue-green: λ = 470 nm and λ = 535 nm, white: λ = 400-700 nm) was assessed by immunoblotting. Five minutes of illumination with a combination of blue-green light as well as with green light alone resulted in increased phosphorylation of Erk, whereas blue or red light alone did not elicit any signaling activation (Figure 5.6). As expected, white light, which includes light of the whole wavelength spectrum of visible light, also activated the MAPK/Erk pathway in murine islets.

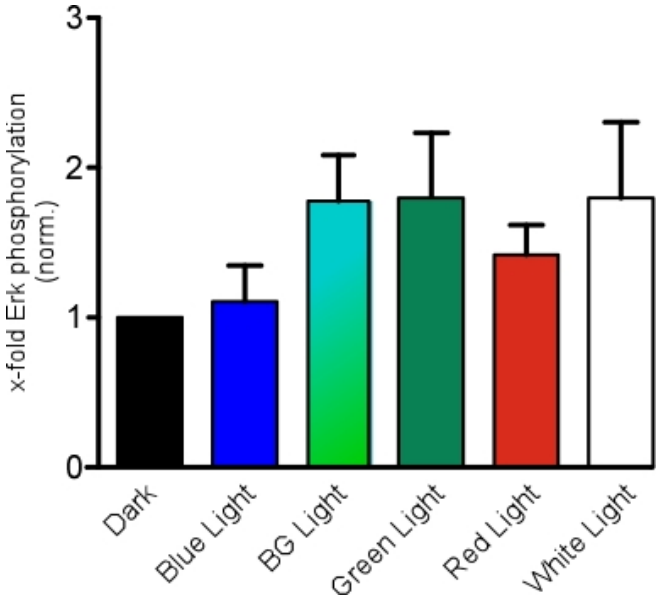

Figure 5.6 Influence of wavelength on light-dependent MAPK/Erk pathway activation in murine islets. Quantification of pErk levels in murine islets assessed by immunoblotting. Light intensity: 64 µW/cm^2 each wavelength; duration of illumination: five minutes; mean values ± SEM are shown for three to four independent experiments.

5.2.3.2 Intensity dependency of MAPK/Erk activation by blue-green light

To investigate how these observed effects depend on light intensity, MAPK/Erk pathway activation upon illumination with different intensities of blue-green light was assessed by immunoblotting. Comparable levels of MAPK/Erk pathway activation over a wide range of intensities from 0.5 µW/cm^2 to 255 µW/cm^2 blue-green light was determined (Figure 5.7), indicating a very robust and light-sensitive mechanism.

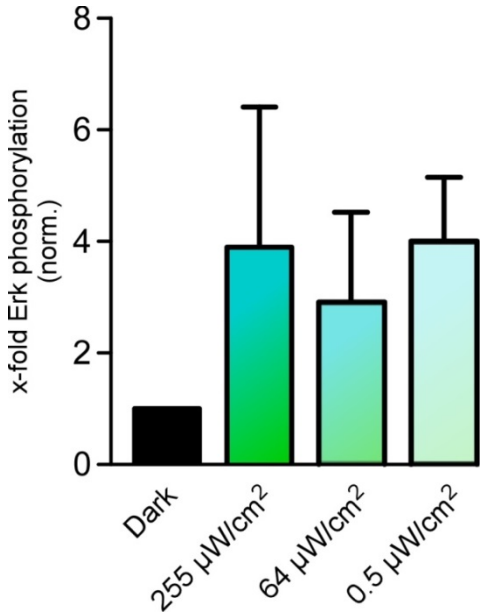

Figure 5.7 Influence of light intensity on BG-light-dependent MAPK/Erk pathway activation in murine islets. Quantification of pErk levels in murine islets assessed by immunoblotting after five minutes illumination with different light intensities of blue-green light. Mean values ± SEM are shown for three to four independent experiments.

5.2.3.3 Alternative protocol for dark samples

To exclude that the observed light-based effects occur due to different sample handling, which results in different sample environment such as temperature differences, control immunoblot experiments were performed. In this control experiment, an additional dark control was included, which was protected from light by foil and placed for the same time period in the light incubator as the light sample. This procedure differed from the “standard” immunoblott procedure, where the dark control was put immediately on ice and lysed. In addition temperature was manually verified during the whole incubation period. There was no increased MAPK/Erk pathway activation in the dark sample placed in the light incubator (Dark(i)), compared to the original dark control (Figure 5.8 A and B), indicating that MAPK/Erk signaling activation is due to illumination with blue-green light and not due to temperature changes resulting from illumination.

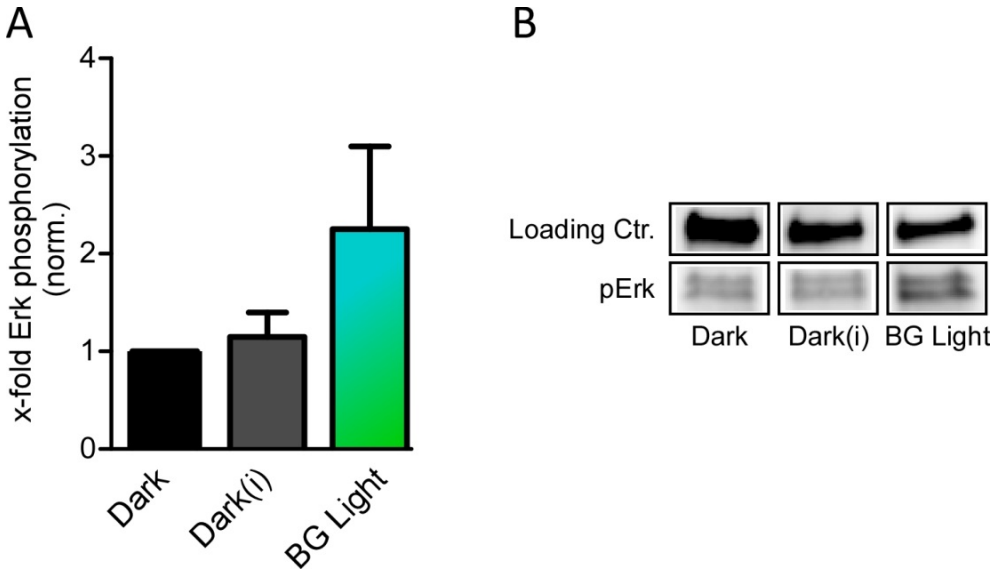

Figure 5.8 MAPK/Erk pathway activation in murine islets including an alternative dark control, to exclude environmental influences due to handling differences. (A) Quantification of pErk levels in murine islets assessed by immunoblotting. Mean values ± SEM are shown for two independent experiments. (B) Representative immunoblot of temperature control experiments. Loading Ctr: vinculin; light intensity: 64 µW/cm^2; duration of illumination: 5 minutes

5.2.3.4 Opsin expression in murine and human islets

To identify opsins expressed in murine and human islets, reverse transcribed cDNA from isolated islet RNA was analyzed by PCR. Insulin as well as β-actin was used as a positive control for RT-PCR, because they are expressed in β-cells. As an additional control a –RT (no added reverse transcriptase) control was introduced to exclude any genomic DNA (gNDA) contamination. Opsin expression was always verified with two primer sets for every specific opsin (Table A3), which were quality tested using gDNA (not shown). Each RT-PCR product was assessed by gel electrophoresis as well as sequencing. Some of the PCR products, such as for murine OPN1WM and Melanopsin, resulted from mispriming, as determined by sequencing, and did not indicate actual opsin expression (Figure 5.9, Table 5.1). Two opsins, OPN3 and rhodopsin, were expressed in both, murine and human islets. OPN3 showed intense bands and its expression was also verified by sequencing analysis (Figure 5.9, Figure 5.10, Table 5.1). Rhodopsin was expressed at lower levels, but also in both, human and murine islets (Figure 5.9, Figure 5.10, Table 5.1). Due to these results, it was hypothesized that OPN3, rhodopsin or a combination of both could be responsible for the blue-green-light-induced effects in pancreatic islets. This hypothesis is also coinciding with the absorption spectrum of these two opsins and the blue-green light illumination regime (Table 1.1).

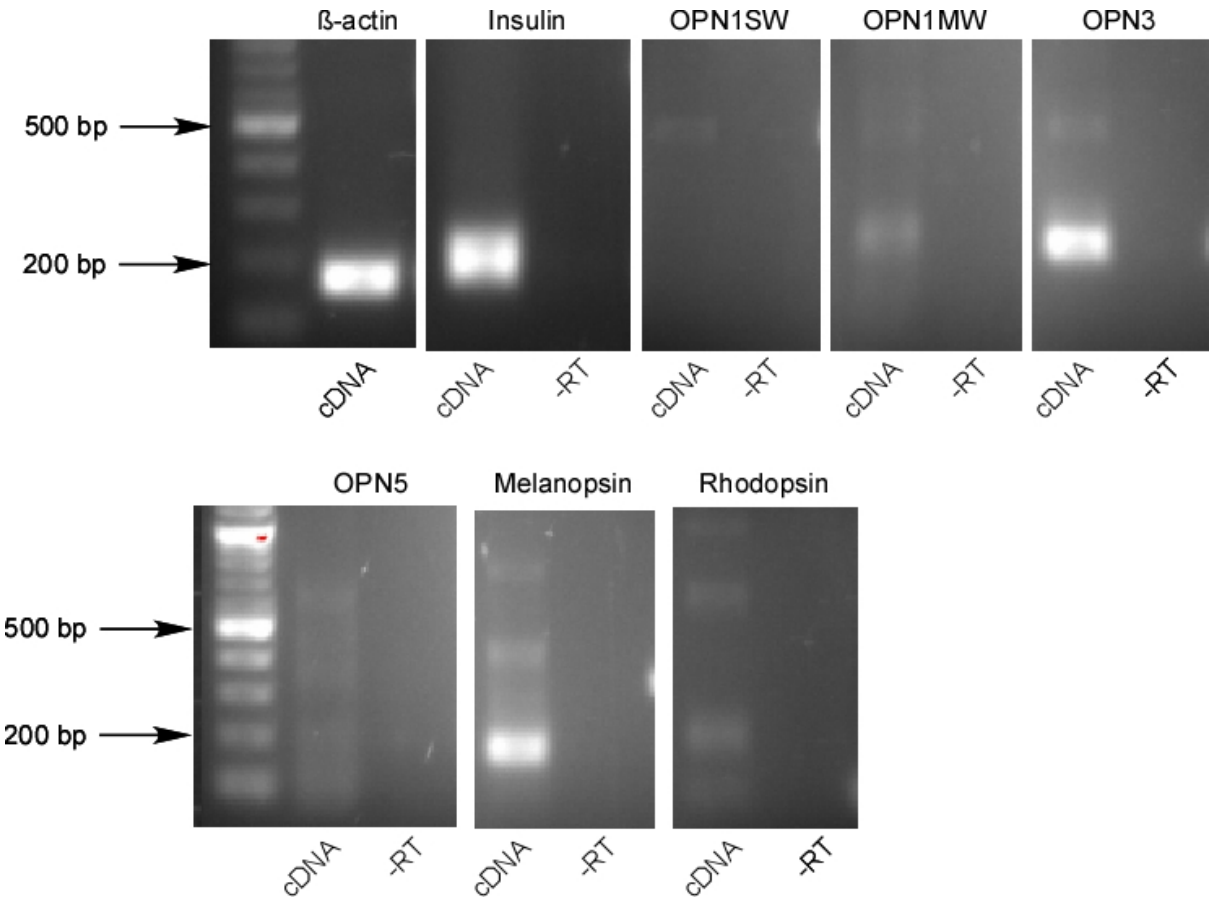

Figure 5.9 Determination of opsin expression in murine islets. Representative agarose gels of RT-PCR products for one primer set for each opsin. A -RT sample was used as control to exclude gDNA contamination. Exposure time was automatically adjusted for each gel.

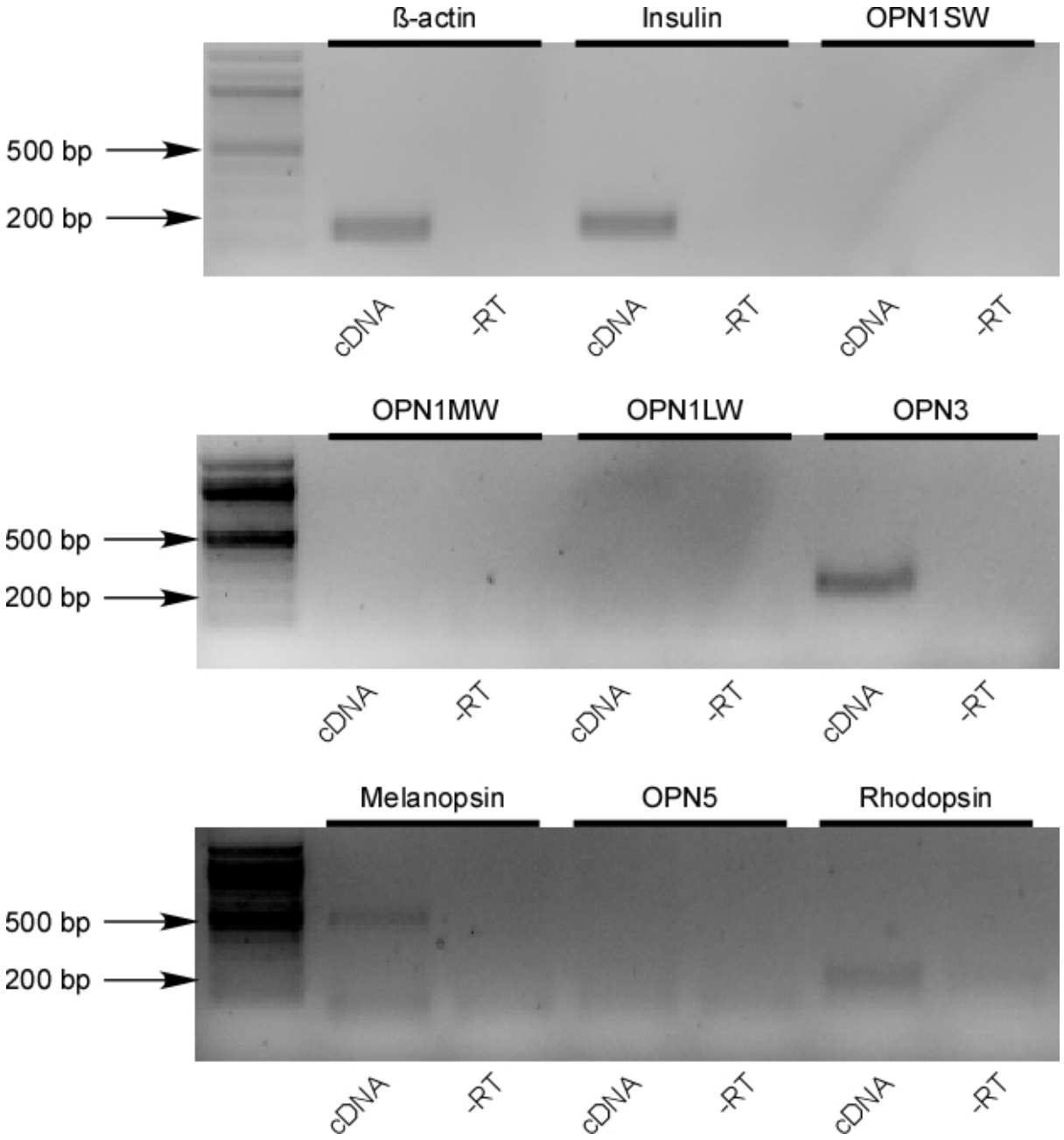

Figure 5.10 Determination of opsin expression in human islets. Representative agarose gels of RT-PCR products for one primer set for each opsin. A -RT sample was used as control for gDNA contamination. Exposure time was automatically adjusted for each gel.

Table 5.1 Summary of murine and human opsin expression. Band appearance, correct band size as well as final sequencing results for each murine and human opsin are displayed.

Opsin	Band	Band size	Sequencing result
MURINE ISLETS			
Rhodopsin	YES	CORRECT	RHODOPSIN
OPN1SW (SW)	NO	-	-
OPN1MW (MW)	YES	CORRECT	INCORRECT
Melanopsin	YES	CORRECT	INCORRECT
OPN3	YES	CORRECT	OPN3
OPN5	NO	-	-
HUMAN ISLETS			
Rhodopsin	YES	CORRECT	RHODOPSIN
OPN1SW (SW)	NO	-	-
OPN1MW (MW)	NO	-	-
OPN1LW (LW)	NO		-
Melanopsin	YES	INCORRECT	INCORRECT
OPN3	YES	CORRECT	OPN3
OPN5	NO	-	-

5.2.3.5 MAPK/Erk signaling activation in murine OPN3$^{-/-}$ islets

To test the hypothesis that OPN3 is responsible for light-induced effects, islets from OPN3$^{-/-}$ mice were investigated. Light-induced MAPK/Erk pathway activation was assessed in islets from OPN3$^{-/-}$ mice and compared to pathway activation in islets from wildtype C57BL/6J by immunoblotting. Whereas all previous experiments were performed in islets from mice with a CD-1 genetic background, OPN3$^{-/-}$ had a C57BL/6J genetic background, therefore an additional C57BL/6J wildtype control was introduced to exclude any variability caused by the genetic background. Islets from OPN3$^{-/-}$ mice showed an increase in signaling, contrary to the expected reduced level of MAPK/Erk pathway activation compared to wildtype upon blue-green light illumination (Figure 5.11). This result indicated that OPN3 alone was not required for the light-induced effects in pancreatic islets.

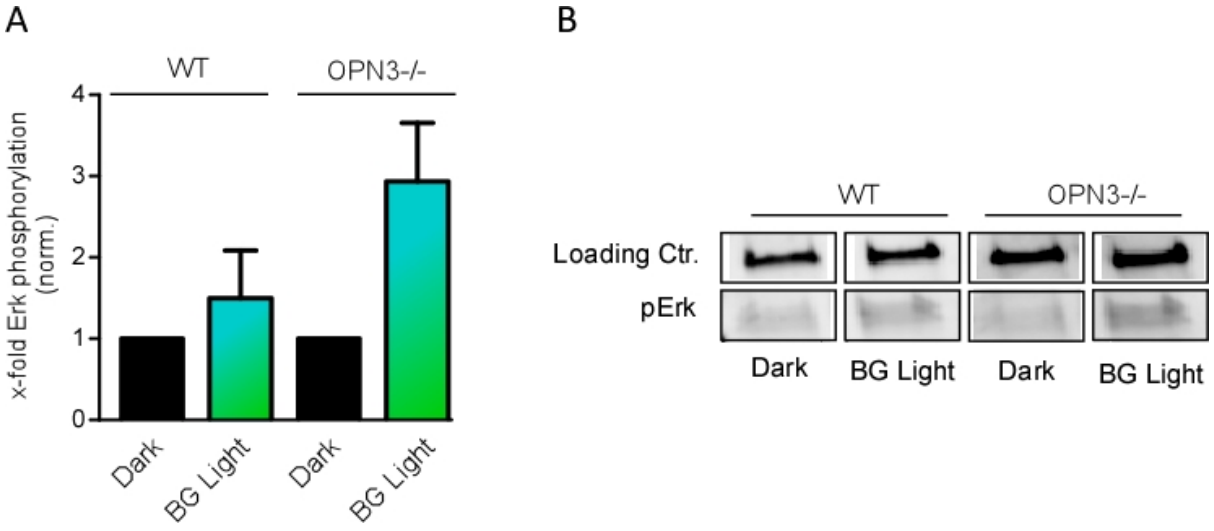

Figure 5.11 Involvement of OPN3 in light-based MAPK/Erk activation in pancreatic islets. (A) Quantification of pErk levels in murine islets from wildtype (WT) and OPN3$^{-/-}$ mice assessed by immunoblotting Mean values ± SEM are shown for three independent experiments. (B) Representative immunoblot of BG-light-induced pErk increase; Loading Ctr: vinculin; light intensity: 64 µW/cm^2; duration of illumination: 5 minutes

5.2.3.6 Influence of blue-green light illumination on ATP levels.

To test as an alternative mechanism, whether blue-green-light-induced effects were triggered by light stimulation of CcO, ATP levels in murine islets, upon blue-green light illumination, were determined at three different time points (2 minutes, 10 minutes, 24 hours). There were no significant changes in ATP levels upon blue-green light illumination at all time points (Figure 5.1). These results suggest that blue-green light illumination did not act through CcO because for this an increase in ATP levels would be expected.

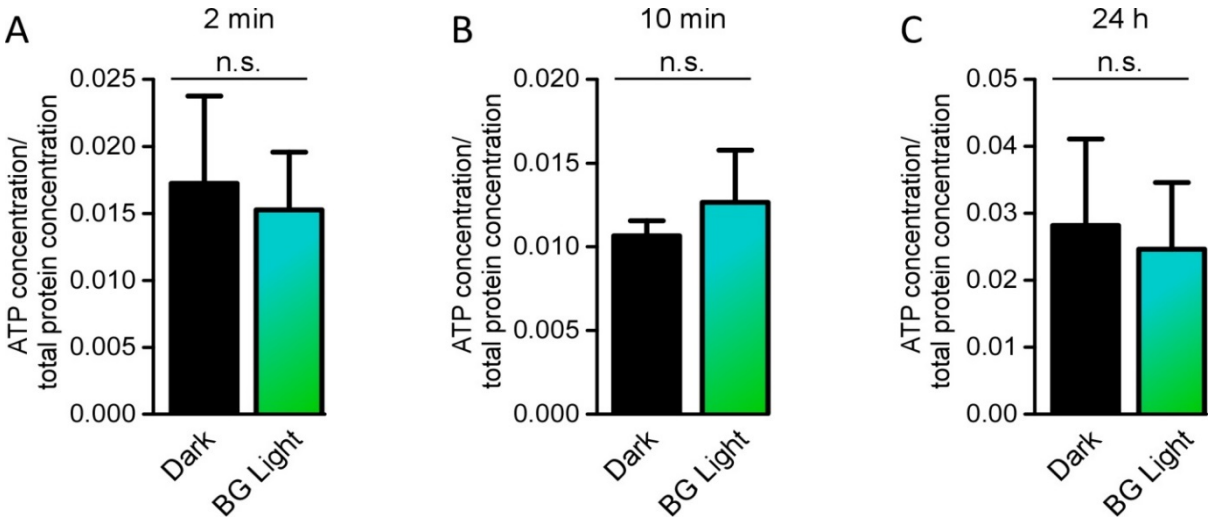

Figure 5.12 Quantification of ATP levels of murine islets upon BG light illumination. (A) ATP levels of murine islets upon 2 minutes (2 min) of BG light illumination normalized to total protein concentration. All Mean values ± SEM are shown for three independent experiments. (B) ATP levels of murine islets upon 10 minutes (10 min) of BG light illumination normalized to total protein concentration. Mean values ± SEM are shown for five independent experiments. (C) ATP levels of murine islets upon 24 hours (24 h) of BG light illumination, normalized total protein concentration. Mean values ± SEM are shown for three independent experiments. (A-C) Light intensity: 64 µW/cm^2; two-tailed, paired Student's t–test; a value of $p \leq 0.05$ was considered to be significant (n.s.: not significant)

5.3 Discussion

The second part of this thesis focused on a light-based approach for pancreatic β-cell expansion, without the necessity of gene transfer, through the discovery and characterization of endogenous light-response mechanisms. To the end, the influence of visible light on cell proliferation and survival in pancreatic islets was investigated. It was shown that blue-green light illumination leads to activation of proliferative and pro-survival signaling pathways and subsequently an increase in cell proliferation. Compared to cell lines or other primary tissues, the level of proliferation increase (1.6- and 1.4-fold, Figure 5.1) appears modest but is considerable in light of the intrinsically low turnover of β-cells. Furthermore, the magnitude of these effects is comparable to published data, where different growth factors or growth factor receptors were used to increase β-cell proliferation.[102,176,179,180] Previous studies also have shown that a rather small increase in β-cell proliferation is sufficient to regulate glucose levels in diabetic disease models.[102,179] In human islets, it was additionally demonstrated that the proliferative effect does not lead to dedifferentiation and subsequent decrease of overall β-cells mass or loss of β-cell functionality, and that illuminated islets even showed an increased number of proliferative β-cells compared to dark controls (Figure 5.2). Furthermore, a trend was observed that islets responded with an increased insulin secretion potential, under high glucose conditions, in response to light treatment. Similarly, the overall amount of internal insulin of illuminated islets stayed constant compared to controls, further indicating that blue-green light illumination had no negative effect on β-cells integrity. These findings are groundbreaking, as previous studies have shown that increased proliferation induced by growth factor administration can lead to decreased insulin levels, presumably because of dedifferentiation of β-cells into non-insulin producing cells.[103,176] The total β-cells mass as well as β-cells specific proliferation was only assessed in human islets and not in murine islets due to their different islet composition. Murine islets innately exhibit a high number of β-cells, up to 80%, whereas human islets exhibit only around 50% β-cells. Therefore an imbalance in islets cell composition, due to β-cells loss is easier to detect and more relevant in human islets.

As it was previously shown that prolonged activation of MAPK/Erk pathway is involved in β-cell proliferation,[181] this was the first pathway that was investigated here. It was demonstrated that five minutes of blue-green light illumination was sufficient to activate MAPK/Erk pathway in murine and human islets. Moreover, activation of the PI3K/Akt signaling cascade, a key player in cell survival, was also found.[181] Together, these results showed that blue-green light can activate both, major proliferative and pro-survival pathways in murine and human islets comparably to growth factors (Figure 5.4, Figure 5.5). This suggests that blue-green light illumination of pancreatic islets as a therapeutical approach for diabetes could have a double effect: first, expansion of the β-cell mass could be generated through inducing proliferation of existing β-cells; and second, both surviving and newly regenerated β-cells could have increased chances of survival.

In order to unravel the detailed characteristics of this endogenous light-sensitive mechanism, the precise light requirements were determined. In particular, it was determined which wavelengths are able to induce pathway activation, and whether a light dose-response curve can be observed. In addition to blue-green light,

interestingly green light alone was also sufficient to activate the MAPK/Erk pathway, but was not enough to increase proliferation of murine islets. The mechanistic background of this inconsistent outcome is yet unknown. A higher sample number for the proliferation assay could potentially clarify this outcome, as a positive effect of green light on islets proliferation was possibly missed due to the small sample size in that particular treatment group. Blue and red light had no effect in murine islets. Observing a similar level of Erk phosphorylation upon white light illumination compared to blue-green light illumination was not surprising, as white light contains all wavelengths, and thus includes both, blue and green light. Blue-green light was further used to determine a possible light dose-response curve with regard to MAPK/Erk pathway activation. It was observed that there was no light intensity dependent phosphorylation of Erk. Every illumination protocol resulted in increased pErk levels, even at very low intensities, indicating that this endogenous light-sensing mechanism is rather robust with regard to light intensities. The fact that the light-dependent effect is visible over a large range of intensities is a good indication regarding future *in vivo* as well as therapeutical uses, as the application of light over wide intensity range is sufficient to induce the positive effects and no highly precise light administration is necessary. The lack of a clear light dose-response curve could also indicate the involvement of two different light-sensing mechanisms, for example two different opsins, with different response curves themselves that together form a non-sigmoidal relationship. This hypothesis is substantiated, by the fact that non mammalian opsins such as JellyOp show a clear dose-response curve over the test intensity range.[182]

Although the behavioral influence of blue-green light as well as the signaling pathway activation was clearly characterized in this study, there are still questions left unanswered. In particular, the exact mechanism of how islets cells sense light and the upstream mechanism of MAPK/Erk and PI3K/Akt pathway activation is still unclear. The observed effects were proven to be not induced by environmental factors such as temperature changes and are really light-induced (Figure 5.8). Based on previous studies[45,168-171] as well as the results of opsin expression experiments (Table 5.1), different hypotheses were developed (Figure 5.13). The first hypothesis was that the non-visual opsin OPN3 plays a major role in the endogenous light-sensing mechanism. This hypothesis was underpinned by the robust expression of the protein in mouse and human pancreatic islets, previously published data that showed OPN3-dependent Erk signaling activation and increased proliferation upon illumination[45,168,169] as well as the consistent excitation profile of OPN3 and the used wavelengths (Table 1.1). By using a knockout mouse model of OPN3[50], the influence of OPN3 on the light-induced effect was investigated. The deletion of OPN3 in murine islets did not result in the expected decrease in light-induced MAPK/Erk activation compared to wild type mice; it rather led to an increase (Figure 5.11). This increase in signaling activation suggests that OPN3 is not required for light-dependent effects, but may work as a light-dependent antagonist of the proliferative effects. Thus the knockout of OPN3 released the antagonistic break and the light-dependent proliferative signal was increased. An observation supporting this theory is that in pufferfish and mosquito OPN3 was shown to couple to $G\alpha_i$, which results in decreased cAMP levels.[46] Previous studies have found that GPCRs including the GLP-1 receptor had a positive effect on β-cell proliferation and survival.[183,184] Notably, the GLP-1 receptor couples to $G\alpha_s$, which leads to an increase in cAMP levels, exactly the opposite effect that results from OPN3 activation in pufferfish and

mosquito. However, for mammalian OPN3, G-protein coupling has not been identified yet. To validate this antagonistic hypothesis, further studies are needed, for example proliferation assays including islets of OPN3$^{-/-}$ mice to show that also proliferation and not only signaling is increased in these islets. Further, a second approach to knock out OPN3 in islets, such as siRNA, would be needed to verify the used OPN3$^{-/-}$ mouse model. The second hypothesis was the involvement of CcO in the light-sensing mechanism. Various previous studies focusing on photobiomodulation, also called low-level light therapy, showed that irradiation of different cells with light lead to an increase in ATP levels and subsequent increase in proliferation was mediated by the light-sensing character of CcO.[171,174] Although all of these studies focused on red/near-infrared light illumination, this option was taken into consideration, as CcO has not only an absorption peak at the red/near-infrared range but also at around 430 nm.[175] While the used activation wavelengths are not at the exact absorption peak, they are still in the range of CcO absorption. Different time intervals of illumination were tested to assess ATP levels of islets. Neither short term illumination, nor long term illumination led to a significant change in ATP levels (Figure 5.12), demonstrating that an ATP-dependent mechanism that would be required for the CcO hypothesis is not involved in blue-green-light-induced signaling activation and proliferation in islets.

After excluding OPN3 and CcO as light-sensing actuator in pancreatic islets, the last remaining option is rhodopsin as actuator of the observed light-dependent effects. It seems that rhodopsin is expressed in lower levels compared to OPN3, but is also found in both mouse and human islets. The absorption maximum of rhodopsin (500 nm) is also consistent with the wavelengths used for islet illumination (Table 1.1).[51] Light-activated rhodopsin in the rodent retina was previously found to induce phosphorylation of the β-subunit of the insulin receptor (IR) in the rod outer segment, which further leads to the activation of PI3K in an arrestin and Src dependent manner.[185] Interestingly, it was also shown that β-arrestin underlies the proliferative effect of GLP-1 in pancreatic β-cells via the interaction of c-Src and the subsequent transactivation of the epidermal growth factor receptor.[186,187] Visual arrestins (arrestin 1 and 4) are expressed only in rod and cone cells, β-arrestin 1 and 2 (arrestin 2 and 3), however, are ubiquitously expressed in mammalian tissue.[188] While arrestins were originally discovered to be responsible for receptor desensitization, they are now also characterized as an adapter molecule to initiate various signaling cascades such as the MAPK/Erk, JNK, and p38 pathway as well as the transactivation of other receptors.[185,186,189,190] These findings strengthen the suspicion that rhodopsin may be the trigger of light-induced proliferation in pancreatic islets via light-dependent coupling to arrestin and subsequent activation of the MAPK/Erk and PI3K/Akt pathway. This hypothesis can be proven by using a rhodopsin knockout mouse model to investigate the influence of rhodopsin on light-dependent signaling and proliferative effects. Additionally, signaling molecules such as c-Src as well as possible transactivated receptors such as IR and epidermal growth factor receptor can be investigated.

In addition to experiments focusing on the characterization of the light-sensing mechanism, also *in vivo* studies will have to be performed to prove the translational potential of this approach. In particular, it has to be shown that blue-green-light-induced β-cell expansion can permanently normalize hyperglycemia in diabetic animal models. Although further investigations are needed, this approach

has great translational capability as it does not include any gene transfer to make the target tissue light responsive. The required implant to enable blue-green light activation is almost negligible, in particular in the context that no gene therapy is needed, because as discussed in section 4.3, red-light-activated systems are also not suitable for an implant-free therapeutical approach for diabetes in humans. As optogenetics is maturing into a candidate for next generation therapeutics, several methods are currently developed to improve light delivery to tissues, such as wireless implants and light guiding hydrogels.[103,191] In addition, non-optical devices for implantation at the pancreas are currently being developed,[192,193] which can be used as a model to engineer a specific illumination device for the pancreas. In addition, to *in vivo* regeneration and expansion of β-cells, another suitable application of this new light-based approach is its use for *ex vivo* expansion of the β-cell mass. E*x-vivo* expansion of human β-cells is considered as a promising approach to provide enough insulin-producing cells for β-cell replacement therapy in diabetes. Expansion of adult β-cells from the limited donor numbers is an attractive prospect. However, attempts at expanding β-cells *ex vivo* frequently result in dedifferentiation of β-cells and consequently loss of the insulin-secreting phenotype, raising doubts about the therapeutic potential of this approach.[194] As mentioned above, β-cells expanded by blue-green light illumination did not dedifferentiate and did not lose their insulin-secreting potential, thus representing the perfect technology for *ex vivo* β-cells expansion, by overcoming the limitations of current techniques. This approach would not only enable the expansion of β-cells *ex vivo* prior to transplantation, thereby lowering the number of required donor tissue, but would also enable the increase of surviving cells after transplantation and further expansion of β-cells by ongoing *in vivo* illumination after transplantation. Summarized, after fully characterizing this light-based approach *ex vivo* and *in vivo*, it has a great potential to overcome various limitations of current methods and will be applicable in a broad spectrum of therapeutical approaches from *ex vivo* β-cells expansion to *in vivo* regeneration of the β-cell mass.

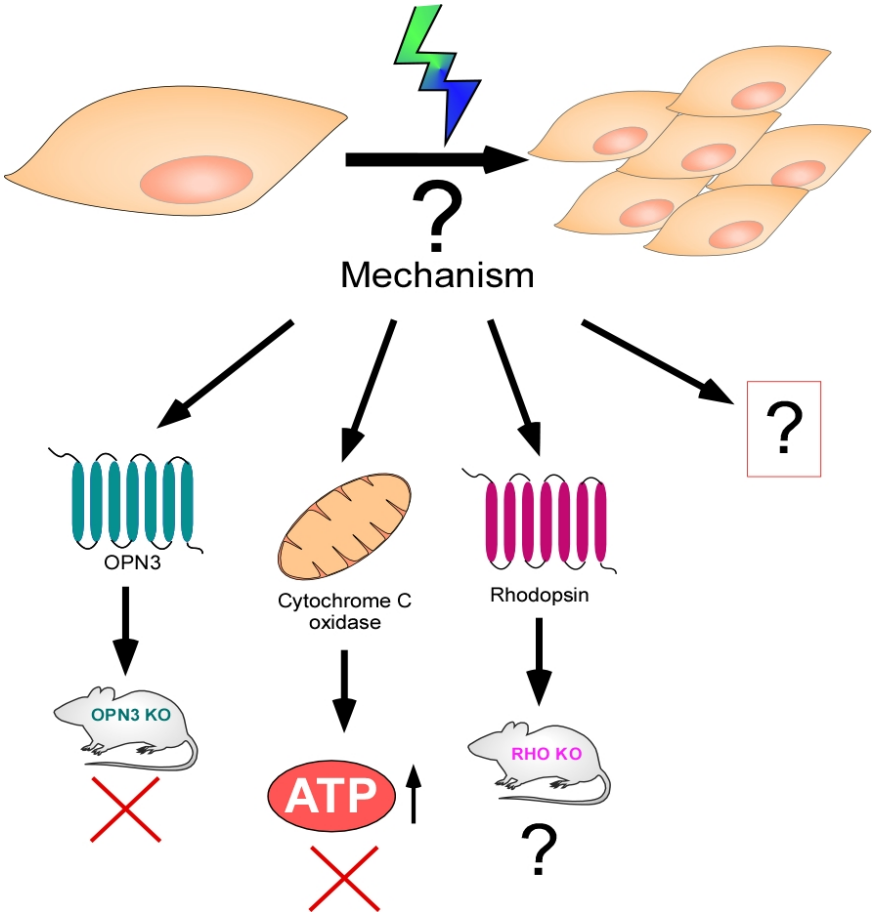

Figure 5.13 Summary and outlook of hypothesis for light-sensing mechanism. It was hypothesized that OPN3, a robustly expressed opsin, or CcO could be responsible for the light-induced proliferative effect in pancreatic islets. These hypotheses were disproved by an OPN3 knockout mouse model (OPN3 KO) and an assay that determined ATP levels after illumination. Another possible mechanism is the involvement of rhodopsin, which has to be verified by a rhodopsin knockout (Rho KO) mouse model.

CHAPTER 6: CONCLUDING REMARKS AND FUTURE DIRECTIONS

The development of red-light-activated RTKs opens a new avenue for optogenetics research by allowing non-invasive activation of RTKs *in vivo*, in particular as red light offers deeper tissue penetration than other wavelengths in the visible spectrum. This strengthens the argument that red-light-activated RTKs can be the ideal tool for many *in vivo* studies, ranging from spatial and temporal analysis of growth factor involvement in degenerative diseases to developmental and behavioral studies. In addition to deep tissue penetration, red light has a further major advantage compared to other wavelengths in the visible spectrum: it does not overlap with the excitation wavelength of commonly used fluorescent probes, and consequently this feature allows the use of red-light-activated RTKs for multi-color cell signaling experiments in an all-optical manner. A blueprint of such a multi-color cell signaling experiment is illustrated in Figure 6.1 A and B, where two different fluorescent reporters were used to determine MAPK/Erk activation (SRE-mCherry) and cell viability (CMV-mCer3) simultaneously. These reporters, combined with red-light-activated RTKs, allow to determine the influence of different small molecules on signaling activation and cell viability in parallel and an all-optical manner. This multi-color cell signaling approach can, in the future, be combined with the previously published approach of an all-optical drug screen,[195] leading to improvement and expansion of applicability and validity of the screening platform. The combination of red-light-activated RTKs with different fluorescent signaling reporters would, for example, enable the screening of small molecules acting on different pathways simultaneously in an unprecedented, rapid and economic way.

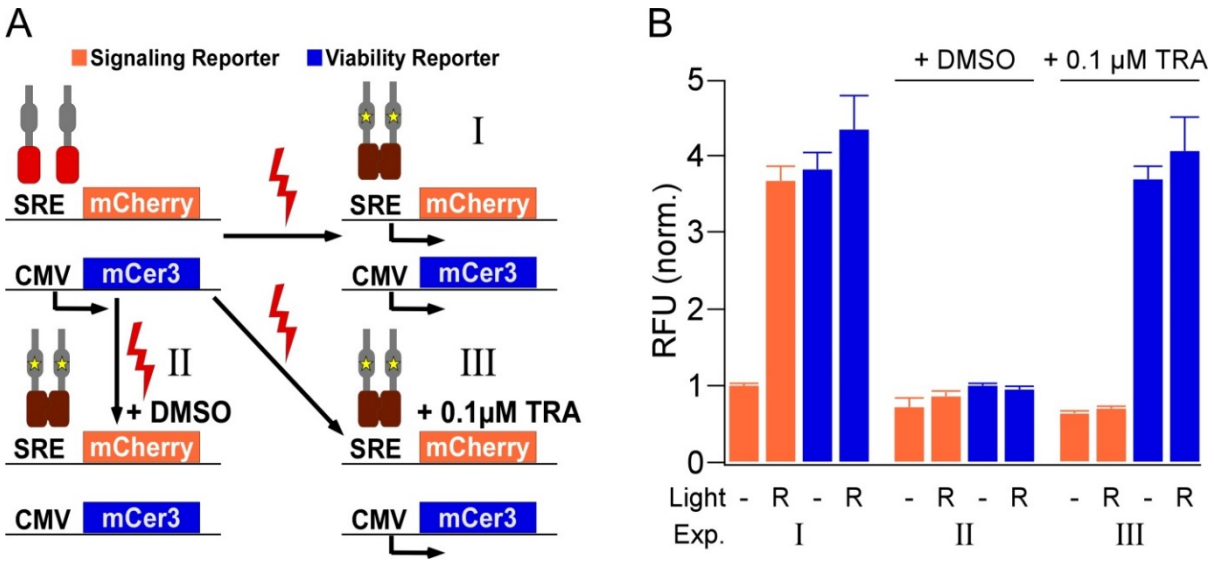

Figure 6.1 Multicolor cell signaling experiment tested receptor/pathway inhibition and cell viability simultaneously in an all optical manner. (A) I) CMV–mCerulean3 is expressed constitutively and acts as viability reporter, whereas SRE–mCherry depends on activation of the MAPK/Erk pathway by light-activated RTKs (mCer3: mCerulean3). II) The addition of a toxin such as DMSO leads to cell death, thereby resulting in expression of neither mCherry nor mCer3. III) The addition of a specific MAPK/Erk pathway inhibitor such Trametinib (TRA) inhibits mCherry expression, whereas viability and therefore mCer3 expression is not affected. (B) Experimental realization of (A). Activation of the MAPK/Erk

pathway in response to red light (R), of untreated cells, DMSO treated cells or TRA (0.1 µM) treated cells. Pathway activation and cell viability is expressed as relative fluorescence units (RFU) of mCherry and mCer3, respectively. Mean values ± SEM for three independent experiments, each performed in triplicate, are shown. Light intensity: 6.2 µW/cm^2; duration of illumination: 18 hours

Another innovative light-based approach is the activation of endogenous light-responsive mechanisms to expand pancreatic islets. As discussed in section 5.3, further studies are essential in order to characterize the light based mechanism in detail, and *in vivo* studies are required to provide insight into the translational potential. Nevertheless, this approach promises great potential for future therapies, as it includes all advantages of common optogenetic approaches, such as temporal and local precision, but additionally, it does not require gene transfer to make tissues light responsive. Gene transfer is a requirement of common optogenetic tools, limiting their use as therapeutics in a broad spectrum, as gene therapy comes with many risk factors and is therefore still not used widely. Because this new approach is based only on the local delivery of visible light to the pancreas and relies solely on endogenous responses to light, it could be the basis for future diabetic therapy without further risks and side effects. Moreover, the light-based expansion of cells is not limited to pancreatic islets,[168] and further investigations can identify other tissue types all over the body which are responsive to visible light. Interestingly, in preliminary cell line based experiments (Figure 6.2) it was shown that not only pancreatic cells (INS-1E and primary islets cells) are light responsive, but also other cell lines such as HEK293 cells. In particular, the responsiveness to light of three different cell lines was tested. Two different signaling cascades were investigated, a cAMP-based cascade and the MAPK/Erk pathway, as well as changes in cell viability upon illumination (Figure 6.2, Figure A1, Figure A2, Figure A3). The results showed that different cell lines were responsive to visible light in different ways. Considering these results, it is worth to further investigate various tissues for their light responsiveness in order to expand the approach of light-induced proliferation by endogenous mechanisms, and to find new therapeutical approaches for various degenerative diseases.

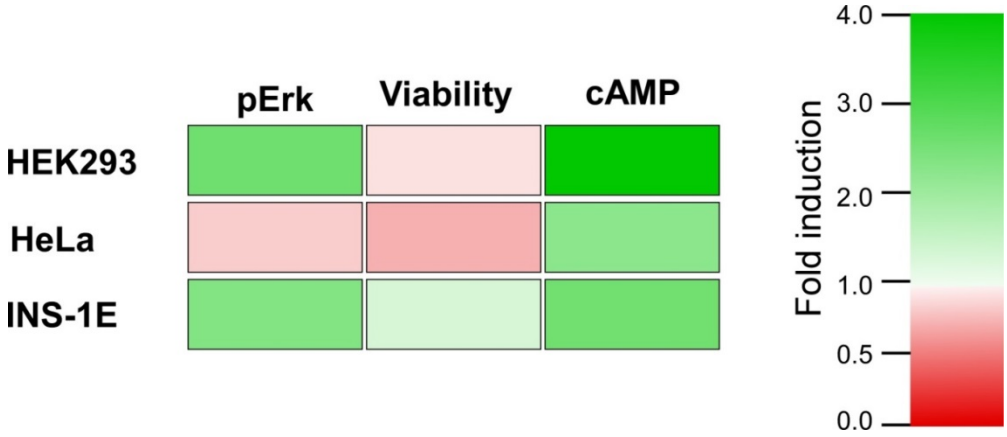

Figure 6.2 Influence of visible light on cellular signaling and cell behavior in different cell lines. Results are displayed as color code translated from fold induction compared to dark controls. Each result indicates the quantification of three independent experiments. HEK293 cells show an increase in pErk levels as well as cAMP levels after illumination. HeLa cells show only a minimal increase in cAMP levels upon illumination. INS-1E cells show increase in pErk levels, increased viability as well as small increased cAMP levels

upon illumination with visible light. Detailed experimental outcomes are depicted in Figure A1, Figure A2 and Figure A3.

To conclude, in this study two different light-based approaches were established and investigated in order to overcome limitations of common optogenetic and pharmacological methods, such as local and temporal precision as well as tissue penetration, and gene delivery. These new approaches are important tools which can be used in basic research as well as for the invention of new therapies for degenerative diseases such as diabetes.

REFERENCES

1 Janovjak, H. Light at the End of the Protein: Crystal Structure of a C-Terminal Light-Sensing Domain. *Structure* 24, 213-215, doi:10.1016/j.str.2016.01.002 (2016).

2 Foster, R. G., Hankins, M. W. & Peirson, S. N. Light, photoreceptors, and circadian clocks. *Methods in molecular biology* 362, 3-28, doi:10.1007/978-1-59745-257-1_1 (2007).

3 Moglich, A., Yang, X., Ayers, R. A. & Moffat, K. Structure and function of plant photoreceptors. *Annual review of plant biology* 61, 21-47, doi:10.1146/annurev-arplant-042809-112259 (2010).

4 Schmidt, D. & Cho, Y. K. Natural photoreceptors and their application to synthetic biology. *Trends in biotechnology* 33, 80-91, doi:10.1016/j.tibtech.2014.10.007 (2015).

5 Heijde, M. & Ulm, R. UV-B photoreceptor-mediated signalling in plants. *Trends in plant science* 17, 230-237, doi:10.1016/j.tplants.2012.01.007 (2012).

6 Ortiz-Guerrero, J. M., Polanco, M. C., Murillo, F. J., Padmanabhan, S. & Elias-Arnanz, M. Light-dependent gene regulation by a coenzyme B12-based photoreceptor. *Proceedings of the National Academy of Sciences of the United States of America* 108, 7565-7570, doi:10.1073/pnas.1018972108 (2011).

7 Jenkins, G. I. The UV-B photoreceptor UVR8: from structure to physiology. *The Plant cell* 26, 21-37, doi:10.1105/tpc.113.119446 (2014).

8 Oravecz, A. *et al.* CONSTITUTIVELY PHOTOMORPHOGENIC1 is required for the UV-B response in Arabidopsis. *The Plant cell* 18, 1975-1990, doi:10.1105/tpc.105.040097 (2006).

9 Rizzini, L. *et al.* Perception of UV-B by the Arabidopsis UVR8 protein. *Science* 332, 103-106, doi:10.1126/science.1200660 (2011).

10 Christie, J. M., Blackwood, L., Petersen, J. & Sullivan, S. Plant flavoprotein photoreceptors. *Plant & cell physiology* 56, 401-413, doi:10.1093/pcp/pcu196 (2015).

11 Conrad, K. S., Manahan, C. C. & Crane, B. R. Photochemistry of flavoprotein light sensors. *Nature chemical biology* 10, 801-809, doi:10.1038/nchembio.1633 (2014).

12 Chaves, I. *et al.* The cryptochromes: blue light photoreceptors in plants and animals. *Annual review of plant biology* 62, 335-364, doi:10.1146/annurev-arplant-042110-103759 (2011).

13 Ahmad, M. & Cashmore, A. R. HY4 gene of A. thaliana encodes a protein with characteristics of a blue-light photoreceptor. *Nature* 366, 162-166, doi:10.1038/366162a0 (1993).

14 Pokorny, R. *et al.* Recognition and repair of UV lesions in loop structures of duplex DNA by DASH-type cryptochrome. *Proceedings of the National Academy of Sciences of the United States of America* 105, 21023-21027, doi:10.1073/pnas.0805830106 (2008).

15 Selby, C. P. & Sancar, A. A cryptochrome/photolyase class of enzymes with single-stranded DNA-specific photolyase activity. *Proceedings of the National Academy of Sciences of the United States of America* 103, 17696-17700, doi:10.1073/pnas.0607993103 (2006).

16 Yu, X., Liu, H., Klejnot, J. & Lin, C. The Cryptochrome Blue Light Receptors. *The Arabidopsis book* 8, e0135 (2010).

17 Liu, B., Liu, H., Zhong, D. & Lin, C. Searching for a photocycle of the cryptochrome photoreceptors. *Current opinion in plant biology* 13, 578-586, doi:10.1016/j.pbi.2010.09.005 (2010).

18 Losi, A. & Gartner, W. The evolution of flavin-binding photoreceptors: an ancient chromophore serving trendy blue-light sensors. *Annual review of plant biology* 63, 49-72, doi:10.1146/annurev-arplant-042811-105538 (2012).

19 Muller, K. & Weber, W. Optogenetic tools for mammalian systems. *Molecular bioSystems* 9, 596-608, doi:10.1039/c3mb25590e (2013).

20 Gomelsky, M. & Klug, G. BLUF: a novel FAD-binding domain involved in sensory transduction in microorganisms. *Trends in biochemical sciences* 27, 497-500 (2002).

21 Meyer, T. E. *et al.* The growing family of photoactive yellow proteins and their presumed functional roles. *Photochemical & photobiological sciences : Official journal of the European Photochemistry Association and the European Society for Photobiology* 11, 1495-1514, doi:10.1039/c2pp25090j (2012).

22 Meyer, T. E. Isolation and characterization of soluble cytochromes, ferredoxins and other chromophoric proteins from the halophilic phototrophic bacterium Ectothiorhodospira halophila. *Biochimica et biophysica acta* 806, 175-183 (1985).

23 Pande, K. *et al.* Femtosecond structural dynamics drives the trans/cis isomerization in photoactive yellow protein. *Science* 352, 725-729, doi:10.1126/science.aad5081 (2016).

24 Tenboer, J. *et al.* Time-resolved serial crystallography captures high-resolution intermediates of photoactive yellow protein. *Science* 346, 1242-1246, doi:10.1126/science.1259357 (2014).

25 Takano, H. *et al.* Involvement of CarA/LitR and CRP/FNR family transcriptional regulators in light-induced carotenoid production in Thermus thermophilus. *Journal of bacteriology* 193, 2451-2459, doi:10.1128/JB.01125-10 (2011).

26 Jost, M. *et al.* Structural basis for gene regulation by a B12-dependent photoreceptor. *Nature* 526, 536-541, doi:10.1038/nature14950 (2015).

27 Perez-Marin, M. C., Padmanabhan, S., Polanco, M. C., Murillo, F. J. & Elias-Arnanz, M. Vitamin B12 partners the CarH repressor to downregulate a photoinducible promoter in Myxococcus xanthus. *Molecular microbiology* 67, 804-819, doi:10.1111/j.1365-2958.2007.06086.x (2008).

28 Takano, H., Beppu, T. & Ueda, K. The CarA/LitR-family transcriptional regulator: Its possible role as a photosensor and wide distribution in non-phototrophic bacteria. *Bioscience, biotechnology, and biochemistry* 70, 2320-2324, doi:10.1271/bbb.60230 (2006).

29 Rockwell, N. C., Su, Y. S. & Lagarias, J. C. Phytochrome structure and signaling mechanisms. *Annual review of plant biology* 57, 837-858, doi:10.1146/annurev.arplant.56.032604.144208 (2006).

30 Burgie, E. S. & Vierstra, R. D. Phytochromes: an atomic perspective on photoactivation and signaling. *The Plant cell* 26, 4568-4583, doi:10.1105/tpc.114.131623 (2014).

31 Ulijasz, A. T. & Vierstra, R. D. Phytochrome structure and photochemistry: recent advances toward a complete molecular picture. *Current opinion in plant biology* 14, 498-506, doi:10.1016/j.pbi.2011.06.002 (2011).

32 Moglich, A. & Moffat, K. Engineered photoreceptors as novel optogenetic tools. *Photochemical & photobiological sciences : Official journal of the European*

Photochemistry Association and the European Society for Photobiology 9, 1286-1300, doi:10.1039/c0pp00167h (2010).

33 Shichida, Y. & Matsuyama, T. Evolution of opsins and phototransduction. *Philosophical transactions of the Royal Society of London. Series B, Biological sciences* 364, 2881-2895, doi:10.1098/rstb.2009.0051 (2009).

34 Nagel, G. *et al.* Channelrhodopsin-1: a light-gated proton channel in green algae. *Science* 296, 2395-2398, doi:10.1126/science.1072068 (2002).

35 Hankins, M. W., Davies, W. I. L. & Foster, R. G. in *In Evolution of Visual and Non-Visual Pigments* (eds D. M. Hunt, M. W. Hankins, S. P. Collin, & Marshall N. J.) (Springer US, 2009).

36 Terakita, A. The opsins. *Genome biology* 6, 213, doi:10.1186/gb-2005-6-3-213 (2005).

37 Arshavsky, V. Y., Lamb, T. D. & Pugh, E. N., Jr. G proteins and phototransduction. *Annual review of physiology* 64, 153-187, doi:10.1146/annurev.physiol.64.082701.102229 (2002).

38 Cameron, E. G. & Robinson, P. R. beta-Arrestin-dependent deactivation of mouse melanopsin. *PloS one* 9, e113138, doi:10.1371/journal.pone.0113138 (2014).

39 Bailes, H. J. & Lucas, R. J. Human melanopsin forms a pigment maximally sensitive to blue light (lambdamax approximately 479 nm) supporting activation of G(q/11) and G(i/o) signalling cascades. *Proceedings. Biological sciences* 280, 20122987, doi:10.1098/rspb.2012.2987 (2013).

40 Hughes, S., Hankins, M. W., Foster, R. G. & Peirson, S. N. Melanopsin phototransduction: slowly emerging from the dark. *Progress in brain research* 199, 19-40, doi:10.1016/B978-0-444-59427-3.00002-2 (2012).

41 Blackshaw, S. & Snyder, S. H. Encephalopsin: a novel mammalian extraretinal opsin discretely localized in the brain. *The Journal of neuroscience : the official journal of the Society for Neuroscience* 19, 3681-3690 (1999).

42 Halford, S. *et al.* Characterization of a novel human opsin gene with wide tissue expression and identification of embedded and flanking genes on chromosome 1q43. *Genomics* 72, 203-208, doi:10.1006/geno.2001.6469 (2001).

43 White, J. H. *et al.* Identification of a novel asthma susceptibility gene on chromosome 1qter and its functional evaluation. *Human molecular genetics* 17, 1890-1903, doi:10.1093/hmg/ddn087 (2008).

44 Barreto Ortiz, S. *et al.* Opsin 3 and 4 Mediate Light-Induced Pulmonary Vasorelaxation that is Potentiated by G-Protein Receptor Kinase 2 Inhibition. *American journal of physiology. Lung cellular and molecular physiology*, ajplung 00091 02017, doi:10.1152/ajplung.00091.2017 (2017).

45 Regazzetti, C. *et al.* Melanocytes sense blue light and regulate pigmentation through the Opsin3. *J Invest Dermatol*, doi:10.1016/j.jid.2017.07.833 (2017).

46 Koyanagi, M., Takada, E., Nagata, T., Tsukamoto, H. & Terakita, A. Homologs of vertebrate Opn3 potentially serve as a light sensor in nonphotoreceptive tissue. *Proceedings of the National Academy of Sciences of the United States of America* 110, 4998-5003, doi:10.1073/pnas.1219416110 (2013).

47 Tarttelin, E. E., Bellingham, J., Hankins, M. W., Foster, R. G. & Lucas, R. J. Neuropsin (Opn5): a novel opsin identified in mammalian neural tissue. *FEBS letters* 554, 410-416 (2003).

48 Kojima, D. *et al.* UV-sensitive photoreceptor protein OPN5 in humans and mice. *PloS one* 6, e26388, doi:10.1371/journal.pone.0026388 (2011).

49 Yamashita, T. *et al.* Opn5 is a UV-sensitive bistable pigment that couples with Gi subtype of G protein. *Proceedings of the National Academy of Sciences of the United States of America* 107, 22084-22089, doi:10.1073/pnas.1012498107 (2010).

50 Buhr, E. D. *et al.* Neuropsin (OPN5)-mediated photoentrainment of local circadian oscillators in mammalian retina and cornea. *Proceedings of the National Academy of Sciences of the United States of America* 112, 13093-13098, doi:10.1073/pnas.1516259112 (2015).

51 Imai, H. *et al.* Molecular properties of rhodopsin and rod function. *The Journal of biological chemistry* 282, 6677-6684, doi:10.1074/jbc.M610086200 (2007).

52 Fasick, J. I., Applebury, M. L. & Oprian, D. D. Spectral tuning in the mammalian short-wavelength sensitive cone pigments. *Biochemistry* 41, 6860-6865 (2002).

53 Deeb, S. S. The molecular basis of variation in human color vision. *Clinical genetics* 67, 369-377, doi:10.1111/j.1399-0004.2004.00343.x (2005).

54 Sun, H., Macke, J. P. & Nathans, J. Mechanisms of spectral tuning in the mouse green cone pigment. *Proceedings of the National Academy of Sciences of the United States of America* 94, 8860-8865 (1997).

55 Walker, M. T., Brown, R. L., Cronin, T. W. & Robinson, P. R. Photochemistry of retinal chromophore in mouse melanopsin. *Proceedings of the National Academy of Sciences of the United States of America* 105, 8861-8865, doi:10.1073/pnas.0711397105 (2008).

56 Deisseroth, K. Optogenetics: 10 years of microbial opsins in neuroscience. *Nature neuroscience* 18, 1213-1225, doi:10.1038/nn.4091 (2015).

57 Reiner, A. & Isacoff, E. Y. The Brain Prize 2013: the optogenetics revolution. *Trends in Neurosciences* 36, 557-560, doi:10.1016/j.tins.2013.08.005 (2013).

58 Tye, K. M. & Deisseroth, K. Optogenetic investigation of neural circuits underlying brain disease in animal models. *Nature Reviews Neuroscience* 13, 251-266, doi:10.1038/nrn3171 (2012).

59 Williams, S. C. & Deisseroth, K. Optogenetics. *Proceedings of the National Academy of Sciences of the United States of America* 110, 16287, doi:10.1073/pnas.1317033110 (2013).

60 Lubbe, A. S., Szymanski, W. & Feringa, B. L. Recent developments in reversible photoregulation of oligonucleotide structure and function. *Chemical Society reviews* 46, 1052-1079, doi:10.1039/c6cs00461j (2017).

61 Toettcher, J. E., Voigt, C. A., Weiner, O. D. & Lim, W. A. The promise of optogenetics in cell biology: interrogating molecular circuits in space and time. *Nature methods* 8, 35-38, doi:10.1038/nmeth.f.326 (2011).

62 Ziegler, T. & Moglich, A. Photoreceptor engineering. *Frontiers in molecular biosciences* 2, 30, doi:10.3389/fmolb.2015.00030 (2015).

63 Wu, Y. I. *et al.* A genetically encoded photoactivatable Rac controls the motility of living cells. *Nature* 461, 104-108, doi:10.1038/nature08241 (2009).

64 Grusch, M. *et al.* Spatio-temporally precise activation of engineered receptor tyrosine kinases by light. *The EMBO journal*, doi:10.15252/embj.201387695 (2014).

65 Kainrath, S., Stadler, M., Reichhart, E., Distel, M. & Janovjak, H. Green-Light-Induced Inactivation of Receptor Signaling Using Cobalamin-Binding Domains. *Angewandte Chemie* 56, 4608-4611, doi:10.1002/anie.201611998 (2017).

66 Kennedy, M. J. *et al.* Rapid blue-light-mediated induction of protein interactions in living cells. *Nature methods* 7, 973-975, doi:10.1038/nmeth.1524 (2010).

67 Taslimi, A. *et al.* An optimized optogenetic clustering tool for probing protein interaction and function. *Nature communications* 5, 4925, doi:10.1038/ncomms5925 (2014).

68 Muller, K. *et al.* A red/far-red light-responsive bi-stable toggle switch to control gene expression in mammalian cells. *Nucleic acids research* 41, e77, doi:10.1093/nar/gkt002 (2013).

69 Dirice, E. & Kulkarni, R. N. in *Islet Cell Growth Factors* (ed R.N. Kulkarni) (Landes Bioscience, 2011).

70 Slack, J. M. Developmental biology of the pancreas. *Development* 121, 1569-1580 (1995).

71 Gittes, G. K. Developmental biology of the pancreas: a comprehensive review. *Developmental biology* 326, 4-35, doi:10.1016/j.ydbio.2008.10.024 (2009).

72 Edlund, H. Developmental biology of the pancreas. *Diabetes* 50 Suppl 1, S5-9 (2001).

73 Steiner, D. J., Kim, A., Miller, K. & Hara, M. Pancreatic islet plasticity: interspecies comparison of islet architecture and composition. *Islets* 2, 135-145 (2010).

74 Kilimnik, G., Jo, J., Periwal, V., Zielinski, M. C. & Hara, M. Quantification of islet size and architecture. *Islets* 4, 167-172, doi:10.4161/isl.19256 (2012).

75 Cabrera, O. *et al.* The unique cytoarchitecture of human pancreatic islets has implications for islet cell function. *Proceedings of the National Academy of Sciences of the United States of America* 103, 2334-2339, doi:10.1073/pnas.0510790103 (2006).

76 Marty, N., Dallaporta, M. & Thorens, B. Brain glucose sensing, counterregulation, and energy homeostasis. *Physiology* 22, 241-251, doi:10.1152/physiol.00010.2007 (2007).

77 MacDonald, P. E., Joseph, J. W. & Rorsman, P. Glucose-sensing mechanisms in pancreatic beta-cells. *Philosophical transactions of the Royal Society of London. Series B, Biological sciences* 360, 2211-2225, doi:10.1098/rstb.2005.1762 (2005).

78 Wilcox, G. Insulin and insulin resistance. *The Clinical biochemist. Reviews* 26, 19-39 (2005).

79 Bratanova-Tochkova, T. K. *et al.* Triggering and augmentation mechanisms, granule pools, and biphasic insulin secretion. *Diabetes* 51 Suppl 1, S83-90 (2002).

80 Dimitriadis, G., Mitrou, P., Lambadiari, V., Maratou, E. & Raptis, S. A. Insulin effects in muscle and adipose tissue. *Diabetes research and clinical practice* 93 Suppl 1, S52-59, doi:10.1016/S0168-8227(11)70014-6 (2011).

81 Wild S, R. G., Green A,SicreeR, King H. Global Prevalence of Diabetes. Estimates for the year 2000 and projections for 2030. *Diabetes Care* 27, 1047–1053 (2004).

82 WHO. Global report on diabetes. (WHO, 2016).

83 Lindenmeyer, A. *et al.* Influence of primary care practices on patients' uptake of diabetic retinopathy screening: a qualitative case study. *The British journal of general practice : the journal of the Royal College of General Practitioners* 64, e484-492, doi:10.3399/bjgp14X680965 (2014).

84 Hughes, R. A. Peripheral neuropathy. *Bmj* 324, 466-469 (2002).

85 Mathis, D., Vence, L. & Benoist, C. beta-Cell death during progression to diabetes. *Nature* 414, 792-798, doi:10.1038/414792a (2001).

86 van Belle, T. L., Coppieters, K. T. & von Herrath, M. G. Type 1 diabetes: etiology, immunology, and therapeutic strategies. *Physiological reviews* 91, 79-118, doi:10.1152/physrev.00003.2010 (2011).

87 Wherrett, D. K. & Daneman, D. Prevention of type 1 diabetes. *Endocrinology and metabolism clinics of North America* 38, 777-790, doi:10.1016/j.ecl.2009.08.006 (2009).

88 Atkinson, M. A., Eisenbarth, G. S. & Michels, A. W. Type 1 diabetes. *Lancet* 383, 69-82, doi:10.1016/S0140-6736(13)60591-7 (2014).

89 Yoon, J. W. & Jun, H. S. Cellular and molecular pathogenic mechanisms of insulin-dependent diabetes mellitus. *Annals of the New York Academy of Sciences* 928, 200-211 (2001).

90 Collaboration, N. C. D. R. F. Worldwide trends in diabetes since 1980: a pooled analysis of 751 population-based studies with 4.4 million participants. *Lancet* 387, 1513-1530, doi:10.1016/S0140-6736(16)00618-8 (2016).

91 Alejandro, E. U., Gregg, B., Blandino-Rosano, M., Cras-Meneur, C. & Bernal-Mizrachi, E. Natural history of beta-cell adaptation and failure in type 2 diabetes. *Molecular aspects of medicine* 42, 19-41, doi:10.1016/j.mam.2014.12.002 (2015).

92 Tremblay, F. & Marette, A. Amino acid and insulin signaling via the mTOR/p70 S6 kinase pathway. A negative feedback mechanism leading to insulin resistance in skeletal muscle cells. *The Journal of biological chemistry* 276, 38052-38060, doi:10.1074/jbc.M106703200 (2001).

93 Gruessner, A. C. 2011 update on pancreas transplantation: comprehensive trend analysis of 25,000 cases followed up over the course of twenty-four years at the International Pancreas Transplant Registry (IPTR). *The review of diabetic studies : RDS* 8, 6-16, doi:10.1900/RDS.2011.8.6 (2011).

94 Shapiro, A. M. *et al.* Islet transplantation in seven patients with type 1 diabetes mellitus using a glucocorticoid-free immunosuppressive regimen. *The New England journal of medicine* 343, 230-238, doi:10.1056/NEJM200007273430401 (2000).

95 Shapiro, A. M. *et al.* Strategic opportunities in clinical islet transplantation. *Transplantation* 79, 1304-1307 (2005).

96 Ryan, E. A. *et al.* Five-year follow-up after clinical islet transplantation. *Diabetes* 54, 2060-2069 (2005).

97 Korsgren, O. *et al.* Current status of clinical islet transplantation. *Transplantation* 79, 1289-1293 (2005).

98 Vasavada, R. C. *et al.* Growth factors and beta cell replication. *The international journal of biochemistry & cell biology* 38, 931-950, doi:10.1016/j.biocel.2005.08.003 (2006).

99 Pepper, A. R. *et al.* Diabetes Is Reversed in a Murine Model by Marginal Mass Syngeneic Islet Transplantation Using a Subcutaneous Cell Pouch Device. *Transplantation* 99, 2294-2300, doi:10.1097/TP.0000000000000864 (2015).

100 Sakata, N. *et al.* Strategy for clinical setting in intramuscular and subcutaneous islet transplantation. *Diabetes/metabolism research and reviews* 30, 1-10, doi:10.1002/dmrr.2463 (2014).

101 Gaddy, D. F., Riedel, M. J., Pejawar-Gaddy, S., Kieffer, T. J. & Robbins, P. D. In vivo expression of HGF/NK1 and GLP-1 From dsAAV vectors enhances pancreatic ss-cell

proliferation and improves pathology in the db/db mouse model of diabetes. *Diabetes* 59, 3108-3116, doi:10.2337/db09-1886 (2010).

102 Kobinger, G. P. *et al.* Pharmacologically regulated regeneration of functional human pancreatic islets. *Molecular therapy : the journal of the American Society of Gene Therapy* 11, 105-111, doi:10.1016/j.ymthe.2004.09.010 (2005).

103 Pais, E. *et al.* Regulated Expansion of Human Pancreatic beta-Cells. *Molecular therapy : the journal of the American Society of Gene Therapy* 18, 1389-1396, doi:10.1038/mt.2010.63 (2010).

104 Kahn, S. E., Cooper, M. E. & Del Prato, S. Pathophysiology and treatment of type 2 diabetes: perspectives on the past, present, and future. *Lancet* 383, 1068-1083, doi:10.1016/S0140-6736(13)62154-6 (2014).

105 Rendell, M. The role of sulphonylureas in the management of type 2 diabetes mellitus. *Drugs* 64, 1339-1358 (2004).

106 Hostalek, U., Gwilt, M. & Hildemann, S. Therapeutic Use of Metformin in Prediabetes and Diabetes Prevention. *Drugs* 75, 1071-1094, doi:10.1007/s40265-015-0416-8 (2015).

107 Pernicova, I. & Korbonits, M. Metformin--mode of action and clinical implications for diabetes and cancer. *Nature reviews. Endocrinology* 10, 143-156, doi:10.1038/nrendo.2013.256 (2014).

108 Chen, Y. *et al.* Discovery of Novel Insulin Sensitizers: Promising Approaches and Targets. *PPAR research* 2017, 8360919, doi:10.1155/2017/8360919 (2017).

109 Janani, C. & Ranjitha Kumari, B. D. PPAR gamma gene--a review. *Diabetes & metabolic syndrome* 9, 46-50, doi:10.1016/j.dsx.2014.09.015 (2015).

110 Aleman-Gonzalez-Duhart, D., Tamay-Cach, F., Alvarez-Almazan, S. & Mendieta-Wejebe, J. E. Current Advances in the Biochemical and Physiological Aspects of the Treatment of Type 2 Diabetes Mellitus with Thiazolidinediones. *PPAR research* 2016, 7614270, doi:10.1155/2016/7614270 (2016).

111 Iltz, J. L., Baker, D. E., Setter, S. M. & Keith Campbell, R. Exenatide: an incretin mimetic for the treatment of type 2 diabetes mellitus. *Clinical therapeutics* 28, 652-665, doi:10.1016/j.clinthera.2006.05.006 (2006).

112 Bae, E. J. DPP-4 inhibitors in diabetic complications: role of DPP-4 beyond glucose control. *Archives of pharmacal research* 39, 1114-1128, doi:10.1007/s12272-016-0813-x (2016).

113 Kushibiki, T., Okawa, S., Hirasawa, T. & Ishihara, M. Optogenetic control of insulin secretion by pancreatic beta-cells in vitro and in vivo. *Gene therapy* 22, 553-559, doi:10.1038/gt.2015.23 (2015).

114 Reinbothe, T. M., Safi, F., Axelsson, A. S., Mollet, I. G. & Rosengren, A. H. Optogenetic control of insulin secretion in intact pancreatic islets with beta-cell-specific expression of Channelrhodopsin-2. *Islets* 6, e28095, doi:10.4161/isl.28095 (2014).

115 Ye, H., Daoud-El Baba, M., Peng, R. W. & Fussenegger, M. A synthetic optogenetic transcription device enhances blood-glucose homeostasis in mice. *Science* 332, 1565-1568, doi:10.1126/science.1203535 (2011).

116 Broichhagen, J. *et al.* Optical Control of Insulin Secretion Using an Incretin Switch. *Angewandte Chemie* 54, 15565-15569, doi:10.1002/anie.201506384 (2015).

117 Robinson, D. R., Wu, Y. M. & Lin, S. F. The protein tyrosine kinase family of the human genome. *Oncogene* 19, 5548-5557, doi:10.1038/sj.onc.1203957 (2000).

118 Lemmon, M. A. & Schlessinger, J. Cell signaling by receptor tyrosine kinases. *Cell* 141, 1117-1134, doi:10.1016/j.cell.2010.06.011 (2010).

119 Gonzalez-Pertusa JA, A. L., Garcia-Ocana A. Hepatocyte Growth Factor (HGF) and the Pancreatic Beta Cell. *Islets Cell Growth Factors* (2011).

120 Kondegowda Nagesha Guthalu , Z. X., Williams Katoura , Mozar Anaïs and & C., V. R. Growth Factor Mediated Regulation of Beta Cell Survival. *The Open Endocrinology Journal* 4, 78-93 (2010).

121 Hart, A. W., Baeza, N., Apelqvist, A. & Edlund, H. Attenuation of FGF signalling in mouse beta-cells leads to diabetes. *Nature* 408, 864-868, doi:10.1038/35048589 (2000).

122 Kilkenny, D. M. & Rocheleau, J. V. Fibroblast growth factor receptor-1 signaling in pancreatic islet beta-cells is modulated by the extracellular matrix. *Mol Endocrinol* 22, 196-205 (2008).

123 Garcia-Ocana, A. *et al.* Adenovirus-mediated hepatocyte growth factor expression in mouse islets improves pancreatic islet transplant performance and reduces beta cell death. *The Journal of biological chemistry* 278, 343-351, doi:10.1074/jbc.M207848200 (2003).

124 Mwangi, S. *et al.* Glial cell line-derived neurotrophic factor increases beta-cell mass and improves glucose tolerance. *Gastroenterology* 134, 727-737, doi:10.1053/j.gastro.2007.12.033 (2008).

125 Shin, S., Li, N., Kobayashi, N., Yoon, J. W. & Jun, H. S. Remission of diabetes by beta-cell regeneration in diabetic mice treated with a recombinant adenovirus expressing betacellulin. *Molecular therapy : the journal of the American Society of Gene Therapy* 16, 854-861, doi:10.1038/mt.2008.22 (2008).

126 Wente, W. *et al.* Fibroblast growth factor-21 improves pancreatic beta-cell function and survival by activation of extracellular signal-regulated kinase 1/2 and Akt signaling pathways. *Diabetes* 55, 2470-2478, doi:10.2337/db05-1435 (2006).

127 Dai, C., Li, Y., Yang, J. & Liu, Y. Hepatocyte growth factor preserves beta cell mass and mitigates hyperglycemia in streptozotocin-induced diabetic mice. *The Journal of biological chemistry* 278, 27080-27087, doi:10.1074/jbc.M211947200 (2003).

128 Dickson, L. M. & Rhodes, C. J. Pancreatic beta-cell growth and survival in the onset of type 2 diabetes: a role for protein kinase B in the Akt? *American journal of physiology. Endocrinology and metabolism* 287, E192-198, doi:10.1152/ajpendo.00031.2004 (2004).

129 Wang, X., Chen, X. & Yang, Y. Spatiotemporal control of gene expression by a light-switchable transgene system. *Nature methods* 9, 266-269, doi:10.1038/nmeth.1892 (2012).

130 Aravanis, A. M. *et al.* An optical neural interface: in vivo control of rodent motor cortex with integrated fiberoptic and optogenetic technology. *Journal of neural engineering* 4, S143-156, doi:10.1088/1741-2560/4/3/S02 (2007).

131 Collins, M. & Thrasher, A. Gene therapy: progress and predictions. *Proceedings. Biological sciences* 282, 20143003, doi:10.1098/rspb.2014.3003 (2015).

132 Naldini, L. Gene therapy returns to centre stage. *Nature* 526, 351-360, doi:10.1038/nature15818 (2015).

133 Reardon, S. Light-controlled genes and neurons poised for clinical trials. *Nature*, doi:doi:10.1038/nature.2016.19886 (2016).

134 Sutherland, S. Revolutionary Neuroscience Technique Slated for Human Clinical Trials. *Scientific American* (2016).

135 Gonzalez-Pertusa JA, A. L., Garcia-Ocana A. *Hepatocyte Growth Factor (HGF) and the Pancreatic Beta Cell*. (Landes Bioscience, 2011).

136 Grusch, M. *et al.* Spatio-temporally precise activation of engineered receptor tyrosine kinases by light. *The EMBO journal* 33, 1713-1726, doi:10.15252/embj.201387695 (2014).

137 Watanabe, N. & Mitchison, T. J. Single-molecule speckle analysis of actin filament turnover in lamellipodia. *Science* 295, 1083-1086, doi:10.1126/science.1067470 295/5557/1083 [pii] (2002).

138 Fan, F. *et al.* Novel genetically encoded biosensors using firefly luciferase. *ACS chemical biology* 3, 346-351, doi:10.1021/cb8000414 (2008).

139 Graham, F. L., Smiley, J., Russell, W. C. & Nairn, R. Characteristics of a human cell line transformed by DNA from human adenovirus type 5. *The Journal of general virology* 36, 59-74, doi:10.1099/0022-1317-36-1-59 (1977).

140 Brown, R. W. & Henderson, J. H. The mass production and distribution of HeLa cells at Tuskegee Institute, 1953-55. *Journal of the history of medicine and allied sciences* 38, 415-431 (1983).

141 Merglen, A. *et al.* Glucose sensitivity and metabolism-secretion coupling studied during two-year continuous culture in INS-1E insulinoma cells. *Endocrinology* 145, 667-678, doi:10.1210/en.2003-1099 (2004).

142 Marquez, G., Wang, L. V., Lin, S. P., Schwartz, J. A. & Thomsen, S. L. Anisotropy in the absorption and scattering spectra of chicken breast tissue. *Appl Opt* 37, 798-804, doi:61135 [pii] (1998).

143 Wan, S., Parrish, J. A., Anderson, R. R. & Madden, M. Transmittance of nonionizing radiation in human tissues. *Photochem Photobiol* 34, 679-681 (1981).

144 Yaroslavsky, A. N., Neel, V. & Anderson, R. R. Demarcation of nonmelanoma skin cancer margins in thick excisions using multispectral polarized light imaging. *J Invest Dermatol* 121, 259-266, doi:12372 [pii] 10.1046/j.1523-1747.2003.12372.x (2003).

145 Sisino, G., Bellavia, D., Corallo, M., Geraci, F. & Barbieri, R. A homemade cytospin apparatus. *Analytical biochemistry* 359, 283-284, doi:10.1016/j.ab.2006.09.002 (2006).

146 Blesch, A. Neurotrophic factors in neurodegeneration. *Brain Pathol* 16, 295-303, doi:BPA036 [pii]10.1111/j.1750-3639.2006.00036.x (2006).

147 Nagahara, A. H. & Tuszynski, M. H. Potential therapeutic uses of BDNF in neurological and psychiatric disorders. *Nat Rev Drug Discov* 10, 209-219, doi:10.1038/nrd3366 (2011).

148 Strauss, H. M., Schmieder, P. & Hughes, J. Light-dependent dimerisation in the N-terminal sensory module of cyanobacterial phytochrome 1. *FEBS letters* 579, 3970-3974, doi:10.1016/j.febslet.2005.06.025 (2005).

149 Welm, B. E. *et al.* Inducible dimerization of FGFR1: development of a mouse model to analyze progressive transformation of the mammary gland. *J Cell Biol* 157, 703-714, doi:10.1083/jcb.200107119 (2002).

150 Lew, E. D., Furdui, C. M., Anderson, K. S. & Schlessinger, J. The precise sequence of FGF receptor autophosphorylation is kinetically driven and is disrupted by oncogenic mutations. *Science signaling* 2, ra6, doi:10.1126/scisignal.2000021 (2009).

151 McCarty, J. H. & Feinstein, S. C. Activation loop tyrosines contribute varying roles to TrkB autophosphorylation and signal transduction. *Oncogene* 16, 1691-1700, doi:10.1038/sj.onc.1201688 (1998).

152 Bae, J. H. *et al.* Asymmetric receptor contact is required for tyrosine autophosphorylation of fibroblast growth factor receptor in living cells. *Proceedings of the National Academy of Sciences of the United States of America* 107, 2866-2871, doi:10.1073/pnas.0914157107 (2010).

153 Wilson, B. C. & Patterson, M. S. The physics, biophysics and technology of photodynamic therapy. *Physics in medicine and biology* 53, R61-109, doi:10.1088/0031-9155/53/9/R01 (2008).

154 Celli, J. P. *et al.* Imaging and photodynamic therapy: mechanisms, monitoring, and optimization. *Chemical reviews* 110, 2795-2838, doi:10.1021/cr900300p (2010).

155 Kubelka, P. New contributions to the optics of intensely light-scattering materials. *Journal of the Optical Society of America* 38, 448-457 (1948).

156 Kim, C. H., Oh, Y. & Lee, T. H. Codon optimization for high-level expression of human erythropoietin (EPO) in mammalian cells. *Gene* 199, 293-301 (1997).

157 Wells, K. D., Foster, J. A., Moore, K., Pursel, V. G. & Wall, R. J. Codon optimization, genetic insulation, and an rtTA reporter improve performance of the tetracycline switch. *Transgenic research* 8, 371-381 (1999).

158 Holm, L. Codon usage and gene expression. *Nucleic acids research* 14, 3075-3087 (1986).

159 McCarty, M. F. Clinical potential of Spirulina as a source of phycocyanobilin. *Journal of medicinal food* 10, 566-570, doi:10.1089/jmf.2007.621 (2007).

160 Strasky, Z. *et al.* Spirulina platensis and phycocyanobilin activate atheroprotective heme oxygenase-1: a possible implication for atherogenesis. *Food & function* 4, 1586-1594, doi:10.1039/c3fo60230c (2013).

161 Liu, J. *et al.* Phycocyanobilin accelerates liver regeneration and reduces mortality rate in carbon tetrachloride-induced liver injury mice. *World journal of gastroenterology* 21, 5465-5472, doi:10.3748/wjg.v21.i18.5465 (2015).

162 Zheng, J. *et al.* Phycocyanin and phycocyanobilin from Spirulina platensis protect against diabetic nephropathy by inhibiting oxidative stress. *American journal of physiology. Regulatory, integrative and comparative physiology* 304, R110-120, doi:10.1152/ajpregu.00648.2011 (2013).

163 Jacobson, S. G. *et al.* Gene therapy for leber congenital amaurosis caused by RPE65 mutations: safety and efficacy in 15 children and adults followed up to 3 years. *Archives of ophthalmology* 130, 9-24, doi:10.1001/archophthalmol.2011.298 (2012).

164 Nathwani, A. C. *et al.* Adenovirus-associated virus vector-mediated gene transfer in hemophilia B. *The New England journal of medicine* 365, 2357-2365, doi:10.1056/NEJMoa1108046 (2011).

165 Kumar, S. R., Markusic, D. M., Biswas, M., High, K. A. & Herzog, R. W. Clinical development of gene therapy: results and lessons from recent successes. *Molecular therapy. Methods & clinical development* 3, 16034, doi:10.1038/mtm.2016.34 (2016).

166 Jimenez, V. *et al.* In vivo genetic engineering of murine pancreatic beta cells mediated by single-stranded adeno-associated viral vectors of serotypes 6, 8 and 9. *Diabetologia* 54, 1075-1086, doi:10.1007/s00125-011-2070-3 (2011).

167 Sako, K. *et al.* Optogenetic Control of Nodal Signaling Reveals a Temporal Pattern of Nodal Signaling Regulating Cell Fate Specification during Gastrulation. *Cell reports* 16, 866-877, doi:10.1016/j.celrep.2016.06.036 (2016).

168 Buscone, S. *et al.* A new path in defining light parameters for hair growth: Discovery and modulation of photoreceptors in human hair follicle. *Lasers in surgery and medicine*, doi:10.1002/lsm.22673 (2017).

169 Ong, W. K. *et al.* The activation of directional stem cell motility by green light-emitting diode irradiation. *Biomaterials* 34, 1911-1920, doi:10.1016/j.biomaterials.2012.11.065 (2013).

170 Halevy, O., Piestun, Y., Rozenboim, I. & Yablonka-Reuveni, Z. In ovo exposure to monochromatic green light promotes skeletal muscle cell proliferation and affects myofiber growth in posthatch chicks. *American journal of physiology. Regulatory, integrative and comparative physiology* 290, R1062-1070, doi:10.1152/ajpregu.00378.2005 (2006).

171 Wu, S. & Xing, D. Intracellular signaling cascades following light irradiation. *Laser Photonics Rev.* 8, 115–130 (2014).

172 Liang, H. L., Whelan, H. T., Eells, J. T. & Wong-Riley, M. T. Near-infrared light via light-emitting diode treatment is therapeutic against rotenone- and 1-methyl-4-phenylpyridinium ion-induced neurotoxicity. *Neuroscience* 153, 963-974, doi:10.1016/j.neuroscience.2008.03.042 (2008).

173 Reinhart, F. *et al.* Near-infrared light (670 nm) reduces MPTP-induced parkinsonism within a broad therapeutic time window. *Experimental brain research* 234, 1787-1794, doi:10.1007/s00221-016-4578-8 (2016).

174 Gao, X. & Xing, D. Molecular mechanisms of cell proliferation induced by low power laser irradiation. *Journal of biomedical science* 16, 4, doi:10.1186/1423-0127-16-4 (2009).

175 Mason, M. G., Nicholls, P. & Cooper, C. E. Re-evaluation of the near infrared spectra of mitochondrial cytochrome c oxidase: Implications for non invasive in vivo monitoring of tissues. *Biochimica et biophysica acta* 1837, 1882-1891, doi:10.1016/j.bbabio.2014.08.005 (2014).

176 Beattie, G. M., Cirulli, V., Lopez, A. D. & Hayek, A. Ex vivo expansion of human pancreatic endocrine cells. *The Journal of clinical endocrinology and metabolism* 82, 1852-1856, doi:10.1210/jcem.82.6.4009 (1997).

177 Maeda, H., Rajesh, K. G., Maeda, H., Suzuki, R. & Sasaguri, S. Epidermal growth factor and insulin inhibit cell death in pancreatic beta cells by activation of PI3-kinase/AKT signaling pathway under oxidative stress. *Transplantation proceedings* 36, 1163-1165, doi:10.1016/j.transproceed.2004.04.018 (2004).

178 Araujo, T. G. *et al.* Hepatocyte growth factor plays a key role in insulin resistance-associated compensatory mechanisms. *Endocrinology* 153, 5760-5769, doi:10.1210/en.2012-1496 (2012).

179 Garcia-Ocana, A. *et al.* Hepatocyte growth factor overexpression in the islet of transgenic mice increases beta cell proliferation, enhances islet mass, and induces mild hypoglycemia. *The Journal of biological chemistry* 275, 1226-1232 (2000).

180 Otonkoski, T. *et al.* Hepatocyte growth factor/scatter factor has insulinotropic activity in human fetal pancreatic cells. *Diabetes* 43, 947-953 (1994).

181 Kulkarni, R. N. *Islet Cells Growth Factors*. (Landes Bioscience, 2011).

182 Bailes, H. J., Zhuang, L. Y. & Lucas, R. J. Reproducible and sustained regulation of Galphas signalling using a metazoan opsin as an optogenetic tool. *PloS one* 7, e30774, doi:10.1371/journal.pone.0030774 (2012).

183 Ahren, B. Islet G protein-coupled receptors as potential targets for treatment of type 2 diabetes. *Nat Rev Drug Discov* 8, 369-385, doi:10.1038/nrd2782 (2009).

184 Doyle, M. E. & Egan, J. M. Mechanisms of action of glucagon-like peptide 1 in the pancreas. *Pharmacology & therapeutics* 113, 546-593, doi:10.1016/j.pharmthera.2006.11.007 (2007).

185 Rajala, R. V., McClellan, M. E., Ash, J. D. & Anderson, R. E. In vivo regulation of phosphoinositide 3-kinase in retina through light-induced tyrosine phosphorylation of the insulin receptor beta-subunit. *The Journal of biological chemistry* 277, 43319-43326, doi:10.1074/jbc.M206355200 (2002).

186 Buteau, J., Foisy, S., Joly, E. & Prentki, M. Glucagon-like peptide 1 induces pancreatic beta-cell proliferation via transactivation of the epidermal growth factor receptor. *Diabetes* 52, 124-132 (2003).

187 Talbot, J., Joly, E., Prentki, M. & Buteau, J. beta-Arrestin1-mediated recruitment of c-Src underlies the proliferative action of glucagon-like peptide-1 in pancreatic beta INS832/13 cells. *Molecular and cellular endocrinology* 364, 65-70, doi:10.1016/j.mce.2012.08.010 (2012).

188 Barki-Harrington, L. & Rockman, H. A. Beta-arrestins: multifunctional cellular mediators. *Physiology* 23, 17-22, doi:10.1152/physiol.00042.2007 (2008).

189 Sonoda, N. *et al.* Beta-Arrestin-1 mediates glucagon-like peptide-1 signaling to insulin secretion in cultured pancreatic beta cells. *Proceedings of the National Academy of Sciences of the United States of America* 105, 6614-6619, doi:10.1073/pnas.0710402105 (2008).

190 Lefkowitz, R. J. & Shenoy, S. K. Transduction of receptor signals by beta-arrestins. *Science* 308, 512-517, doi:10.1126/science.1109237 (2005).

191 Choi, M. *et al.* Light-guiding hydrogels for cell-based sensing and optogenetic synthesis in vivo. *Nature photonics* 7, 987-994, doi:10.1038/nphoton.2013.278 (2013).

192 Byrne, J. D. *et al.* Local iontophoretic administration of cytotoxic therapies to solid tumors. *Science translational medicine* 7, 273ra214, doi:10.1126/scitranslmed.3009951 (2015).

193 Byrne, J. D. *et al.* Iontophoretic device delivery for the localized treatment of pancreatic ductal adenocarcinoma. *Proceedings of the National Academy of Sciences of the United States of America* 113, 2200-2205, doi:10.1073/pnas.1600421113 (2016).

194 Efrat, S. Ex-vivo Expansion of Adult Human Pancreatic Beta-Cells. *The review of diabetic studies : RDS* 5, 116-122, doi:10.1900/RDS.2008.5.116 (2008).

195 Ingles-Prieto, A. *et al.* Light-assisted small-molecule screening against protein kinases. *Nature chemical biology* **11**, 952-954, doi:10.1038/nchembio.1933 (2015).

APPENDIX

Table A1 Oligonucleotides for genotyping of OPN3$^{-/-}$ mice.

Number	Name	Sequence
1	OPN3WT_F	TGTACCGTGGACTGGAGATCCAAG
2	OPN3$^{-/-}$_F	TTATGGCCCACACCAGTGGC
3	FOPN3_R	GTTCCCACA CACGACCTGCTC

Table A2 Oligonucleotides utilized in genetic engineering. Restriction sites are underlined.

Number	Name	Sequence
1	CPH1S_XmaI_F	GCTACCCGGGGCCACCACCGTACAACTCAG
2	CPH1S_XmaI_R	GCTACCCGGGTTCTTCTGCCTGGCGCAAAAT
3	CPH1So_XmaI_F	GATCCCCGGGGCAACTACTGTTCAACTGTCT
4	CPH1So_XmaI_R	GATCCCCGGGTTCTTCAGCTTGGCGCAGAAT
5	truncated	TGGGAGGTCTATATAAGCAGAGC
6	truncated	GGCGGGCCATTTACCGTAAG
7	mF_inverse_SgrAI_F	GATCCACCGGTGGAGCAACTACTGTTCAACT
8	mF_ inverse_SgrAI_R	GATCCACCGGTGACGTCGAGGCGCTG
9	rtrkB_BspEI_F	GATCTCCGGAAAGTTTGGCATGAAAG
10	rtrkB_AgeI_R	CAGAAACCGGTGCCTAGGATGTCCAG
11	mF_YY271/2FF_F	GAGACATTCATCATATCGACTTCTTCAAGAAA
12	mF_YY271/2FF_R	GGCCGTTGGTGGTTTTCTTGAAGAAGTCGAT
13	mF_R195E_F	TACAGGCCCGGGAGCCTCCTGGGCTGGAGT
14	mF_R195E_R	TTATAGCAGTACTCCAGCCCAGGAGGCTCCC
15	TrkB-CP1 K131A F	TGGCCGTGGCGACGCTGAAGGAC
16	TrkB-CP1 K131A R	GTCCTTCAGCGTCGCCACGGCCA
17	pGL4_inverse_AscI_F	GATCATGGCGCGCCCTAAGGCCGCGACTCTA
18	pGL4_inverse_ AscI_R	ATGATCGGCGCGCCGGTGGCTTTACCAACAG
19	mCherry_AscI_F	CATCAGGCGCGCCATGGTGAGCAAGGGCGA
20	mCherry_AscI_R	GATCAGGCGCGCCTTACTTGTACAGCTCGTC

Table A3 Oligonucleotides utilized for RT-PCR to determine opsin expression in mouse, humane islets.

Number	Name	Sequence
1	m-bActin _F	CCTGAACCCTAAGGCCAACC
2	m-bActin _R	CTCGTAGATGGGCACAGTGTG
3	mInsulin _F	GCGTGGCTTCTTCTACACAC
4	mInsulin _R	GTTCTCCAGCTGGTAGAGGG
5	mOPN1SW _F1	GTCATCTGTAAACCCTTCGGC
6	mOPN1SW _R1	GTACTCGCTTCGATACTTGGTG
7	mOPN1SW _F2	CTGCTACGTGCCCTATGCTG
8	mOPN1SW _R2	GATGGTGACAAGCCGTAAGTCC
9	mOPN1MW _F1	GCAGTTGCTGACCTAGCAGAG
10	mOPN1MW _R1	CTTGCAGACCACCAGCCATC
11	mOPN1MW _F2	GCCCTTTGGCAATGTGAGAT
12	mOPN1MW _R2	CCAGACCCAGGAGAAGACGAT
13	mOPN3 _F1	CCATTACCACCCTCACTGTGC
14	mOPN3 _R1	CAGCCCAGTCCATGTATGTC
15	mOPN3 _F2	GATGGCCTTTGTCTTTCTCACC
16	mOPN3 _R2	GGTGTCCATAGCCATTGACCA
17	mMelanopsin _F1	CTCTTTGGGGAGACAGGTTG
18	mMelanopsin _R1	CAGGGCATAAAGCCAGACGCC
19	mMelanopsin _F2	GATACTCGCACATCCTGACGC
20	mMelanopsin _R2	AATGGGATTGTGGATGGCAG
21	mOPN5 _F1	CCATACAGCTCTCCGTGGTG
22	mOPN5 _R1	GATGGATCTCCAGCACAGCAG
23	mOPN5 _F2	CCATGTACTTGAGGTGAAGCTG
24	mOPN5 _R2	GCTGATTTTGCAAGGAGTGTGG
25	mRhodopsin _F1	CCTTAGGACTGAGAAAGCATCGAG
26	mRhodopsin _R1	GCTGAGAGACATGAGGCAAGGT
27	mRhodopsin _F2	CCACCCTCTACACATCACTCC
28	mRhodopsin _R2	GAAGACCACACCCATGATAGC

29	h_b-actin _F	CCACACCTTCTACAATGAGCTG
30	h_b-actin _R	CCTGGATAGCAACGTACATGG
31	hInsulin _F	GATCACTGTCCTTCTGCCATG
32	hInsulin_R	GTTCCCCGCACACTAGGTAG
33	hOPN1SW _F1	GACTTACGGCTTGTCACCATTC
34	hOPN1SW_R1	GGGTAGACGAGACAGTAGAAAC
35	hOPN1SW _F2	CTTCCTGGCCTTTGAGCGC
36	hOPN1SW_R2	GCAGAAGATGAAGAGGAACCAC
37	hOPN1MW _F	CACCTACACCAACAGCAACTC
38	hOPN1MW _R	GTTCACCAGGATCCAGTTCAG
39	hOPN1MW _F	CCACGGCCTGAAGACTTCATG
40	hOPN1MW _R	CAGGACCATCACCACCACC
41	hOPN1LW_ F	CACCTACACCAACAGCAACTC
42	hOPN1LW _R	GTTCACCAGGATCCAGTTCAG
43	hOPN1LW_ F	CTGGGAGAGATGGATGGTGG
45	hOPN1LW _R	GGTACGAGCTGCCGCTGAA
46	hOPN3 _F	CGTACCTCTTTGCTAAATCGAAC
47	hOPN3 _R	CCTGTCCCCATCTTTCTGTG
48	hOPN3 _F	CTCACCTCCTCCTGGTCAAC
49	hOPN3 _R	CTACAAAGGACGAACTTGGATTACATC
50	hMelanopsin _F	GACACGAAGCAGAGACTCCAG
51	hMelanopsin _R	CTCACAGCATAATCCTGGGTC
52	hMelanopsin _F	CGAGGGGTTGCTGACATCC
53	hMelanopsin _R	CTTGCACTCGCTCTGCAGCC
54	hOPN5 _F	CTGTGATCGTGTTCTCCTACG
55	hOPN5 _R	CCTTCCAAAAGCTGACCACAC
56	hOPN5 _F	GACTATCAATTTAGCAGTCTGTGATC
57	hOPN5 _R	GATCCAGGCTGACAGCAGTC
58	hRhodopsin_F	CTCAACTACATCCTGCTCAACC
59	hRhodopsin _R	CAAGGACCACAGGGCAATTTC

60	hRhodopsin_F	CAAGCCGGAGGTCAACAACG
61	hRhodopsin _R	GCCACGCTGGCGTAGGG

Table A4 Donor details

Donor number	Gender	Age	Weight (kg)	BMI	Purity
1	Male	47	95.3	31.0	85%
2	Female	44	106.0	34.5	90%
3	Male	59	94.8	26.8	85%
4	Male	34	181.0	49.9	95%

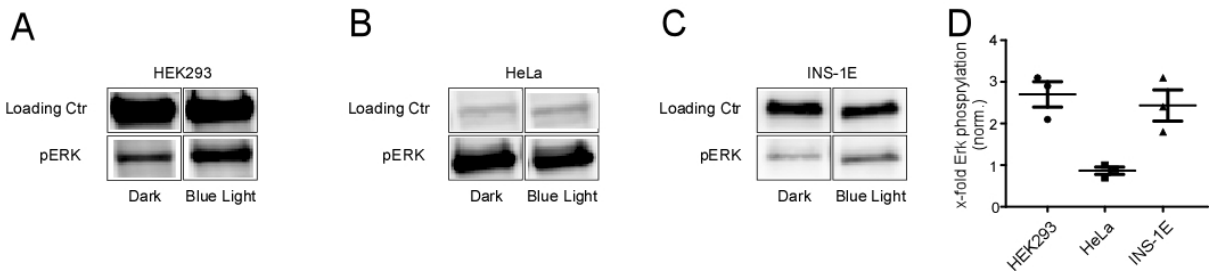

Figure A1 Light-dependent MAPK/Erk pathway activation in different cell lines (A) Representative immunoblot of blue-light-induced pErk increase in HEK293 cells. Loading Ctr: calnexin. (B) Representative immunoblot of blue-light-induced pErk increase in HeLa cells. Loading Ctr: calnexin. (C) Representative immunoblot of blue-light-induced pErk increase in INS-1E cells. Loading Ctr: total Akt. (D) Quantification of blue-light-induced pErk increase for each cell line, normalized to dark control. Mean ± SEM are shown for three independent experiments for each cell line. (A-D) Light intensity: 255 µW/cm^2; duration of illumination: 5 minutes

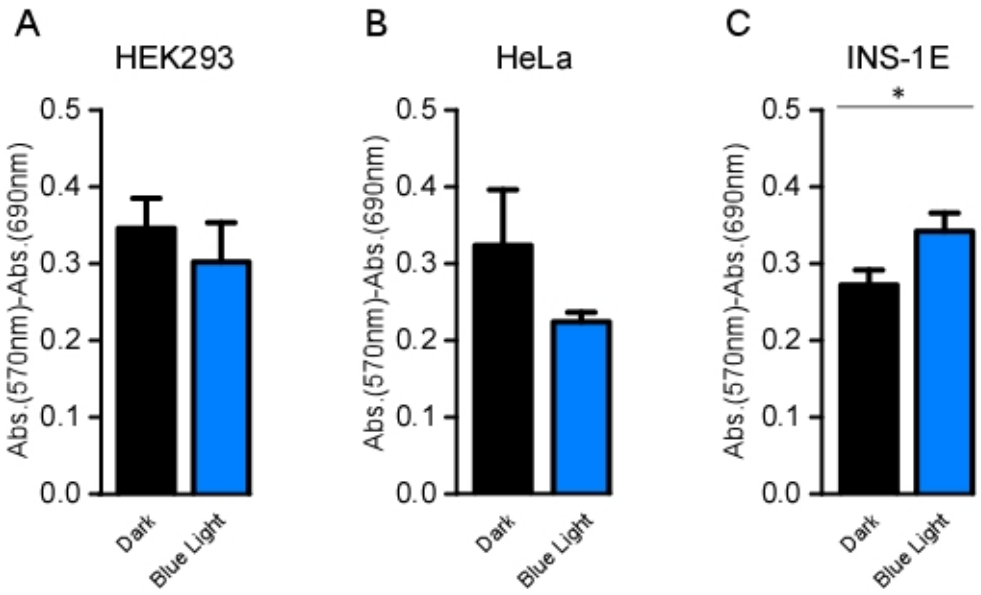

Figure A2 Light-dependent variations in cell viability of different cell lines. Cell viability was assessed by a MTT assay. Cell viability is expressed as absorbance (Abs.) at 570 nm subtracted by the background (Abs. 690 nm). (A) HEK293 cells showed no significant change in cell viability after blue light illumination with an intensity of 64 μW/cm^2. (B) HeLa cells showed a decreasing trend in cell viability after blue light illumination with an intensity of 64 μW/cm^2. (C) INS-1E cells showed a significant increase in cell viability after blue light illumination with an intensity of 255 μW/cm^2. (A-C) Mean ± SEM are shown for three to seventeen independent experiments for each cell line. A value of $p \leq 0.05$ was considered to be significant. Duration of illumination: 24 hours

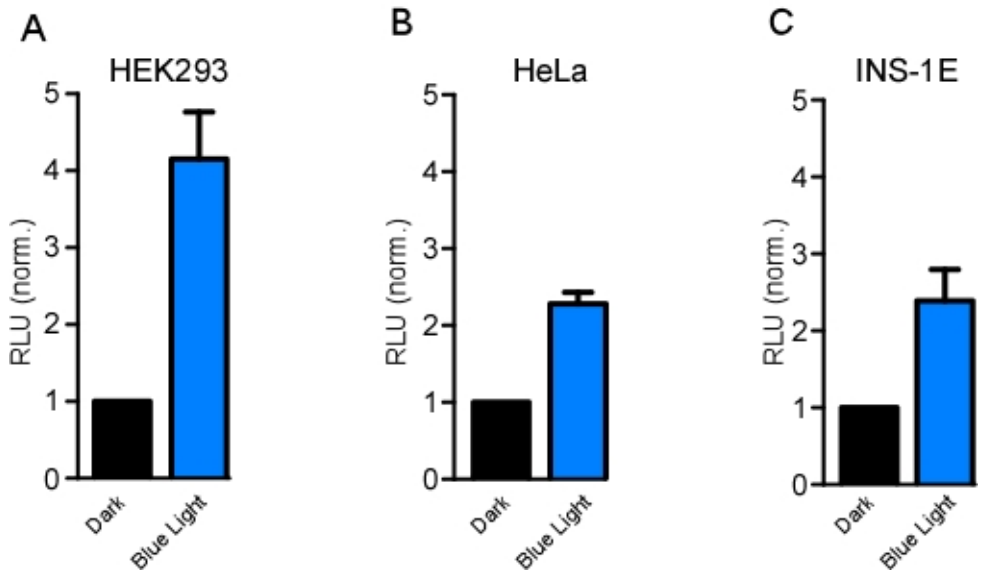

Figure A3 Light-dependent cAMP level changes in different cell lines. cAMP levels are expressed as RLU. Results are normalized to dark values. (A) HEK293 cells showed an increase in cAMP levels after blue light illumination. (B) HeLa cells showed a small increase in cAMP levels after blue light illumination. (C) INS-1E cells showed a small increase in cAMP levels after blue light illumination. (A-C) Mean ± SEM are shown for three independent experiments for each cell line. Light intensity: 9.6 mW/cm^2; duration of illumination: 3 seconds